TWO-DIMENSIONAL TRANSITION METAL DICHALCOGENIDE (TMDC) ALLOYS AND DEVICES

PhD Dissertation
Mehmet BAY

Eskişehir, 2019

TWO-DIMENSIONAL TRANSITION METAL DICHALCOGENIDE (TMDC) ALLOYS AND DEVICES

Mehmet BAY

PhD DISSERTATION

Programme in Electronics

Department of Electrical and Electronics Engineering

Supervisor: Assoc. Prof. Dr. Nihan KOSKU PERKGÖZ

Eskişehir

Eskişehir Technical University

Institue of Graduate Programs

August 2019

FINAL APPROVAL FOR THESIS

This thesis titled “Two-Dimensional Transition Metal Dichalcogenide (TMDC), Alloys and Devices” has been prepared and submitted by Mehmet BAY in partial fulfillment of the requirements in “Eskişehir Technical University Directive on Graduate Education and Examination” for the Degree of Doctor of Philosophy (PhD) in Electrical and Electronics Engineering Department has been examined and approved on 08/08/2019.

Committee Members	**Title Name Surname**	**Signature**
Member (Supervisor)	: Assoc. Prof. Dr. Nihan K. PERKGÖZ	……
Member	: Assoc. Prof. Dr. Feridun AY	……
Member	: Assist. Prof. Dr. Suzan BİRAN AY	……
Member	: Assoc. Prof. Dr. Urartu Özgür Şafak ŞEKER	……
Member	: Assist. Prof. Dr. Faruk DİRİSAĞLIK	……

Prof. Dr. Murat TANIŞLI

.

Director of Institute of Graduate Programs

ABSTRACT

TWO-DIMENSIONAL TRANSITION METAL DICHALCOGENIDE (TMDC), ALLOYS AND DEVICES

Mehmet BAY
Department of Electrical and Electronics Engineering
Eskisehir Technical University, Graduate School of Sciences
Supervisor: Assoc. Dr. Nihan KOSKU PERKGÖZ

Two-dimensional transition metal dichalcogenide (2-D, TMDC) and their alloys have attracted significant attention due to their extraordinary optical and electronic properties such as high mobility, high photosensitivity, direct bandgap that does not exist in their bulk forms. Molybdenum sulphide (MoS_2), molybdenum sulphoselenide ($MoS_{2(1-x)}$-Se_{2x} (x=0-1)), molybdenum selenide ($MoSe_2$), and their alloys are candidates for new devices in optoelectronics, semiconductor electronics, photodetectors, photovoltaics and energy harvesting. In this thesis, we present repeatable MoS_2, $MoS_{2(1-x)}$-Se_{2x}, $MoSe_2$ monolayer formation with a systematical investigation of chemical vapor deposition (CVD) growth parameters including gas flow rates, substrate temperature and precursor concentration (S/Se ratio). We have achieved a complete control of x value (x=0-1) allowing for bandgap change in between 1.82 eV (MoS_2) and 1.56 eV ($MoSe_2$). In general, the sizes of the obtained monolayer flakes have been as large as 150 μm on SiO_2 (300 nm)/Si substrates. The reaction temperature and S/Se ratio have been found to be the most critical parameters to control the composition (x= 0-1) of the monolayer alloy TMDCs. The growth of Se rich alloys at a higher growth temperature is explained with the chalcogen exchange mechanism (CEM) in relation with substitution of S atoms in as grown alloy host lattice site with Se atoms present in the Se rich vapor. Additionally, NaCl salt involvement in the CVD process is investigated to enable large area $MoSe_2$ monolayer flake growth with full substrate coverage, which is proven successful. We performed different characterizations, which include photoluminescence (PL), Raman spectroscopy, and optical and dark field image, atomic force microscopy (AFM), and scanning electron microcopy (SEM) measurements. We also fabricated field effect transistor (FET) devices using our 2D $MoSe_2$ flakes and performed device performance measurements.

Keywords: CVD, $MoS_{2(1-x)}Se_{2(x)}$, MoS_2, $MoSe_2$, 2D TMDCs alloy, FET, Two-dimensional materials

ÖZET

İKİ BOYUTLU GEÇİŞ METAL
DİKALKOGENİT (GMDK) ALAŞIMLARI VE AYGITLARI

Mehmet BAY
Elektrik ve Elektronik Mühendisliği
Eskişehir Teknik Üniversitesi, Lisansüstü Eğitim Enstitüsü
Supervisor: Assoc. Dr. Nihan KOSKU PERKGÖZ

İki-boyutlu geçiş metalleri dikalkojenitler (2-B GMK) alaşımları elektronik özellikleri, mobilite, ışık hassasiyeti, kitle formda olmayan direkt bant aralığı gibi üstün özellikleri nedeniyle büyük ilgi çekmiştir. Molibden sülfit (MoS_2), molibden sülfoselenit ($MoS_{2(1-x)}$-Se_{2x}), molibden selenit ($MoSe_2$), ve alaşımları optoelektronik, yarıiletken elektroniği ışık detektörleri ışık pilleri ve enerji hasadı alanlarında üretilen yeni cihazlar için adaydır. Bu tez çalışmasında, tek katmanlı MoS_2, $MoS_{2(1-x)}$-Se_{2x}), $MoSe_2$ yapıların tekrarlanabilir olarak üretimi, gaz akış oranları, alttaş sıcaklığı kimyasal toz oranları (S/Se) gibi kimyasal buhar biriktirme (KBB) parametrelerinin sistematik şekilde araştırılması sunulmuştur. SiO_2 (300 nm)/Si alttaşları üzerinde üretilen tek tabakalı yaprakların boyutunun 150 μm kadar büyük olduğu ölçülen ve bant aralığının 1.82 eV (MoS_2) ile 1.56 eV ($MoSe_2$) arasında değişmesine izin veren x (x= 0-1) kompozisyonunun tam olarak kontrolünü elde ettik. Reaksiyon sıcaklığı ve S/Se oranı te katmanlı GMK alaşımlarının bileşim değerinin (x=0-1) kontrolünde en önemli parametrelerdir. Selenyum bakımından zengin alaşımların daha yüksek bir büyüme sıcaklığında büyümesi, Se zengin buharında mevcut Se atomları ile büyütülmüş alaşım konak kafes bölgesi olarak S atomlarının ikame edilmesi kalkojen değişim mekanizmasına (KDM) atfedilir. KBB işleminde NaCl katılımı, alttaşın tüm yüzeyini kaplanmış ve tuzsuz bir işlemle mümkün olmayan geniş alanlı $MoSe_2$ üretimini sağlar. Fotoluminesans (FL) ölçümü, Raman spektroskopi ölçümü, karanlık alan ölçümü, aydınlık alan ölçümü atomik güç mikroskobu (AGM) ölçümü, taramalı elektron mikroskobu (TEM) gibi bazı analiz ölçümlerini tatbik ettik. Alan etki transistörü (AET) cihazı 2B $MoSe_2$ yaprağı üzerine fabrike edildi ve performans ölçümü gösterildi.

Anahtar Kelimeler: KBB, $MoS_{2(1-x)}Se_{2(x)}$, MoS_2, $MoSe_2$, 2B-GMK alaşımları, FET, 2-Boyutlu malzemeler

ACKNOWLEDGEMENTS

Firstly, I would like to special thanks to founders of Micro Nano Devices and Systems (MIDAS) Laboratory; Assoc. Prof. Dr. Nihan KOSKU PERKGÖZ, Assoc. Prof. Dr. Feridun AY, Assoc. Prof. Dr. Cem SEVİK for their valuable contributions, comments on this work.

I would like sincere thanks to Assoc. Prof. Dr. Nihan KOSKU PERKGÖZ for considerate and emphatic leadership, motivational support and guidance in the Ph.D work. You are my academic idol and I am grateful to be your Ph.D student.

I would like thank to my colleagues, Dr. Ayberk Özden, Dr. Aydan YELTİK, Mustafa DEMİRTAŞ, Hüseyin ŞAR, Merve ÖPER, Cem ODACI, Yahaya SHEHU, Wonge Lisheshar İBRAHİM, Tuğbey KOCABAŞ and all member of Micro Nano Devices and Systems Research Group (MIDAS) for their contributions.

I would like to thank to my thesis committee members: Assist. Prof. Dr. Suzan Biran Ay, Assoc. Prof. Dr. Faruk DİRİSAĞLIK, Prof. Dr. Urartu Özgür Şafak Şeker for their valuable contributions on this work.

I would like to thank Assist. Prof. Dr. Yasemin Çelik for your cooperation and for using your laboratory facilities.

I would like to thank the hospitality and support from Eskişehir Technical University and Scientific Research Project Units of Eskişehir Technical University with Grants: 1306F174, 1404F214, 1407F335, 1505F271, 150BF228, 1705F265, 1804F085.

I would like to thank to my mother Hacer BAY and my father for raising and educating me as a good person. I would like to thank to my sister Tuğba BAY for being my best friend in my life.

Finally, I would like to special thanks to my wife Zaliha Betül BAY, my daughters Rana Elif BAY and Ceyda Gökçe BAY for their love, this thesis is dedicated to them.

08/08/2019

STATEMENT OF COMPLIANCE WITH ETHICAL PRINCIPLES AND RULES

I hereby truthfully declare that this thesis is an original work prepared by me; that I have behaved in accordance with the scientific ethical principles and rules throughout the stages of preparation, data collection, analysis and presentation of my work; that I have cited the sources of all the data and information that could be obtained within the scope of this study, and included these sources in the references section; and that this study has been scanned for plagiarism with "scientific plagiarism detection program" used by Eskişehir Technical University, and that "it does not have any plagiarism" whatsoever. I also declare that, if a case contrary to my declaration is detected in my work at any time, I hereby express my consent to all the ethical and legal consequences that are involved.

Mehmet BAY

TABLE OF CONTENTS

Page

LIST OF TABLES

Page

LIST OF FIGURES

Page

INDEX OF ABBREVIATIONS AND SYMBOLS

2D : Two Dimensional

PL : Photoluminescence

TMDC : Transition Metal Dichalcogenide

FLIM : Fluorescence Lifetime Imaging

CVD : Chemical Vapor Deposition

b_{Gap} : Band gap

σ : Electrical Conductivity

μ : Charge Carrier Mobility

n : Charge Carrier Density

e : Electrical Charge

E_g : Electronic Band Gap

TEM : Transmission Electron Microscope

SEM : Scanning Electron Microscope

AFM : Atomic Force Microscope

DF : Dark Field

BF : Bright Field

1. INTRODUCTION

In this thesis, we research producing two-dimensional (single layer) transition metal dichalcogenide (TMDC) structures and their alloys such as molybdenum sulphide (MoS_2), molybdenum sulphoselenide ($MoS_{2(1-x)}$-Se_{2x} (x=0-1)), and molybdenum selenide ($MoSe_2$), by using CVD method. Controlling monolayer growth via changing CVD parameters, and characterizations of produced monolayer flakes are investigated. The field effect transistor (FET) devices using 2D $MoSe_2$ flakes are fabricated and the performance measurements are demonstrated. In the introduction part of this dissertation, a summary of the 2D materials basics, our motivation to study in this field and the current problems are summarized.

1.1. Overview

The most famous member of 2D materials is graphene, which is a mono atomic layer of graphite. Many scientific groups have studied graphene due to its extra-ordinary electronic and optical properties such as very high mobility in addition to its peculiar mechanical properties such as high strength and flexibility [1-6].. Andre K. Geim and Konstantin S. Novoselov won Nobel Prize in 2010 due to their scientific contribution about graphene (Figure 1-1) [6-9]. Graphene is monolayer form of sp2 carbon and the lattice structure is hexagonal same as lattice structure of diamond [10-13]. After the discovery of graphene, it is realized that there are hundreds of 2D materials waiting to be discovered [14-25]. Among these 2D materials, two-dimensional TMDCs and their alloys have also attracted considerable attention due to their optical and electronic properties such as high ON/OFF ratio, and high photosensitivity.

Molybdenum sulphide (MoS_2), molybdenum sulphoselenide ($MoS_{2(1-x)}$-Se_{2x} (x=0-1)), molybdenum selenide ($MoSe_2$), their alloys are some of the candidates for new potential devices in optoelectronics [1-5]. Bandgap tuning of 2-dimensional TMDCs via changing process parameters is an attention grabbing method for enhanced light absorption, and responsivity [6, 7].

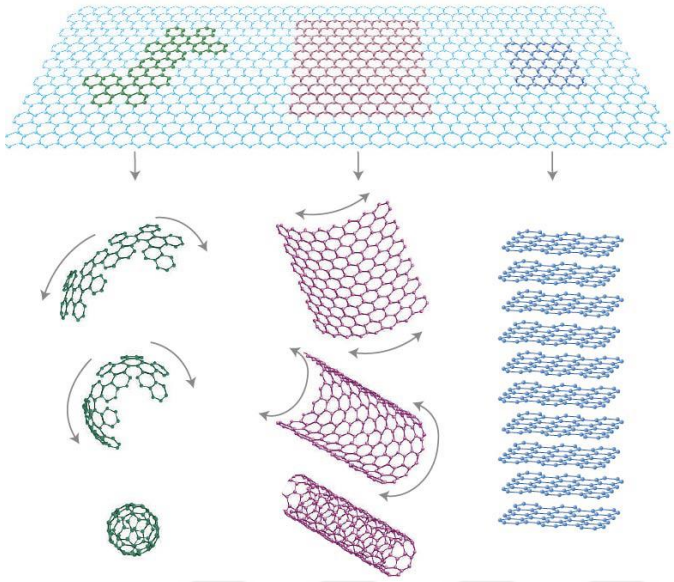

Figure 1-1 *Monolayers of carbon atoms arranged in a hexagonal lattice [6].*

Members of TMDCs family such as, $MoS_{2(1-x)}Se_{2x}$, MoS_2, $MoSe_2$ structures and their alloys was studied in many scientific groups. However, controlling of monolayer growth with high coverage is still a challenging issue. There are various external critical CVD parameters such as pressure, reaction temperature, precursor ratios, gas flow rates. Hence, optimization of CVD parameters is under research [26-33].

Chemical vapor deposition (CVD) is facile process for producing monolayer flakes. By using CVD it is possible to produce most metals and non-metallic elements due to [26]. This CVD technology is important factor in producing semiconductor and in optoelectronic applications [30, 34]. CVD system is user friendly and cost effective comparing other techniques such as evaporation, sputtering and ion plating, CVD [30, 35-37]. The approximated production market for CVD was 3 billion dollars, soon after the market has been rapidly increasing to approximately 30 billions of dollars. The promising improvements of the technology and the growth of the market are predicted to progress in near future [34]. Produced two-dimensional TMDCs their alloys with high coverage are used for device fabrications such as field effect transistor (FET) devices [38, 39]. Device fabrication process are consist of, monolayer growth process, lithography process, metal coating process, lift off process and electrical measurements [39, 40].

1.2. Motivational

The promising improvements of production of two-dimensional semiconductor materials technology predicted to progress in near future [41]. Two-dimensional TMDCs

molybdenum sulphide (MoS_2), molybdenum sulphoselenide ($MoS_{2(1-x)}$-Se_{2x} (x=0-1)), molybdenum selenide ($MoSe_2$), their alloys are intensely studied due to this potential [42-46]. Chemical vapor deposition (CVD) process consists of critical external process parameters to produce monolayer flakes. Some of the important parameters are the reaction temperature of the substrate, the temperature of the powders such as, selenium (Se), (280 ^oC), sulphur (S), (180 ^oC), Molybdenum trioxide (750 ^oC), the amount of carrier gases, and the temperature of the system. In addition, the distances between powders, the distance 300 nm SiO_2 coated silicon substrate and powders has important role in CVD reactions. Bandgap models for single layer $MoS_{2(1-x)}Se_{2x}$ (x=0-1), MoS_2, $MoSe_2$ are shown in Figure A1-3. Bandgap energy of single layer $MoS_{2(1-x)}Se_{2(x)}$, (x=0-1), and x value is calculated by bowing parameter equation [47]. Sulphurization and selenization play key role in CVD surface reaction, it is more challenging to grow large-area and defect-free 2D $MoSe_2$ flakes since selenization is relatively harder than sulphurization. However, sulphurization has disadvantage that sulfur vacancies sharply disturb the electrical and optoelectronic properties of MoS_2 nano-sheets [38, 41, 48].

Two-dimensional TMDCs molybdenum sulphide (MoS_2), molybdenum sulphoselenide ($MoS_{2(1-x)}$-Se_{2x} (x=0-1)), molybdenum selenide ($MoSe_2$), their alloys are used in many applications such as fast photodetectors, solar cells, light emitting diodes (LEDs), field effect transistors (FET) [38, 39, 49-51]. Fabrication of field effect transistor (FET) has many steps such as, production of monolayer structure, transferring of monolayer structures, AFM measurements, lithography process, metal coating process, and electrical measurement. In regard to overview and motivational given above this thesis aims producing mono layer molybdenum sulphide (MoS_2), molybdenum sulphoselenide ($MoS_{2(1-x)}$-Se_{2x} (x=0-1)), molybdenum selenide ($MoSe_2$), and their alloys two-dimensional TMDCs structures and their alloys by using CVD method.

2. REVIEW OF TMDC MATERIALS AND CHARACTERIZATIONS

In the Chapter 2, the material properties of TMDCs including molybdenum sulphide (MoS_2), molybdenum sulphoselenide ($MoS_{2(1-x)}$-Se_{2x} (x=0-1)), and molybdenum selenide ($MoSe_2$) are detailed. In addition, characterization techniques such as, confocal Raman, photoluminescence spectroscopies, bright field and dark field microcopies, atomic force microcopy (AFM), scanning electron microscopy (SEM), transmission electron microscopy (TEM) methods are explained.

2.1. TMDC Materials

The contributions of graphene studies open new research areas about TMDCs family. Two-dimensional transition metal dichalcogenide (TMDC) MX2 (M = Mo, W; X = S, Se, Te) are widely used in many device application areas due to their important properties such as, optical and electronic properties and their potential to be used in catalysis, microelectronics, batteries, hydrogen storage, medical applications, and optoelectronics [51-55]. Band gap of monolayer $MoSe_2$ is 1.56 and band gap of monolayer MoS_2 is 1.82 eV. Both are chemically stable materials and direct bandgap, which does not exist in its bulk form [53, 55]. Besides the controlling growth of two dimensional materials, many scientific groups also research the controlling of band gap for produced alloys such as, $MoS_{2(1-x)}$-Se_{2x} (x=0-1). Alloying of such semiconductors, tuning the bandgap is of significance as it presents additional prospects in terms of novel functionalities such as tuning photoluminescence, absorption and mobility [29, 43, 44]. Also, intentional doping of TMDCs has been used as a method to regulate such electrical and magnetic properties. For instance, Sb doping of SnS_2 enhances the metal-semiconductor interface by reducing Schottky barrier height Pb doping of $SnSe_2$ reduces the Fermi level and increases the on/off ratio of the $SnSe_2$ based transistors. Fe doped of SnS_2 flakes show ferromagnetic ordering with a Curie temperature. Furthermore, careful adjustment of doping and growth parameters can be utilized to synthesize new 2D materials such as CoS_2 film on MoS_2 with new functionalities such as half metallicity. [29].

2.1.1. Crystal structure of MoS_2, $MoS_{2(1-x)}Se_{2x}$ (x=0-1), $MoSe_2$

Crystal structure of MoS_2, $MoS_{2(1-x)}Se_{2x}$ (x=0-1), $MoSe_2$ has been studied by different groups, showing that they have a direct band gap in their monolayer form [56-58]. In this regard, the reports on 2D $MoSe_2$ is comparatively few among the TMDCs,

however, it also presents a high potential considering its high mobility [41, 51, 59-62]. As their thickness are reduced to a single layer, there is a transition from indirect band gap to direct band gap tunable band gap that is useful for the applications such as sensors, catalysis, optoelectronics, and photonics [56, 63-67]. Atomic structures of single layer MX_2 are shown in Figure 2-1 where the phases are presented as 2H, as a stable hexagonal phase, 1T as a metastable and 3R as a metastable phase [68]. Monolayer flakes can be in metallic phase 1T $MoS_{2(1-x)}Se_{2(x)}$, 1T MoS_2, 1T $MoSe_2$, 1T is metallic phase that, in a unit cell 3 molybdenum atoms have chemical bonding with selenium or sulphur atoms, there is trimerization and the structure have metallic phase [41].

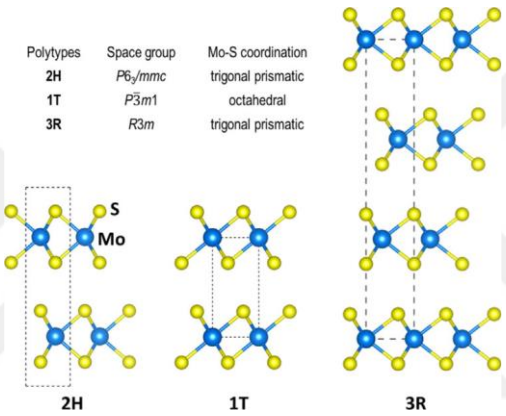

Figure 2-1 *Structural polytopes of MX_2 crystals including 2H phase, 1T phase and 3R phase [68].*

2.2. Synthesis Strategies of TMDCs

2.2.1. Top-down approaches

1.1.1.1 Micromechanical Exfoliation

Using micromechanical exfoliation method, two-dimensional TMDCS can be produced from bulk materials such as, Graphene is monolayer form of sp2 carbon and the lattice structure is hexagonal same as lattice structure of diamond. By using top-bottom configuration, graphene layers can be exfoliated. Exfoliated layers can be produced from bulk graphene due to broken Van der Waals bonds between interlayers of bulk graphene. There are two routes for exfoliation of TMDCs normal and lateral forces. Normal forces are applied through Van der Walls bonding between interlayers; lateral forces are applied through self-lubricating in lateral direction (Figure 2-2) [6, 69].

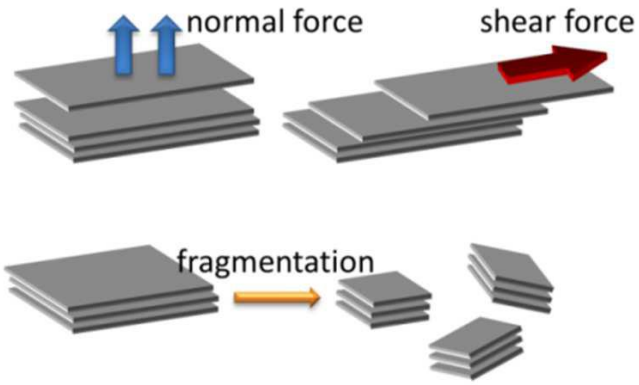

Figure 2-2 *Two routes for exfoliation of TMDCs [69].*

1.1.1.2 Liquid Phase Exfoliation

By using liquid phase exfoliation method, two-dimensional TDCMs can be produced from bulk materials [15]. Liquid phase exfoliation is basically micro exfoliation by using chemical solvents, liquids, polymers etc. Sonication device and high shear mixing devices are generally used to increase exfoliation. Sonication exfoliation method is very effective producing monolayer TMDCs from bulk materials [15]. Sonication device produces ultrasonic waves that causes vibration in Vander Walls bonding between interlayers of a bulk material. Sonication create pull and push forces in interlayer bonds. These forces break these bonds. Monolayer flakes are produced via sonication mechanism (Figure 2-3) [15].

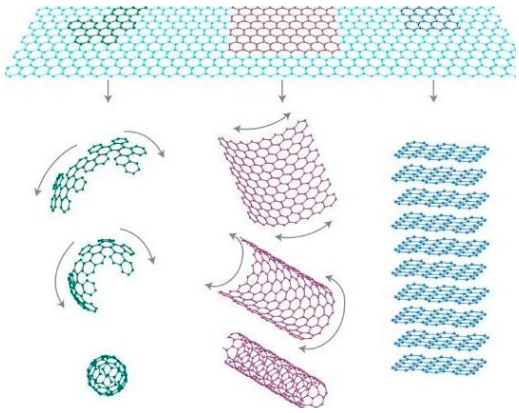

Figure 2-3 *Graphene is a 2D TMDC material for carbon materials[69]*

2.2.2. Bottom-up approaches

1.1.1.3 Physical Vapor Deposition (PVD)

Physical Vapor Deposition (PVD) technique is expensive and difficult method to produce monolayer TMDCs materials such as $MoSe_2$ and MoS_2. PVD system scheme is shown in Figure 2-4. There are two electrodes on inside of chamber. Substrates are located on the center and nitrogen gas is use as a precursor. TMDC materials are heated under vacuum conditions. They are condensed and vaporized for physical vapor deposition process. Reaction temperatures are between 200 ^oC and 500 ^oC which is low comparing CVD reaction temperatures [39, 70].

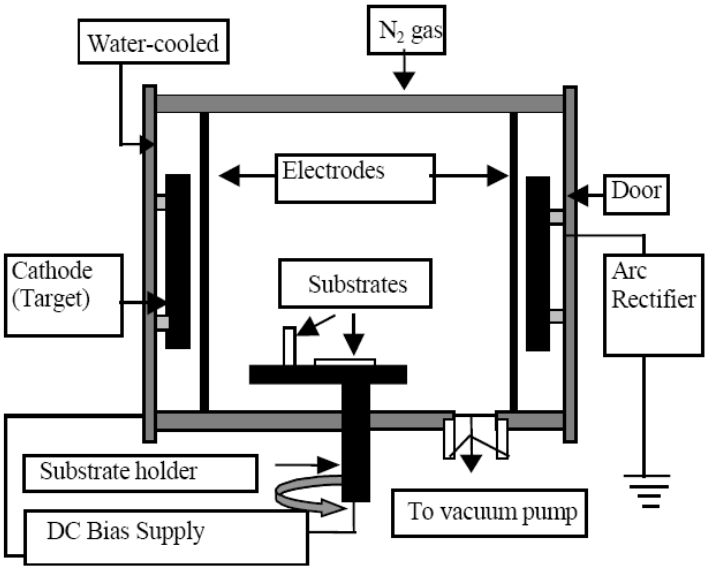

Figure 2-4 *Physical vapor deposition system scheme [70]*

1.1.1.4 Atomic Layer Deposition (ALD)

Atomic layer deposition (ALD) is another potential technique to grow 2D TMDCs materials such as $MoSe_2$ and MoS_2. The most important facility of ALD method is controlling the thickness of deposited layers. Deposition are uniformly coated and surface coverage is homogeneous which is important for device quality. Atomic layer deposition (ALD) system scheme is shown in Figure 2-5. The substrate is located on center of the chamber (Figure 2-5 a) and Precursor is pulsed in to the chamber for ALD reactions (Figure 2-5 b). By using inert gases such as nitrogen (N_2), excess precursors are purged out of the chamber (Figure 2-5 c and Figure 2-5 d). Other precursor is pulsed for ALD reactions (Figure 2-5 d). ALD processes are done cycle by cylices, until targeted thickness is reached [31, 71].

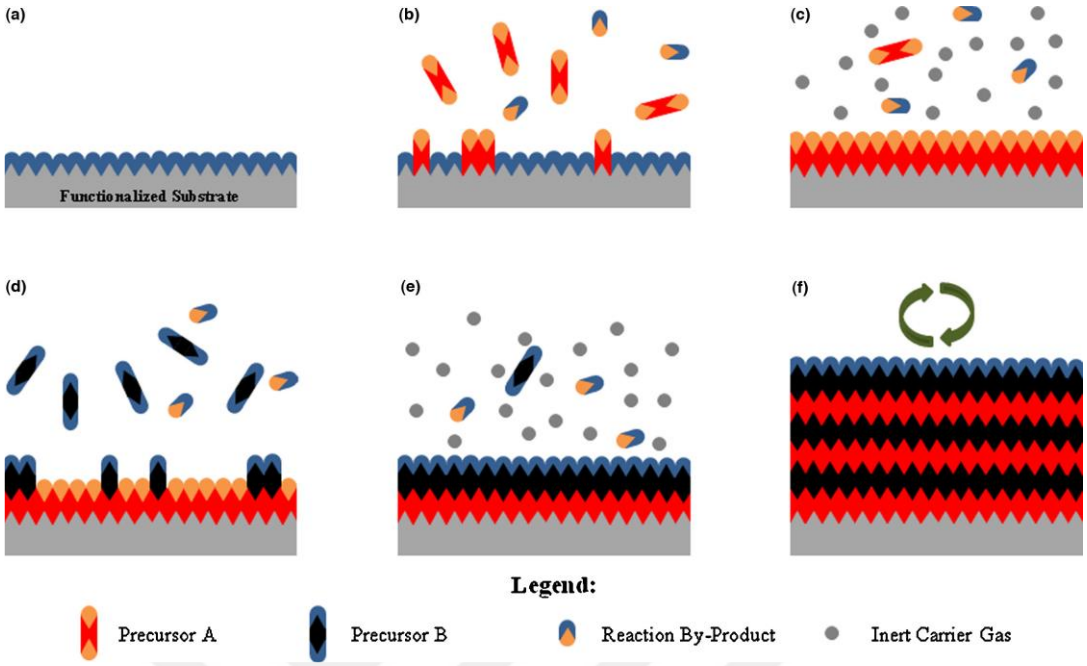

Figure 2-5 *Schematic of ALD process. a) Substrate. b) Precursor A is pulsed c) Excess precursors are purged d) Precursor B is pulsed e) Excess precursor are purged. f) Steps 2–5 are repeated [71].*

1.1.1.5 Chemical Vapor Deposition (CVD)

Chemical vapor deposition (CVD) is a widely used technique to grow monolayer TMDCs such as $MoSe_2$, MoS_2. CVD system is facile, cheap, maintenance friendly and user friendly (Figure 2-6). Chemical vapor deposition is the deposition of reacted and vaporized solid precursors in the heated medium [27]. Carrier gases with distinct flow rate carry vaporized precursors through substrate to produce monolayer structures. With CVD it is possible to produce most metals and non-metallic elements [26, 72]. This technology is an important factor in mass-production of semiconductor and in optoelectronic applications [34, 73]. CVD system is user friendly and cost effective comparing other techniques such as evaporation, sputtering, molecular beam epitaxy, and ion plating, CVD [74-79]. The CVD has water-cooling system is placed between quartz walls [72, 78-80].

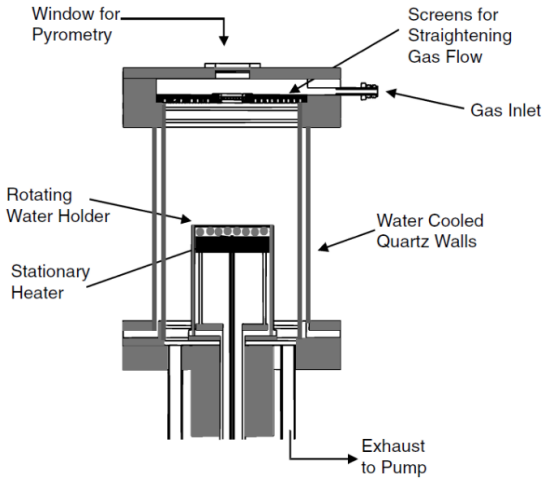

Figure 2-6 *CVD system scheme [80]*

2.3. TMDC Device Applications

2.3.1. Field-effect transistors (FETs)

Two-dimensional TMDCs have widely studied in many scientific groups due to electronic and optical properties such as high mobility and high photosensitivity [81, 82]. These TDMCs have important potential as candidates for new devices in optoelectronics, semiconductor electronics, photodetectors, photovoltaics and energy harvesting (Table 2-1) [2, 38, 81, 83]. Graphene is widely studied two dimensional material. It has high carrier mobility (about 2*10^5 cm^2 V^{-1}) with zero band gap. Monolayer MoS_2, $MoS_{2(1-x)}$-Se_{2x}, $MoSe_2$ structures have direct band gap and high mobility thus: they are new candidates for device applications field-effect transistors (FETs). Configuration of MoS_2 FET device is shown in Figure 2-7 [83, 84].

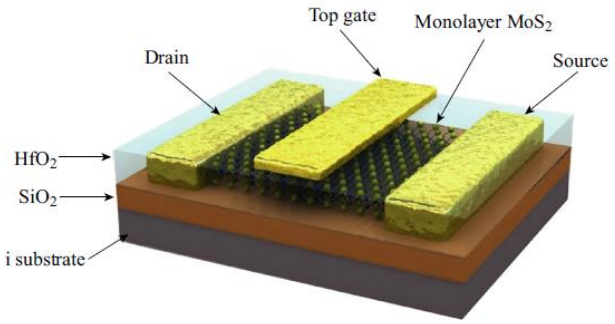

Figure 2-7 *Configuration of MoS_2 FET device [84]*

Table 2-1 *2D materials family [84]*

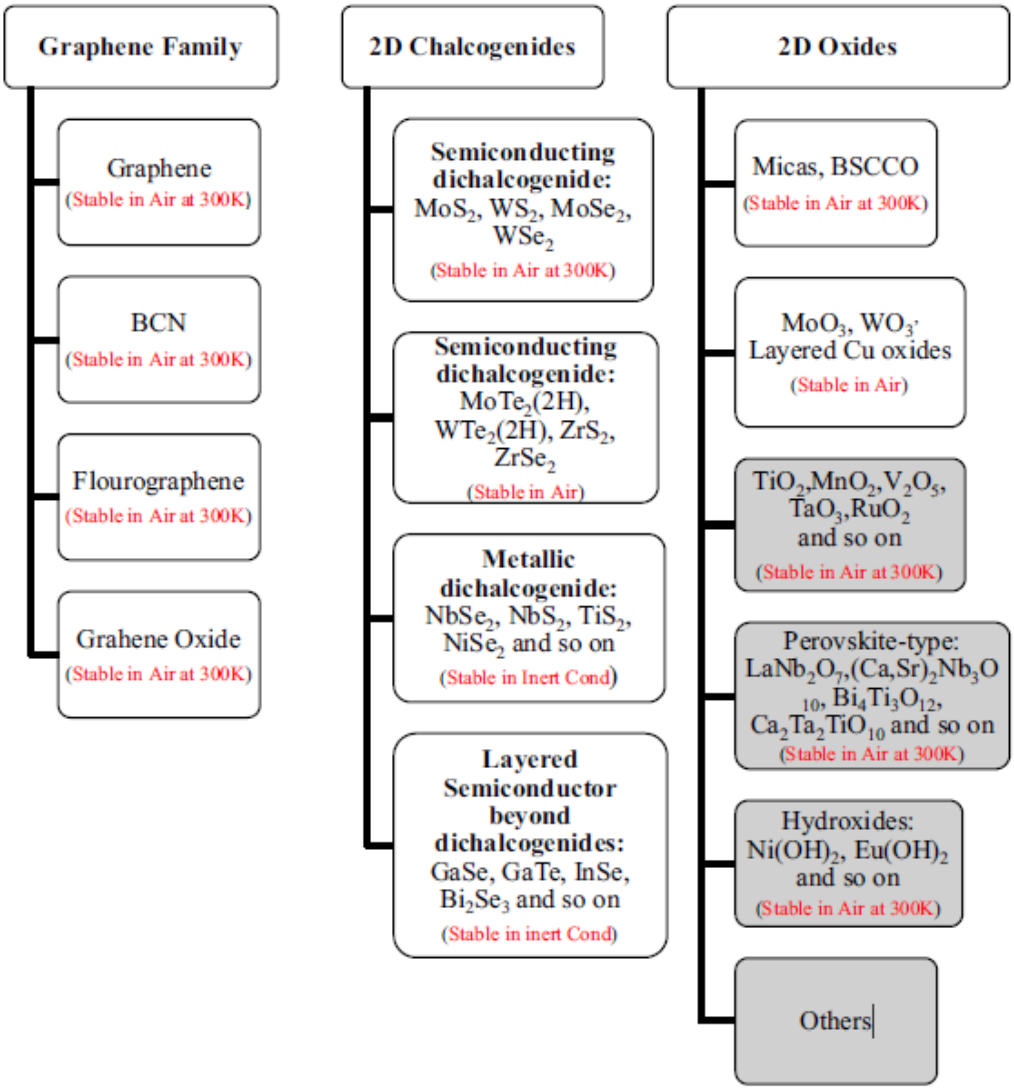

2.3.2. Photodetectors

TMDCs based photodetectors have widely studied in many scientific groups due to optical properties such as high photosensitivity [46, 51, 85]. Photo-detector devices, which are produced from TMDCs, are widely used in electronic applications it is simply converting light in to electrical signal by using absorbed light [86]. There are three steps of photo detecting processes, the first one is carrier generation, the second one is carrier transport and the third one is extraction of carrier [86]. Simple model of photo detector and performance measurements are shown in Figure 2-8.

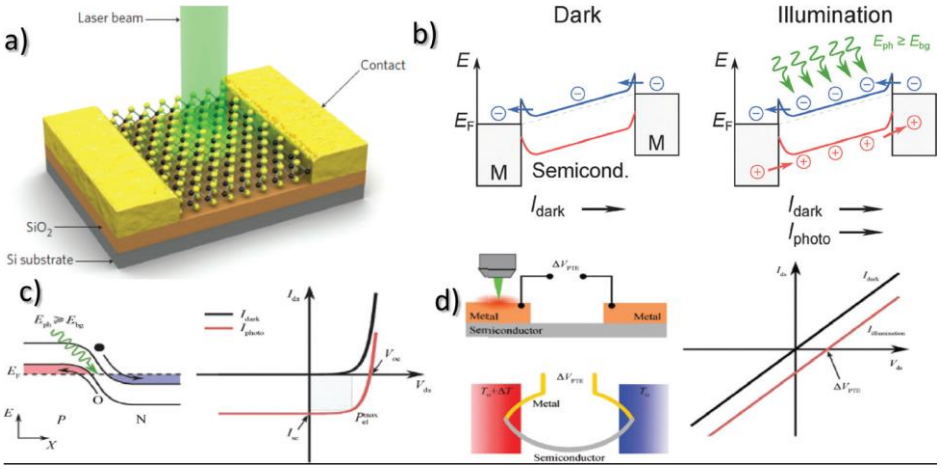

Figure 2-8 *(a) Structure of photodetector. (b) Photoconductive effect (c) Photovoltaic effect (d) Photo-thermoelectric effect [86]*

2.3.3. Energy storage

2DTMDCs have widely studied in many scientific groups due to energy storage capacity Li-ion batteries (LIBs) are rising for the usage in energy storage systems [4, 87, 88]. Producing and performance measurement of energy storage device are shown in Figure 2-9.

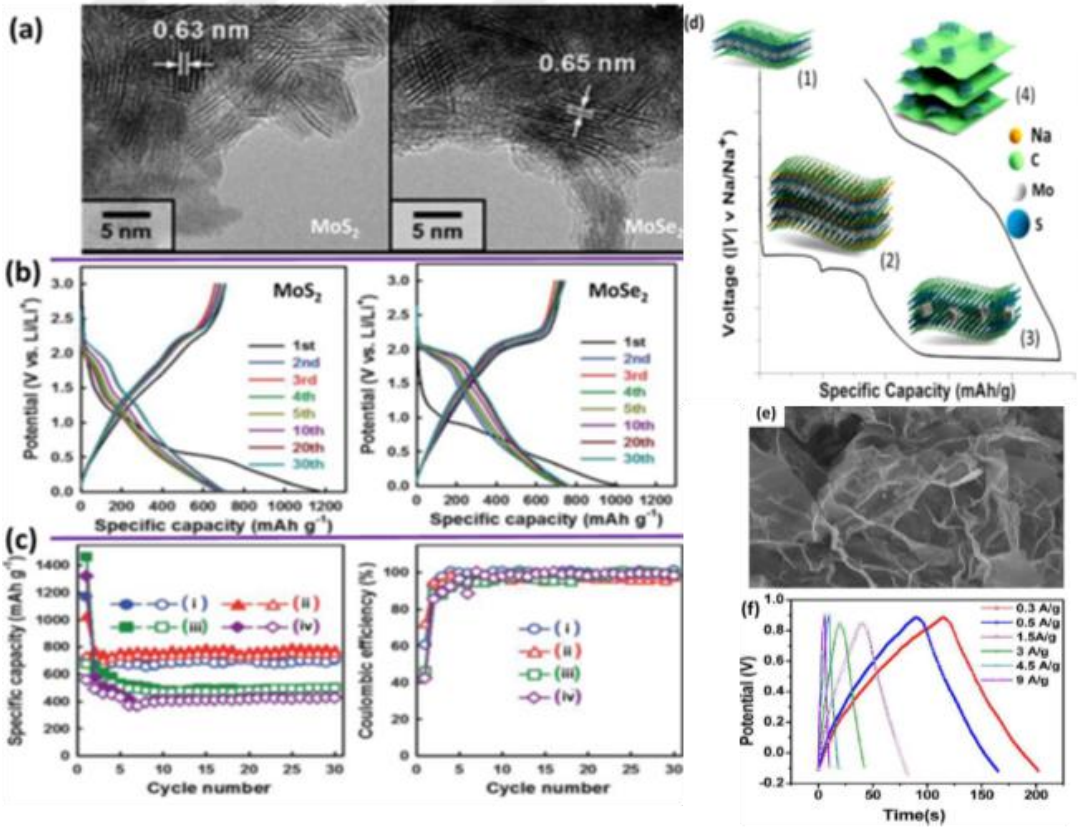

Figure 2-9 *a) HR-TEM images and b) discharge-charge profiles TMDCs c) Cycling performance d) Acid-exfoliated few-layer MoS_2 flakes e) Low-magnification FESEM image f) Charge-discharge curves [86]*

2.4. Characterizations

2DTMDCs, namely molybdenum sulphide (MoS_2), molybdenum sulphoselenide ($MoS_{2(1-x)}$-Se_{2x} (x=0-1)), and molybdenum selenide ($MoSe_2$), are characterized by characterization techniques such as, Confocal Raman, Photoluminescence spectroscopies, Bright field and Dark field microcopies, Atomic force microcopy (AFM), Scanning electron microscopy (SEM), Transmission Electron Microscope (TEM). These techniques are explained briefly.

2.4.1. Confocal Raman and Photoluminescence Spectroscopies

Confocal Raman spectroscopy is used to investigate the monolayer structure of produced flakes, Raman spectroscopy measurements excited by 532 nm continuous laser. There are two distinctive Raman peaks of MoS_2; in plane 380 cm^{-1} (E^1_{2g}) and out of plane vibration of S atoms 400 cm^{-1} (A^1_g) and there is a distinctive Raman peak of $MoSe_2$; out of plane vibration of Se atoms 238 cm^{-1} (A^1_g) reveal produced structures are monolayer. [29, 55, 89-91]. Bright field and Dark field microcopies shows the boundaries, surface coverage, cleanness of the surface, size distribution of the produced flakes. 10x, 20x, 50x, and 100x lenses are used to observe surface of TCMDs.

There are two scatterings, first one is inelastic scatterings and the second one is elastic scattering. When there is elastic scattering, photon energy does not change. However, elastic scattering cause change in photon energy [89].

The elastic scattering takes place without change in photon energy; whereas the inelastic scattering take place with change in photon energy [89, 92]. In Rayleigh scattering. The light scattered having same wavelength and frequency. In Raman scattering, light scatters partially inelastic because there is a change in frequency and energy. We use Raman scattering to analyze the monolayer TMDCs structures. In Stokes Raman scattering, molecules of TMCDs gain energy from incident light. In anti-Stokes Raman scattering, molecules of TMCDs loss energy from incident light. There is a strong fluorescent background of Raman signal (Figure 2-11).

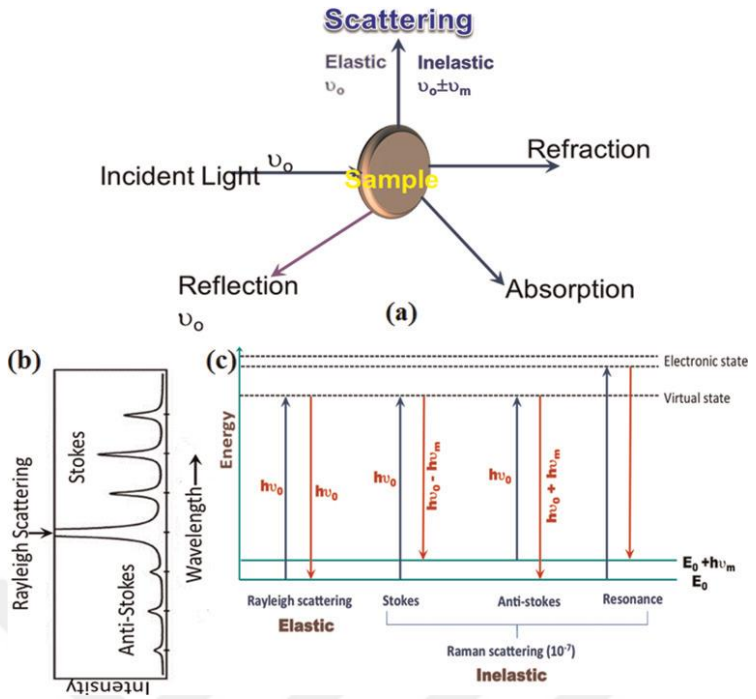

Figure 2-10 *(a) Scattering mechanism (b) spectrum shows Raman (stokes and anti-stokes) and Rayleigh scattering components (c) energy transitions for Rayleigh and Raman scattering [89]*

2.4.2. Photoluminescence spectroscopy

Photoluminescence spectroscopy isused to investigate the monolayer structure of produced flakes, PL spectroscopy measurements excited by 532 nm continuous laser. Photoluminescence spectra of monolayer MoS_2 has a Gaussian peak at 680 nm and for monolayer, $MoSe_2$ has a Gaussian peak at 810 nm. There is a strong fluorescent background of Raman signal (Figure 2-11). To analyze monolayer formation, Raman spectrometer can be used for performing laser-excited PL [89-92]. Luminescence occurs when some form of energy excites solids and energy is released in the form of photons. When solid is excited by short-wavelength light (usually UV radiation), the phenomenon is known as photoluminescence. There are two kind of photoluminescence first one is intrinsic luminescence and the second one is extrinsic luminescence. Intrinsic luminescence comes from crystal structure of TMDCs.

- Band-to-Band Luminescence: Recombination of an e^- in the conduction band (CB) with h^+ in the valence band (VB).
- Cross-luminescence: e^- in (CB) recombines with h^+ created in the outermost core band.
- Exciton Luminescence: Recombination of e^- ^{and} h^+ due to exciton that moves through the crystal.

Extrinsic Luminescence is incorporation defects into a phosphor and in ionic crystals and semiconductors [93].

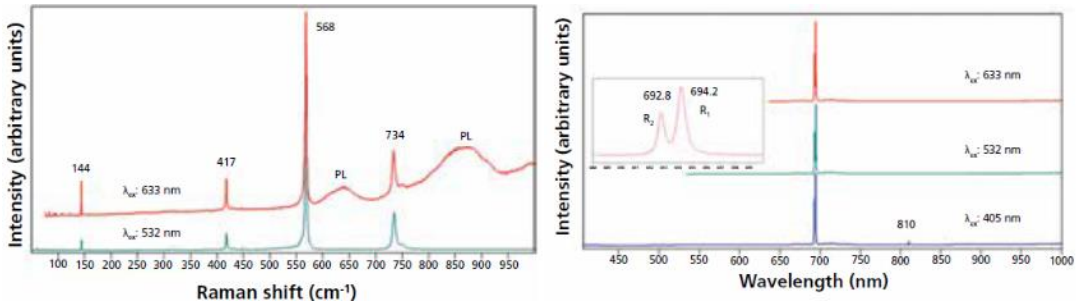

Figure 2-11 *Raman spectra of Al_2O_3 [89]*

2.4.3. Atomic force microcopy (AFM)

Atomic force microscopy (AFM) is a versatile method for surface characterization of two-dimensional TMDCs materials. AFM can have three usage modes. First one is contact mode in which the needle touches to the surface. Second one is non-contact mode and third one is tapping mode (Figure 2-12). Atomic force microcopy (AFM) is used to measure the thickness of produced flakes and observe the surface of the flake. A monolayer flake has a thickness about 0.70 nm [43]. Thickness measurement is taken in contact mode and HeNe laser is used in AFM system [71].

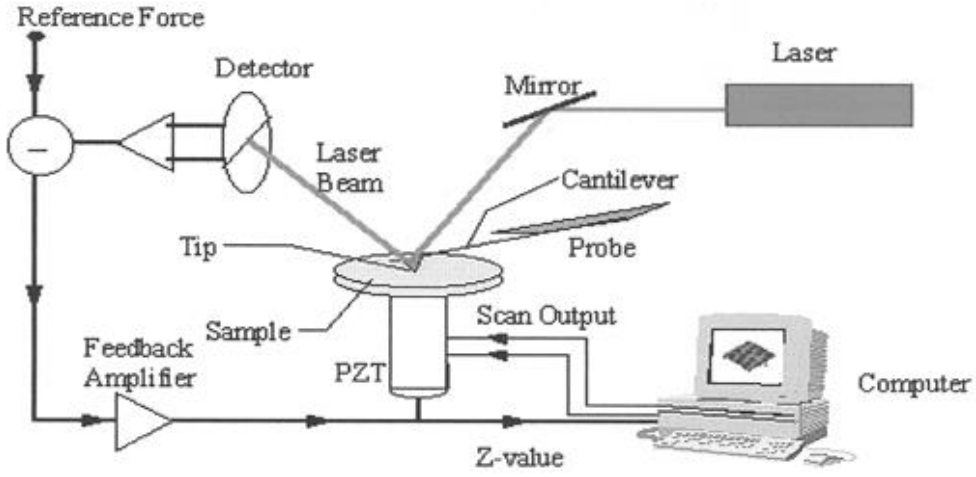

Figure 2-12 *AFM scheme* [71]

2.4.4. Scanning electron microscopy (SEM)

Scanning electron microscopy (SEM) is an important method for surface and morphology characterization of two-dimensional TMDCs materials Figure 2-16 [94]. SEM image of MoS_2 flake is shown in Figure 2-17 a.

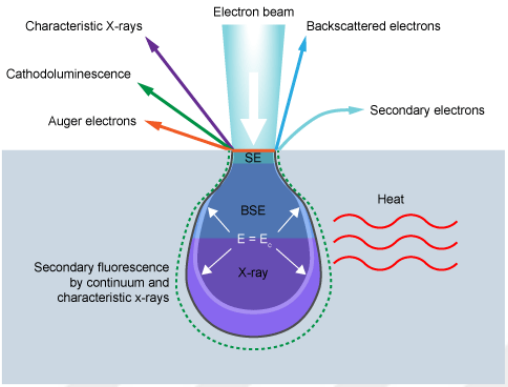

Figure 2-13 *Scattering circled in purple is elastic, scattering circled in orange is Inelastic[95]*

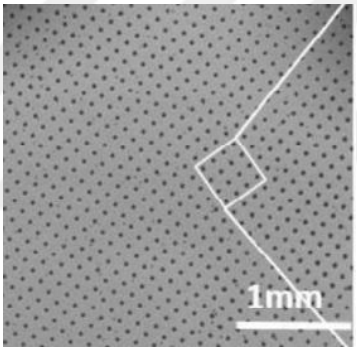

Figure 2-14 *SEM image of monolayer MoS_2 flake [96]*

2.4.5. Transmission electron microscope (TEM)

Transmission electron microscope (TEM) is a facile method for surface and morphology characterization of two-dimensional TMDCs materials [97]. It is used to reveal sub-micrometer, internal fine structure of TMDCs Figure 2-15 [97]. There are four parameters of TEM characterization: the resolving power of the microscope, the thickness of the specimen, the composition of the specimen, the stability of the specimen. There are two scatterings, first one is inelastic scatterings and the second one is elastic scattering. When there is elastic scattering, photon energy does not change. However, elastic scattering cause change in photon energy [97].

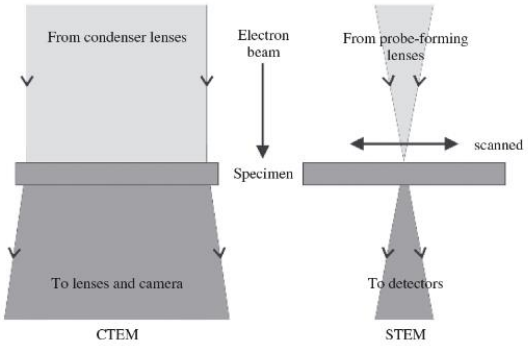

Figure 2-15 *The electron beam in CTEM and STEM systems* [97].

3. CHEMICAL VAPOR DEPOSITION TECHNIQUE

In the Chapter 3, definition of chemical vapor deposition (CVD) technique, CVD equipment's and the experiments having different parameters such as cleaning procedures, amount of precursors, carrier gases and flow rate, reaction temperature and period, pressure distance and locations of precursors and substrates, substrates are explained.

3.1. Definition Chemical Vapor Deposition Technique

CVD is the deposition of reacted and vaporized solid precursors in the heated medium [27]. Carrier gases with distinct flow rate carry vaporized precursors through substrate to produce monolayer structures. CVD is facile process for producing monolayer flakes. With CVD it is possible to produce most metals and non-metallic elements [26, 72]. This CVD technology is important factor in producing semiconductor and in optoelectronic applications [34, 73]. CVD system is user friendly and cost effective comparing other techniques such as evaporation, sputtering, molecular beam epitaxy, and ion plating, CVD [27].

3.2. Our Chemical Vapor Deposition System

The usage of CVD method has grown rapidly in the last decade and this prominent method is widely used in many areas and different applications such as optoelectronics, semiconductors, fast photodetectors, and many other applications [32, 98, 99]. The approximated production market for CVD was 3 billion dollars, soon after the market has been rapidly increasing to approximately 30 billions of dollars [26, 100, 101]. The promising improvements of the technology and the growth of the market are predicted to progress in near future.

CVD method is popular because it is simple and flexible technology, which is appropriate for large range of materials. The coating performance of the CVD system is adequate to have large and smooth coated materials [53, 98].

CVD system has many parameters such as reaction temperature, flow rates of the carrier gases, quantity of powders, location of the chemical powders, substrates, etc.[28, 55, 102]. These parameters should be carefully optimized and every experiment has

unique recipe which is only one parameter changed otherwise it is cannot exactly known which parameter is effect and how its effect. The basic system schemes for monolayer $MoS_{2(1-x)}Se_{2(x)}$, MoS_2, $MoSe_2$ flakes are shown in the Figure 3-1 and Figure 3.2.

Different CVD configurations are tried for optimization of the CVD parameters, such as face up con figuration and facedown configuration [55, 101]. In the face down configuration the 300 nm SiO_2 coated side of the silicon substrate is face down where the monolayer flakes is produced. However, CVD production results have poor coverage and small size in one side of the flakes. CVD general scheme for producing monolayer $MoS_{2(1-x)}Se_{2(x)}$, MoS_2, $MoSe_2$ flakes facedown configuration is shown in Figure 3.1

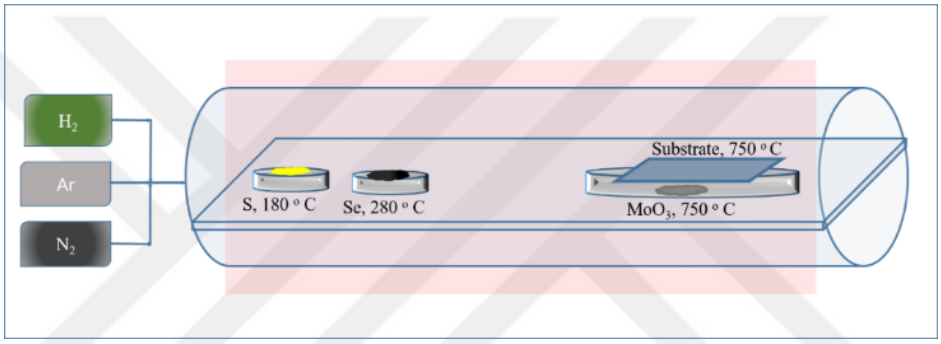

Figure 3-1 *Chemical vapor deposition (CVD) general scheme for producing monolayer $MoS_{2(1-x)}Se_{2(x)}$, MoS_2, $MoSe_2$ flakes facedown configuration*

Producing monolayer $MoS_{2(1-x)}Se_{2(x)}$, MoS_2, $MoSe_2$ flakes with face up configuration has many advantages such as, larger flakes, high coverage, and smoother surface. In the face up configuration the 300 nm SiO_2 coated side of the silicon substrate is face up where the monolayer flakes is produced. CVD production results have good coverage and large size in one side of the flakes up to 150 micrometers in one side of the flakes. The general scheme of ourCVD for producing monolayer $MoS_{2(1-x)}Se_{2(x)}$, MoS_2, $MoSe_2$ flakes face up configuration is shown in Figure 3.1a. Illustration at the close range of face up configuration is shown in Figure 3-2 b.

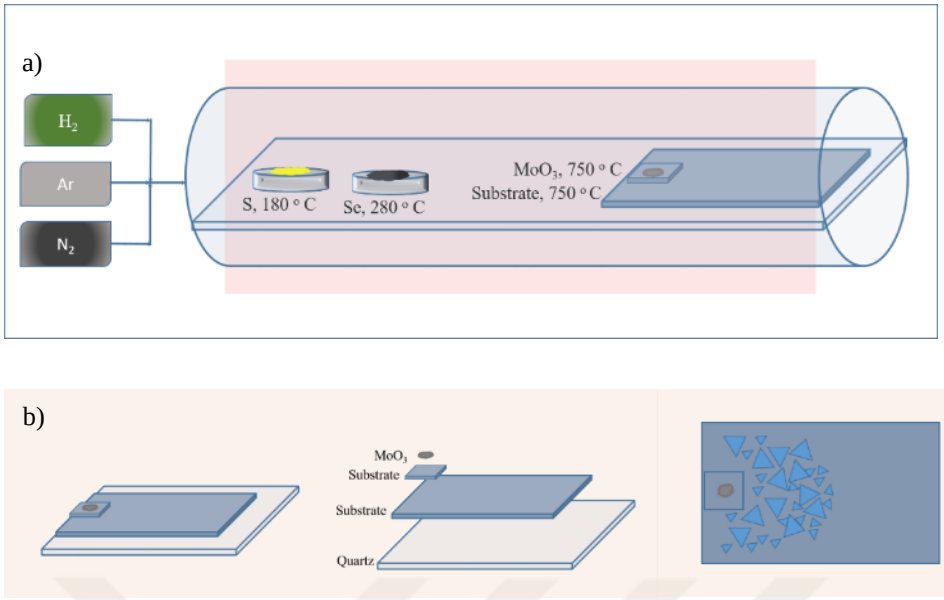

Figure 3-2 a) *Chemical vapor deposition (CVD) general scheme for producing monolayer* $MoS_{2(1-x)}Se_{2(x)}$, MoS_2, $MoSe_2$ *flakes face up configuration b) 300 nm* SiO_2 *coated Si substrate configuration and* $MoS_{2(1-x)}Se_{2(x)}$ *flake location on silicon substrate*

3.2.1. CVD system equipment

Our CVD system has different components such as, 2 zoned furnace, quartz tube, quartz holders, cold trapper, vacuum controller, vacuum valve, vacuum pump, precursor gas line, ventilation system, gas proof flanges, connectors, rubber gaskets etc.

The furnace has two heating zones separated by isolator material, which can be used for two different temperatures concurrently. In addition, the furnace can be heated up to 1250 ^oC with temperature rate 1-25 ^oC/min. There are five heating programs for each zone. It is movable in left and right directions. If the cover of the furnace is accidentally opened or manually opened, the heating system of the furnace automatically is closed for safety conditions (Figure 3-3).

Figure 3-3 *Chemical vapor deposition system two heat zoned furnace*

Quartz materials are non-reactant materials and it is easy to clean them from chemical residues and cylindrical shape of tube is advantageous because, CVD reactions have, carrying gas, vapor phase of precursor such as sulphur (S), selenium (Se), molybdenum (Mo). Melting point of the quartz materials is 1785 ºC, it makes possible to have CVD reactions until its melting point. Quartz tube (70 mm diameter) should have minimum 3 mm thickness due to possible breakage and cracking of the quartz tube (Figure 3-4). Quartz tube can be 80 mm, 70 mm, and 25.4 mm (1 inch) diameters. When diameter size is changes, CVD parameters can be changes due to flow rate and CVD reactions. Quartz holders (plate, boat and pot) are important pieces because, precursors and substrates and placed on them. All of them have 3 mm thickness to prevent from possible breakage and cracking conditions. One of them is quartz plate, rectangular shape 60 mm * 300 mm, it is designed to have a flat area for precursors and substrate in cylindrical quartz tube. The other holder is a pot, selenium (Se), sulphur (S) precursors are put in it (Figure 3-4).

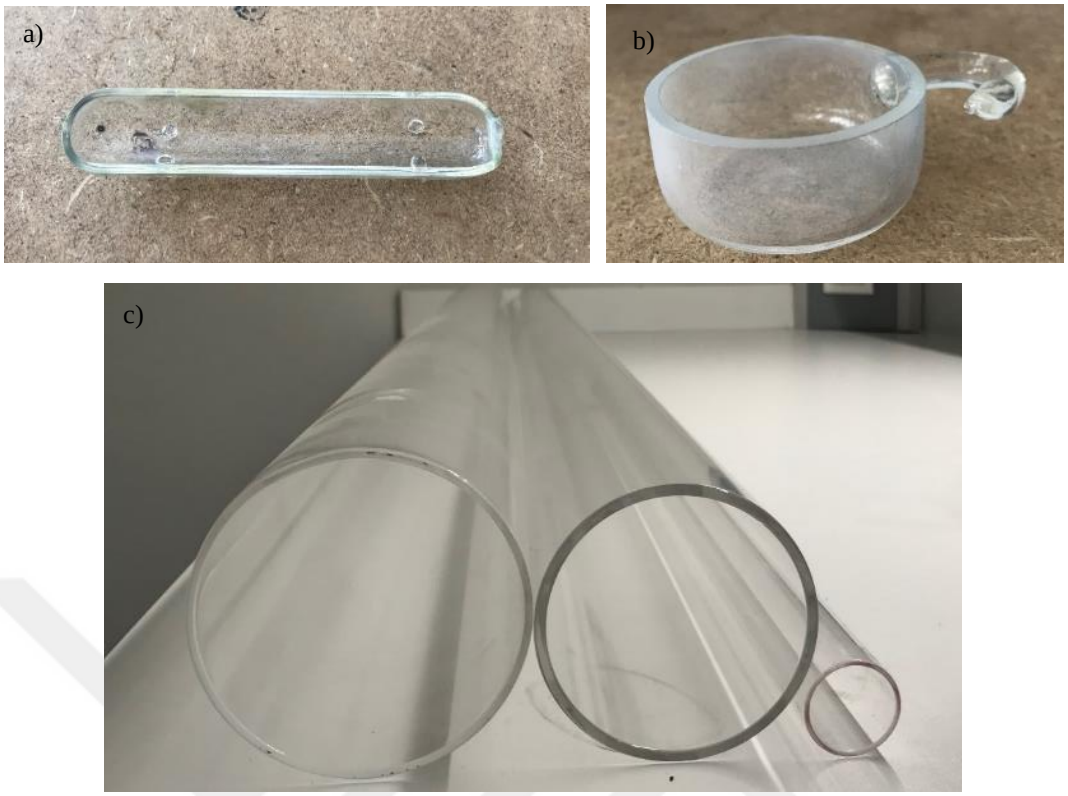

Figure 3-4 *a) Quartz boat b) Quartz pot c) Quartz tubes (80 mm, 70 mm, 25mm)*

Cold trapper is placed between pressure controller and vacuum valve; it prevents the vacuum system by cooling vaporized residues, the temperature of cold trapper is adjustable between 24 ^{o}C and -50 ^{o}C (Figure 3-5).

Figure 3-5 *Cold trapper*

The pressure can be stabilized to the value by vacuum system that includes a display, vacuum pump, vacuum valve, and vacuum controller. Desired pressure data entry is chosen on display. When the pressure is higher than the value, Vacuum controller sends a feedback to open the valve, until the pressure is decreased down to the desired pressure level (Figure 3-6 and Figure 3-7).

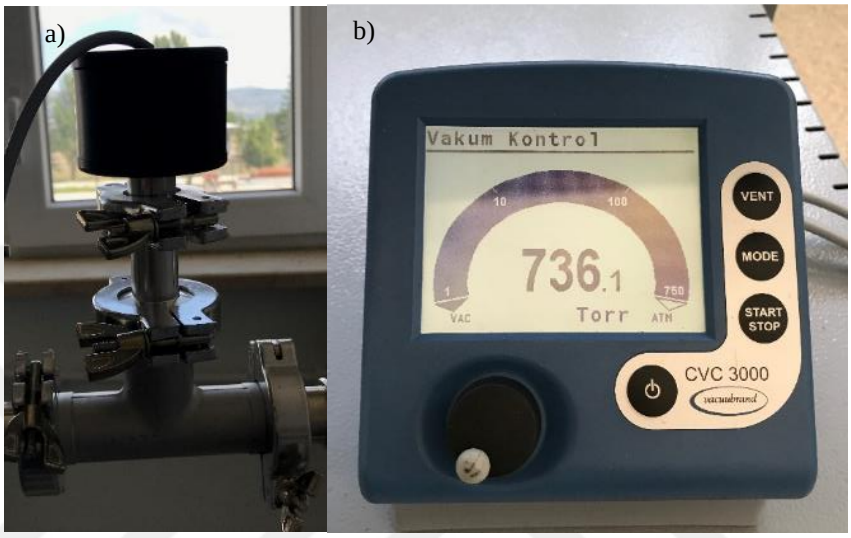

Figure 3-6 *a) Vacuum controller b) Vacuum control system monitor*

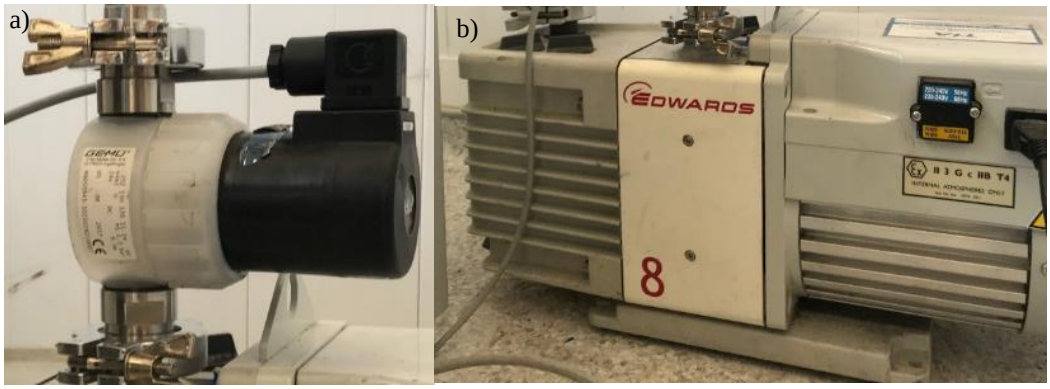

Figure 3-7 *a) Vacuum valve b) Vacuum pump*

Precursor gas line has three inlets for three kinds of gases; argon (Ar), nitrogen (N_2), and hydrogen (H_2) gases, they can be used at the same time with gas outlet up to 500 sccm. The carrier gases are used for carrying the vaporized precursor powders to produce monolayer flakes (Figure 3-8).

Figure 3-8 *Carrier gases line (argon (Ar), hydrogen (H_2), nitrogen (N_2)).*

Ventilation system is important because, opening gas proof flanges, there are vaporized residues in the laboratory, and this is dangerous for human health. The ventilation system should be worked, until all CVD processes are finished (Figure3-9). In our laboratory, there are three CVD system, each have one ventilation system, and there is bench ventilation system. According to on/off condition, these ventilation systems can effect monolayer growth in reaction period due to reverse/fore airflow. In Figure 3-10, on/off conditions of ventilation systems are shown. When ventilation of CVD1 is off and other ventilation systems are off, there is a reverse air flow adversely effects the growth, because this flow cools the quartz tube in which CVD reactions take place (Figure 3-10 a). Experiments with this ventilation conditions are unsuccessful. When ventilation of CVD1 is on and other ventilation systems are on, there is a fore air flow adversely effects the growth, because this flow cools the quartz tube in which CVD reactions take place (Figure 3-10 b). Experiments with this ventilation conditions are unsuccessful. When ventilation of CVD1 and other ventilation systems are off, there is a stable air ventilation conditions. Experiments with this ventilation conditions are successful. The size of produced monolayer flakes are up to 80 μm.

Figure 3-9 *Ventilation System*

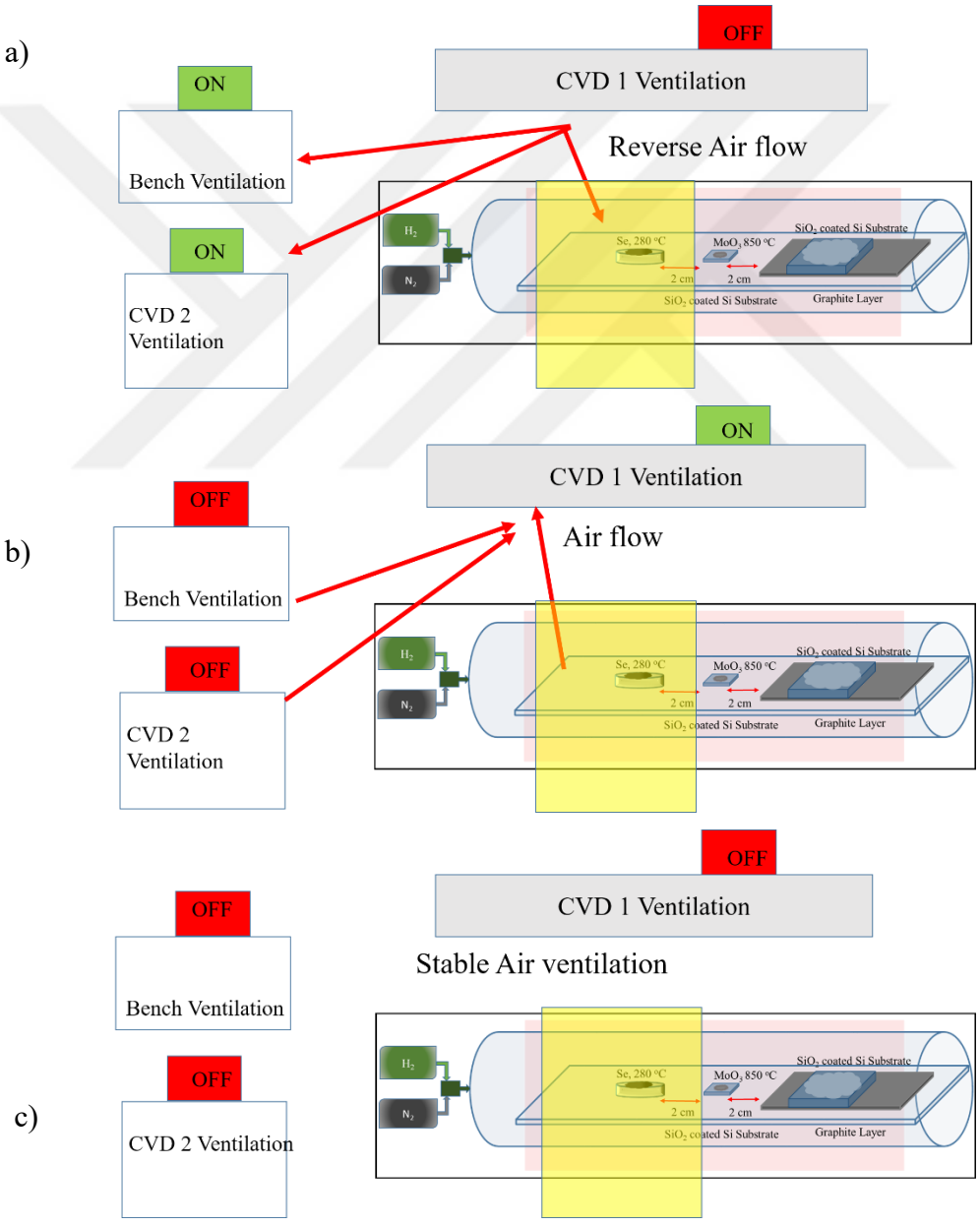

Figure 3-10 *a), b), b) Ventilation system on/off conditions*

We design gas proof flanges is made up of stainless steel, it has cooling channels to prevent from high temperature, and surface of the flanges should be cleaned carefully before every experiment shown in Figure 3-11.

Figure 3-11 *Images of gas proof steel flanges*

Clamp segments and rubber gaskets are connectors of any two part of the CVD system; they should be fitted appropriately in the system to avoid possible gas leakage (Figure 3-12).

Figure 3-12 *Rubber gaskets*

3.3. CVD Parameters

There are various critical parameters such as pressure, location of the powders and substrates, reaction time, reaction temperature, temperature increase rate, flow rates of the carrier gases, quantity of chemical powders, location of the substrates, kind of substrates, etc.[28, 38, 55, 102, 103]. The amount of the powders are the most important parameters such as, 0.1 mg for molybdenum (Mo), 20 - 120 mg for sulphur (S), 20 - 600 mg selenium (Se), to control the surface reaction kinetics. Carrier gases such as argon (Ar), nitrogen (N_2), and hydrogen (H_2) are used to carry the vaporized molecules of the precursor powders such as, molybdenum (Mo), sulphur (S), selenium (Se) [32, 44]. Gas flow rates are varying between 400 sccm and 0 sccm for nitrogen (N_2), 50 sccm and 100 sccm for argon (Ar), 5 sccm and 50 sccm for hydrogen (H_2) [53, 55]. The reaction temperature varies between 650 ^oC and 900 ^oC for 2D materials $MoS_{2(1-x)}Se_{2(x)}$, MoS_2, $MoSe_2$ [102]. The reaction period is depending on the molar weight of the powders [30, 31]. The pressure plays key role in surface reactions of CVD; ambient pressure is the most common. Whatever the pressure is, the critical key is having constant pressure and the controlled pressure for repeatable results [98]. The substrates can be located face up and face down [55, 101]. TDMCs are produced on a substrate, 300 nm SiO2 coated Si substrate is the most common substrate, it is advantageous such as cheapness and abundant, 300nm SiO_2 coated by thermal etching at 1200 ^oC [28, 37].

3.3.1. Cleaning procedures

One of the most critical parameter of CVD method is cleanness of the system. Cleaning procedures should be applied carefully because it is hard to produce homogeneous and large two-dimensional materials. Impurities of system and unclean substrate etc. adversely affect production of monolayer MoS_2, $MoSe_2$, $MoS_{2(1-x)}Se_{2(x)}$ [30]. Before starting an experiment, the CVD system should be cleaned perfectly. Cleaning process takes place at 1000 ^oC for 60 minutes with is 500-sccm flow rate of nitrogen gas to clean impurities and residues of the last experiment, which are, coated inside of the quartz tube and quartz holders. The furnace of CVD system is movable in left and right directions and the furnace is positioned on far left end of quartz tube because the entry of the carrier gases is in the left. Before starting cleaning process quartz holders are put in quartz tube. When the temperature of the furnace is reached at 1000 ^oC with maximum temperature rate (25 ^oC/min), the furnace is shifted 20 cm to the right end of the quartz

tube for every 10 minutes. Shifting of the furnace should be done slowly, otherwise residues in vapor phase can move reverse direction, through which cleaned part of the tube due to rapid change in temperature. After that, by opening the cover of the furnace, it is cooled naturally until the temperature is about room temperature. The gas proof flanges are connected both left and right ends, the residues of the last experiment, should be removed by using acetone and sterile fabric. In the CVD system, there are 8 rubber gaskets which are connect the CVD equipment, for example one of them connect gas inlet and flange, if there is a residue or impurity, there can be gas leakage from rubber gasket, gas leakage affects CVD reactions negatively. To prevent from gas leakage, rubber gaskets should be cleaned carefully by using acetone and sterile fabric. We should wear laboratory gloves and laboratory coat and mask in all CVD cleaning process. In case of tearing of the gloves or mask, it should be changed with the new ones because, breathing of or touching to these residues of the chemicals can be dangerous for human health. In addition, we can contaminate the system by touching without gloves and breathing without mask, which can disturb CVD reactions and the experiments can be unsuccessful eventually. Cleanness and preparation of the chemicals quartz holders, substrates, tweezers, spatulas etc. are critically important. 300 nm coated SiO_2 silicon substrate should be is cut carefully and cleaned by distilled water, acetone, and isopropanol (5 minutes for each step) in sonication device. After that, the substrate is purged with nitrogen gas to remove residues.

3.3.2. Amount of precursors

To control by surface reaction kinetics, the amount of the powders are the most important parameters such as, 0.1 mg for molybdenum (Mo), 100-300 mg for sulphur (S), 400-600 mg selenium (Se), the amounts of the powders are changing according to other reaction parameters like temperature, flow rates of the carrier gases, diameter of the quartz tube [26-28]. To produce $MoS_{2(1-x)}Se_{2(x)}$, MoS_2, $MoSe_2$, every TDMC has different amount of powder in CVD reactions. For instance, MoS_2, $MoSe_2$ are straight forward we use 300 sulphur (S) and 600 mg selenium (Se) but $MoS_{2(1-x)}Se_{2(x)}$ (x=0-1) is little complicated because there is x value (x=0-1). When the x value is equal to 1, $MoSe_2$ is produced. When the x value is equal to 0, MoS_2 is produced. Any value between 0 and 1, $MoS_{2(1-x)}Se_{2(x)}$ alloy is produced by changing amount of selenium (Se) and sulphur (S) powders. The amount of molybdenum (Mo) powder (0.1 mg) is always limiter of the

CVD reactions, to produce monolayer $MoS_{2(1-x)}Se_{2(x)}$, MoS_2, $MoSe_2$ flakes; molybdenum powder has to be very little. Otherwise, multilayer and bulk structures can be produced [29].

3.3.3. Carrier gases and gas flow rate

Carrier gases such as argon (Ar), nitrogen (N_2), and hydrogen (H_2) are used to carry the vaporized molecules of the precursor powders for instance, molybdenum (Mo), sulphur (S), selenium (Se) [32, 44, 104]. According to the diameter of the quartz tube and reaction temperature, gas flow rates are varying between 0 sccm and 100 sccm for nitrogen (N_2), 0 sccm and 100 sccm for argon (Ar), 5 sccm and 20 sccm for hydrogen (H_2) [53, 55, 105].

3.3.4. CVD reaction temperature and reaction period

For a good recipe the CVD reaction temperature plays a critical role in producing monolayer materials, in fact it depends on the vaporize point and vapor pressure of the powders [98, 106]. When the reaction starts, all powders have to be in vaporized phase, otherwise the powders has inefficient reaction and inadequate quality for monolayer films. The reaction temperature varies between 650 ^oC and 900 ^oC for 2D materials $MoS_{2(1-x)}Se_{2(x)}$, MoS_2, $MoSe_2$ [102]. The reaction period is depending on the molar weight of the powders [30, 31]. A sample route of the CVD reaction temperature is shown in Figure 3-13, optimization of CVD parameters by changing reaction temperature is one of the critical parameters because, it effects the geometry of monolayer $MoS_{2(1-x)}Se_{2(x)}$, MoS_2, $MoSe_2$ [50]. At reaction temperature, S vapor decreases MoO_3 / WO_3 powder to volatile sub oxides to produce MoO_2 and WO_2 and the produced radicals diffuse on the substrate reacting with S (1-2) and (3-4), for MoS_2 and WS_2 [107].

$$MoO_3 + (x/2)\ S \rightarrow MoO_{3-x} + (x/2)\ SO_2 \quad (1)$$

$$MoO_{3-x} + (7-x)/2\ S \rightarrow MoS_2 + (3-x)/2\ SO_2 \quad (2)$$

$$7S + 2WO_3 \rightarrow 2WS_2 + 3SO_2 \quad (3)$$

$$WO_3 + 3S + H_2 \rightarrow WS_2 + SO_2 + H_2O \quad (4)$$

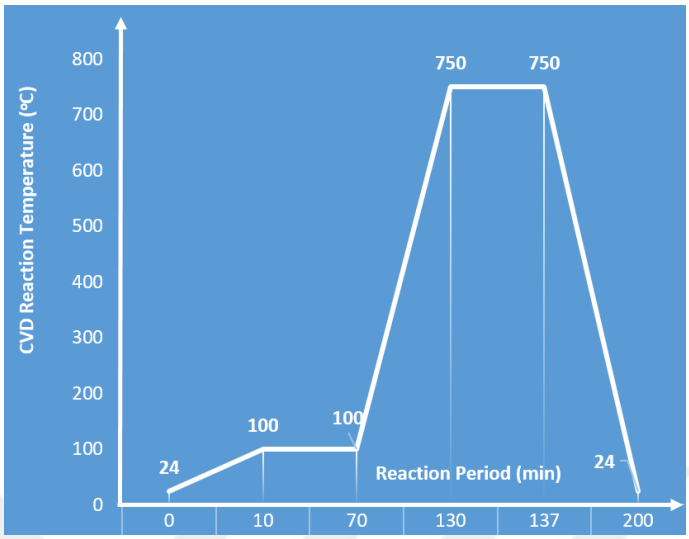

Figure 3-13 *CVD reaction temperature (°C) versus reaction period (min)*

3.3.5. Pressure

The pressure plays key role in surface reactions of, because the vapor of the powders affected by the pressure of the system. It is shown in Figure 3-14, according to phase diagram one can have gas phase under low pressure and at the triple point one powder can be 3 phases; solid, liquid, and gas. Ambient pressure is the most common but substantially under vacuum condition are used in CVD system. Whatever the pressure is, the critical key is having constant pressure and the controlled pressure for repeatable results [51, 98].

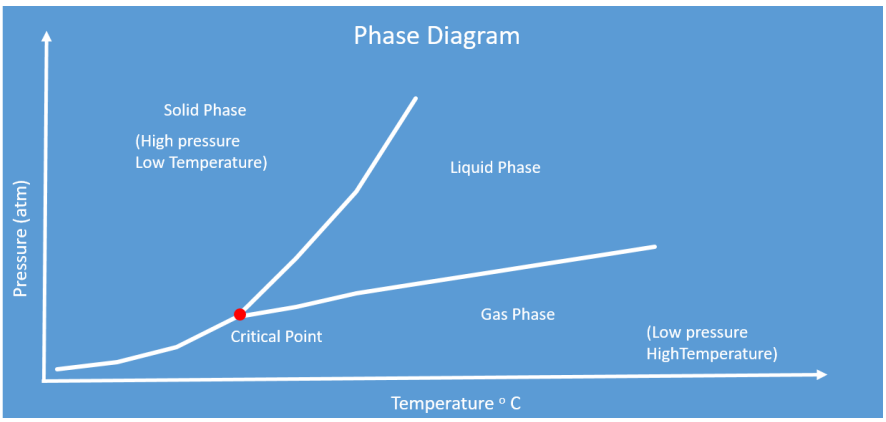

Figure 3-14 *Sample phase diagram*

3.3.6. Locations of precursors and substrates in CVD system

Carrier gases inject in to quartz tube from a noddle. The gas profile is reverse exponential, therefore the distance between powders and substrates are important. In addition, the locations depend on the diameter of the quartz tube. Different CVD configurations are tried for optimization of the CVD parameters, such as face up con figuration and facedown configuration [55, 101]. In the face down configuration the 300 nm SiO_2 coated side of the silicon substrate is face down where the monolayer flakes is produced. However, CVD production results have poor coverage and small size in one side of the flakes Producing monolayer $MoS_{2(1-x)}Se_{2(x)}$, MoS_2, $MoSe_2$ flakes with face up configuration has many advantages such as, larger flakes, high coverage, and smoother surface. In the face up configuration the 300 nm SiO_2 coated side of the silicon substrate is face up where the monolayer flakes is produced. CVD production results have good coverage and large size in one side of the flakes up to 150 micrometers in one side of the flakes.

3.3.7. Substrates

Two-Dimensional TMDCs and monolayer materials produced on a substrate, 300 nm SiO_2 coated Si substrates are used as a substrate. There are also copper, gold, and glass substrates.

Glass substrates have advantages and disadvantages, the most important advantages is produced monolayer $MoS_{2(1-x)}Se_{2(x)}$, MoS_2, $MoSe_2$ flakes have high coverage and large flakes size. However, the produced flakes have to be transferred to the SiO_2 substrate using different steps. Other disadvantage is that the produced monolayer flakes can be in metastable metallic phase 1T $MoS_{2(1-x)}Se_{2(x)}$, 1T MoS_2, 1T $MoSe_2$, 1T is metallic phase that, in a unit cell 3 molybdenum atoms have chemical bonding with selenium or sulphur atoms, there is trimerization and the structure have metallic phase. Super structure of atom is semiconducting with trimerized molybdenum atoms and super structure of atom is metallic with dimerization of molybdenum atoms [41]. Using glass as a substrate is reported to be favorable in CVD reactions, extending the lateral growth of monolayer $MoS_{2(1-x)}Se_{2(x)}$, MoS_2, $MoSe_2$ [3, 4]. However, there are several issues to be clarified regarding the role of a glass substrate in monolayer formation. For example, it is not fully understood whether the glass surface reactions or glass impurities such as Na, Mg, Ca

and etc. function as a catalyzer or supporter to produce homogeneous, large-area and monolayer $MoS_{2(1-x)}Se_{2(x)}$, MoS_2, $MoSe_2$ flakes. NaCl involvement in CVD process enables large area $MoSe_2$ flakes with full substrate coverage, which was not possible with process without any salt [29]. Hence, we confirm that NaCl develops CVD kinetics via reducing strength of interlayer bonds of $MoSe_2$ flakes and enlarges homogeneous, laterally grown monolayer device-quality $MoSe_2$ flakes, which is crucial for practical applications of 2D TMDCs. NaCl supported CVD growth does not need to be transferred because the flakes are produced on SiO2 coated silicon substrate. There are other salt can be used as a catalyzers such as potassium chloride (KCl), potassium iodite (KIO_2), potassium hydroxide (KOH), Copper chloride ($CuCl_2$). Results of using different salts are explained in Chapter 6.

4. INVESTIGATION OF MONOLAYER MOLYBDENUM DISULPHIDE (MoS_2) MONOLAYER FLAKES GROWN BY CVD

4.1. Introduction

In tChapter 4, investigation of monolayer molybdenum disulfide (MoS_2) monolayer flakes grown by CVD is explained and the experimental details, the characterization of the produced monolayer MoS_2 is interpreted.

This work was published in the journal of Nano-Micro Letters (Investigation of Single-Wall MoS_2 Monolayer Flakes Grown by Chemical Vapor Deposition, (2016)) [55].

4.2. Experimental

For the few years single layer molybdenum disulfide (MoS_2) have attracted considerable attention due to their high potential in different device applications including photo detectors, solar batteries, and energy storages, sensors [107-112]. Many scientific groups intensively studied CVD growth of 2D-TMDC molybdenum disulfide (MoS_2) due to its properties such as mobility, direct band gap (1.82 eV) in monolayer form [55, 88, 113-117]. However, controllable CVD growth of monolayer MoS_2 is a still unclear. A systematical investigation of producing monolayer MoS_2 is studied by changing CVD parameters such as, reaction period, reaction temperature. SEM results indicates that monolayer MoS_2 flakes can grow inclined at different angles or flat on the surface due to possible CVD reactions [55, 68]. Reaction periods influences the amount of MoO_3/MoO_2 on the substrate. Surface coverage of the film and the number of produced layers are directly related to the desorption–adsorption of radicals with sulfurization rates and sensitive CVD parameters [57, 118, 119]. Formation of the produced MoS_2 flakes are different from general growth trend of MoS_2 the flakes are heterogeneous with MoS_2 nanowalls. Photoluminescence peak is located around 675 nm [32, 55, 106]. CVD system scheme is shown in Figure 4-1.

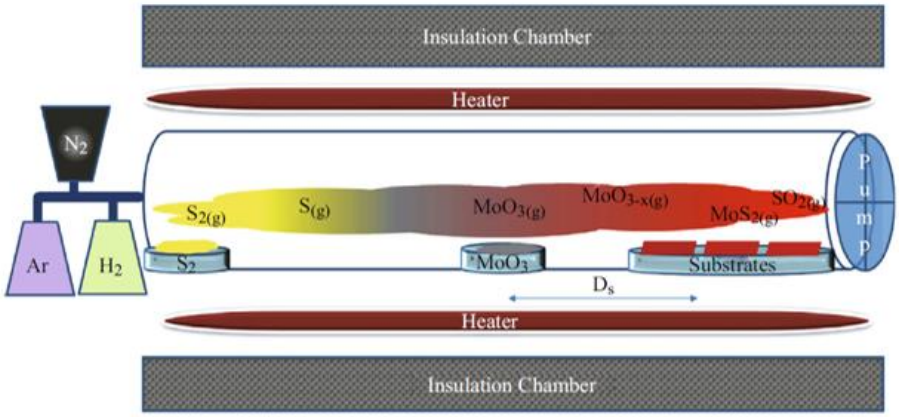

Figure 4-1 *CVD system scheme [55]*

4.3. Results and Discussions

The quartz boats containing MoO_3 (14 mg, 99.9 %, Aldrich) and sulphur (S) precursor (1400 mg, 99.5 %, Alfa) were placed at the temperature zones, 700 ^oC for MoO_3 and 150 ^oC for sulfur[55]. We investigated varying the distance between boats of MoO_3 precursor, (Ds) from 9 cm to 13 cm. 300 nm SiO_2 coated silicon substrates are cleaned using piranha etch solution and the RCA technique [55]. Carrier gases are delivered to CVD chamber with gas flow rates 17 sccm argon (Ar) and 10 sccm hydrogen (H_2) [55]. Reaction periods are 10 minutes, 5 minutes and 3 minutes to observe growth of monolayer MoS_2 structures. After reaction period, fast cooling of the CVD chamber is critical process to finish the CVD reactions. This cooling process is carried out by purging of 500 sccm nitrogen (N_2). Fast cooling process is prevent from multilayer MoS_2 formation on SiO_2 substrate and supports monolayer formation due to distinct reaction periods.

Produced molybdenum disulphide MoS_2 flakes are characterized by Raman spectroscopy, photoluminescence (PL), scanning electron microscopy (SEM), and transmission electron microscopy (TEM) [55]. PL and Raman measurements excited by 532 nm continuous laser. There are two Raman peaks, which are located at 379 cm^{-1} E^1_{2g}, (in-plane mode) and 402 cm^{-1}, A^1_g (out of plane mode). They are fingerprints of monolayer MoS_2 flakes and the peak at 299 cm^{-1}, B^3_g twist mode is a sign of MoO_3 flakes [55]. Photoluminescence measurements give knowledge about multi-layer MoS_2 and monolayer MoS_2 structures. A1 excitation peak of MoS_2 is located at 675 nm; B1 excitation peak of MoS_2 is located at 645 nm [36, 55, 113, 114, 120]. In the CVD configuration, quartz pot, MoO_3 and S as precursors are placed at specific positions, the

distance between MoO_3 and SiO_2 substrate is abbreviated as Ds (Figure 4-1). CVD reaction period is kept constant (10 minutes) and Ds is modified for 10 cm , 11 cm, 12 cm, 13 cm.

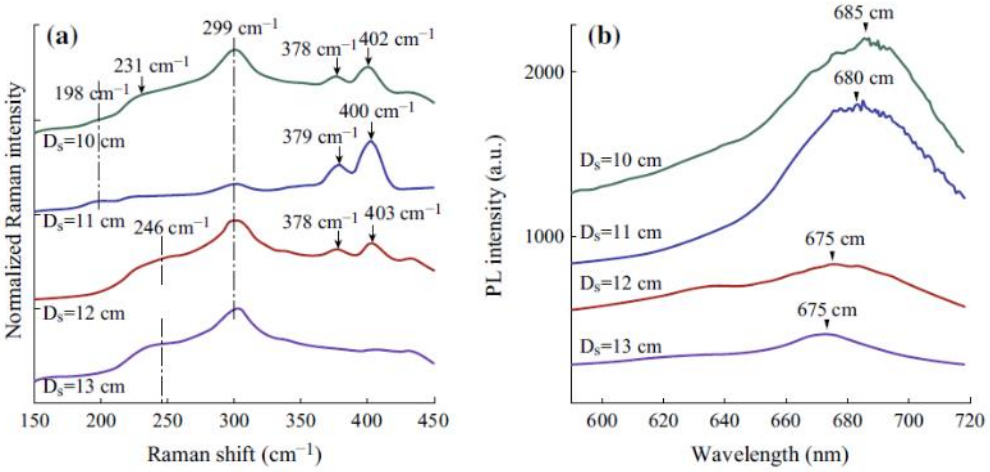

Figure 4-2 *a) Raman scattering spectra and b) PL spectra of MoS_2 the reaction period is 10 minutes [55]*

Raman peak is located at 231 cm^{-1} is observed for D_S = 10 cm, due to possible sign of 1-D MoO_2 nanorods. Raman peak is located at 198 cm^{-1} is explained by the forming of MoO_3 sheets. Surface coverage of produced structures are not homogeneous. Photoluminescence peak is located at 680 nm, which is the sign of monolayer MoS_2 flakes, especially Ds is11 cm, the coverage is more homogeneous (Figure 4-2). The SEM images of the produced MoS_2 with different D_S ($D_{S=}$ 10 cm, 11 cm, 12 cm, 13 cm) are shown in Figure 4-3, SEM measurements give knowledge about surface coverage, boundary of the flakes, homogeneity, size, formation of the structures and shape of the produced MoS_2 flakes [55, 94]. On SiO_2 substrate, nanowalls and nanoribbons are produced which have a high potential to be used in device applications such as, photodetectors and supercapacitors [32, 55].

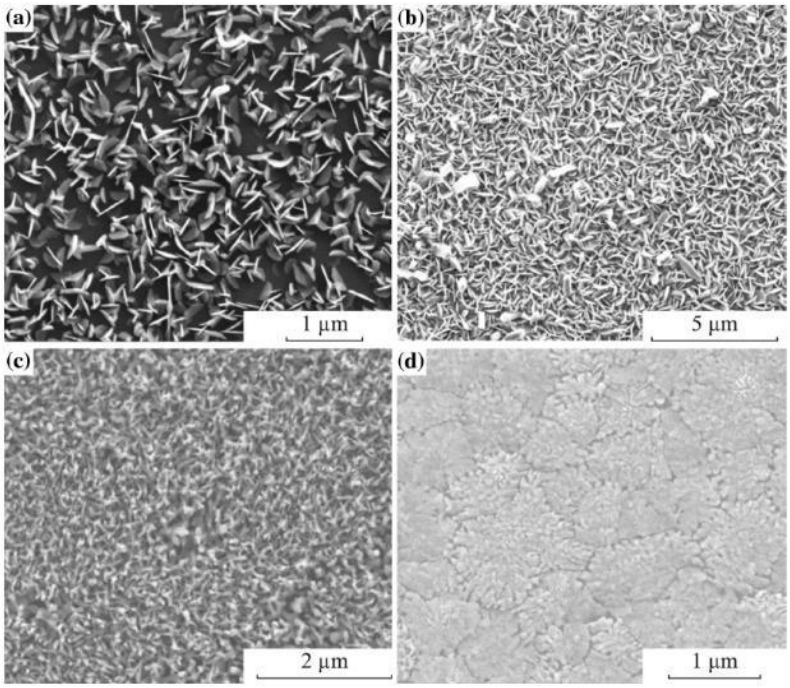

Figure 4-3 *SEM Images for the flakes produced when Ds = a) 10 cm, b) 11 cm, c) 12 cm, and d) 13 cm with a reaction period of 10 minutes [55]*

Surface coverage of the films are not homogeneous. At Ds is 13 cm, the reduced temperature of the SiO_2 substrates effects nanowall formation adversely (Figure 4-3 d). Reaction period and concentration of precursors have important role in producing MoS2 flakes. Therefore, the reaction period is changed to 5 minutes to investigate the effect of the CVD reaction period on $MoSe_2$ flakes. Raman scattering and photoluminescence spectra show that produced flakes are more homogeneous. Raman peak at 299 cm-1 is almost invisible, and the difference in MoS_2 Raman peaks is about 22 cm^{-1}. Important enhancement in the photoluminescence characteristics of produced MoS_2 flakes in 5 minutes (Figure 4-4 b) compared to produce MoS_2 flakes with a reaction period of 10 minutes (Figure 4-3 b). PL spectra shows that there is only one peak at 680 nm with no shoulder peak at 630 nm, which is assign to monolayer MoS_2 [79, 80, 121-125]. Therefore, we successfully produce high quality, homogeneous monolayer MoS_2 flakes at a DS of 11 cm [55, 114].

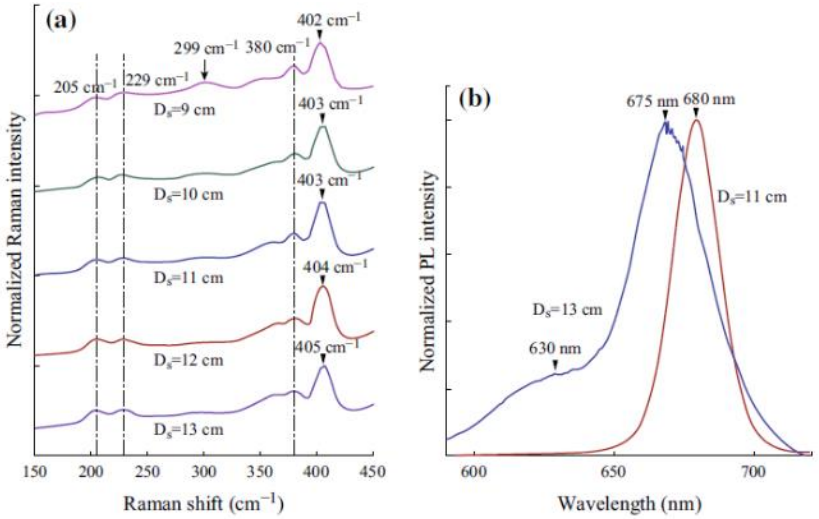

Figure 4-4 *a) Raman scattering spectra for the flakes produced at D_S= 9 cm, 10 cm, 11 cm, 12 cm, 13 cm b) PL spectra for the flakes produced at D_S = 11 and 13 cm while the reaction period is 5 minutes [55]*

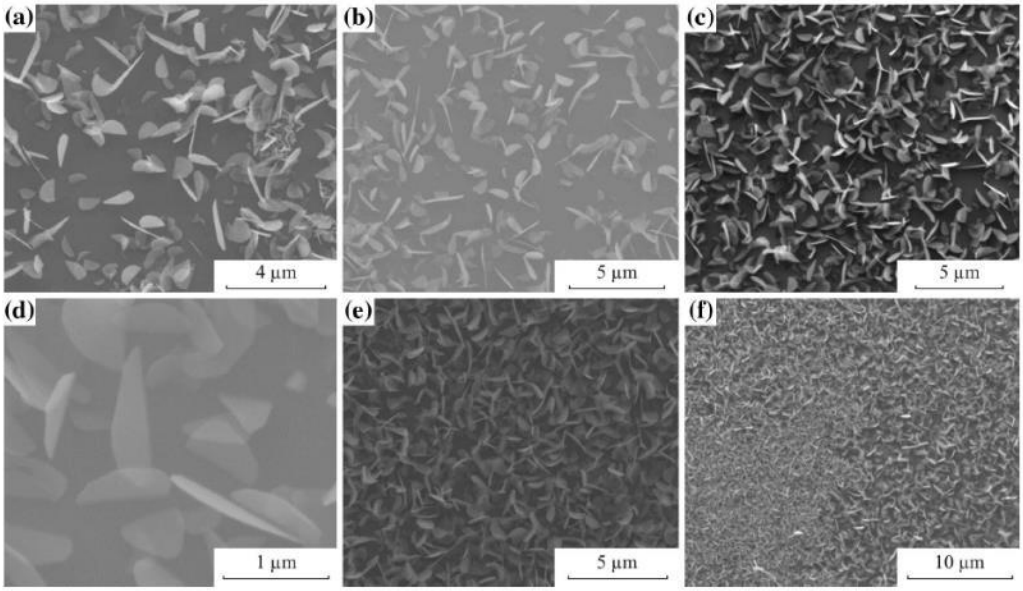

Figure 4-5 *SEM Images for CVD MoS_2 when Ds = a) 9 cm, b) 10 cm, c), d) 11 cm, e) 12 cm, and f) 13 cm with a reaction period of 5 minutes [55]*

SEM images of produced MoS_2 flakes with 5 minutes reaction period. MoS_2 flakes are easily distinguished; surface coverages of the films are homogeneous. However, different than general trend, shapes of MoS_2 flakes are not triangle or hexagonal, they are like half pringles which consist of many triangles of MoS_2 flakes. Reaction period is changed to three minutes thus; decreasing the reaction period improves forming MoS_2 flakes[55]. Raman scattering spectra shows the produced MoS_2 flakes in 3 minutes, 5 minutes, and 10 minutes when Ds is 11 cm. Raman peak at 299 cm^{-1} is

related to MoO_3 sheets due to inadequate reaction period to produce monolayer MoS_2 structures (Figure 4-6 a) [55]. MoS_2 flakes produced with 3 minutes reaction period are smaller than MoS_2 flakes produced with 5 minutes reaction period (Figure 4-6 b).

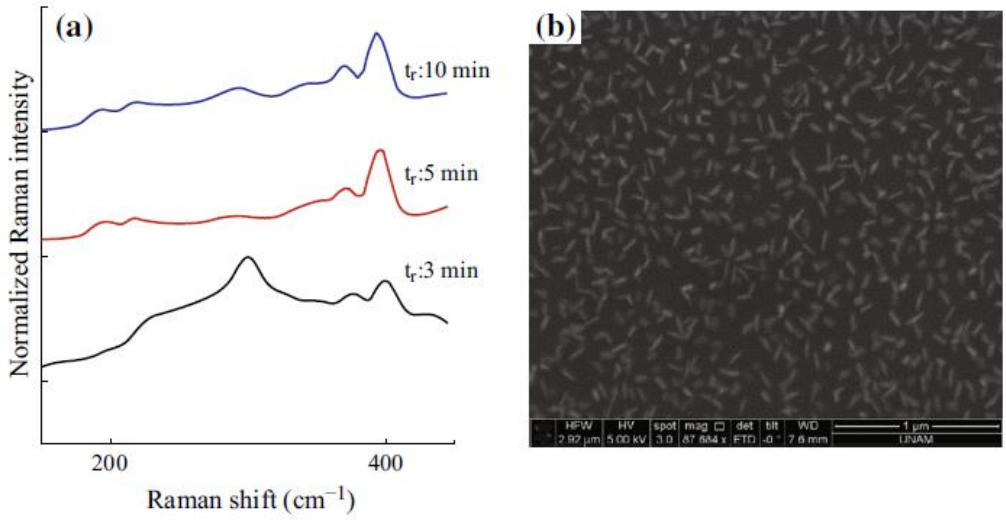

Figure 4-6 *a) Raman spectra for CVD MoS_2 the reaction period is fixed to 3, 5, and 10 minutes when D_S=11 cm; b) SEM image with a reaction period of 3 minutes [55]*

Figure 4-7 c illustrates atomic arrangement of monolayer MoS_2 flake. In Figure 4-6 b SEM image, triangular MoS_2 and chip like MoS_2 structures are formed over the SiO_2 substrate as seen in Figure 4-7 a & Figure 4-7 b . Diffraction patterns of triangular MoS_2 is shown in Figure 4-7 d . CVD grown MoS_2 structures are single crystal thus; there is symmetry in the diffraction spots shown in TEM images (Figure 4-7 a & Figure 4-7 b)[48, 55, 94].

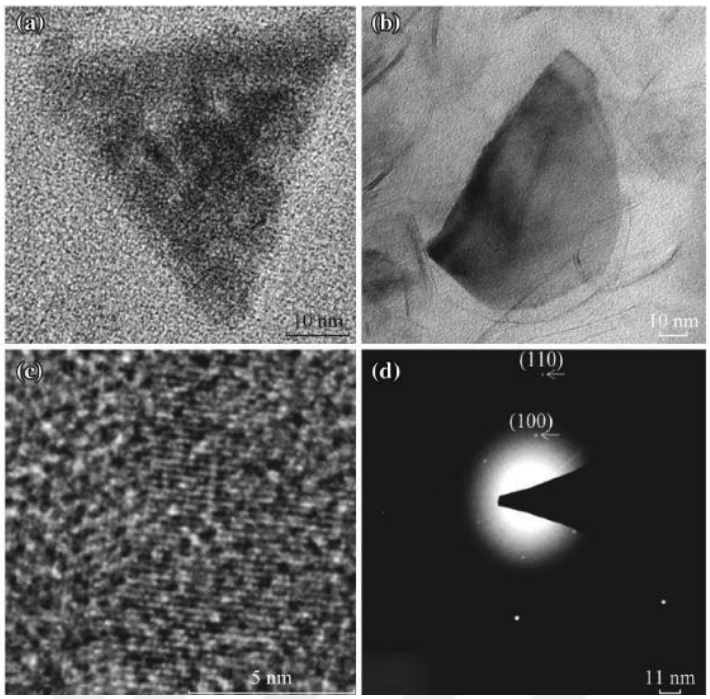

Figure 4-7 *TEM Image of a triangular and b chips-like shapes c periodic atomic arrangement, d diffraction patterns of a monolayer triangular flake [55]*

4.4. Conclusions

Controllable CVD growth of monolayer MoS_2 flakes are carried out by changing CVD parameters such as, substrate temperature, reaction period. We obtain different shapes of MoS_2 such as, triangular, rounded shapes, unified triangles, which are not smooth and formed with different angles on SiO_2 substrate. Single-wall MoS_2 flakes produced CVD method with high surface coverage, can be useful in applications such as solar cells, supercapacitors, photodetectors [55].

5. CONTROLLING BANDGAP AND SIZE OF $MoS_{2(1-x)}$-Se_{2x} ALLOY VIA CVD SYNTHESIS

5.1. Introduction

In Chapter 5, controlling bandgap and size of $MoS_{2(1-x)}Se_{2(x)}$ alloy via CVD synthesis and the experimental details are explained. The characterization of the produced monolayer $MoS_{2(1-x)}Se_{2(x)}$ (x=0-1) such as, optical measurements, photoluminescence and photoluminescence mapping measurement, Raman spectroscopy and Raman imaging measurement, bright field and dark field optical measurements, atomic force microcopy measurement are interpreted. Moreover, $MoS_{2(1-x)}S_{2(x)}$, x value (x=0-1) is alloys are calculated by using bowing parameter and MATLAB programming.

This work was published in the journal of Materials Science in Semiconductor Processing (Bandgap tuning of Monolayer $MoS_{2(1-x)}Se_{2x}$ alloys by optimizing parameters, (2019)) [29].

2-D transition-metal dichalcogenide (TMDC) monolayer alloys attract important interest, due to their properties such as mobility, chemical stability, tunable band gap that is useful for the applications such as sensors, catalysis, optoelectronics, and photonics [56, 63-67]. In this work we present CVD growth of single layer molybdenum sulphoselenide ($MoS_{2(1-x)}$-Se_{2x}) by changing growth parameters such as, reaction temperature locations of powders, locations of substrates and sulphur/selenium ratio [29, 126, 127]. X value is changed between 0 and 1. $MoS_{2(1-x)}Se_{2x}$ alloy is pure MoS_2 (1.82 eV), when x value is 0 there is no selenium atom in the structure. $MoS_{2(1-x)}Se_{2x}$ alloy is pure $MoSe_2$ (1.56 eV),when x is 1 there is no sulphur atom in the structure. By changing CVD parameters x value is it is possible to controlled in alloy structure. It is founded sulphur/selenium ratio is the most important CVD parameters for bandgap tuning of $MoS_{2(1-x)}Se_{2x}$ alloy. Size of monolayer flakes are up to 150 μm on SiO_2 substrate. To grow sulphur rich alloy, reaction temperature is optimized as 750 ^oC, to grow sulphur rich alloy, reaction temperature is optimized as 900 ^oC [128, 129]. Two temperature regimes is due to, formation of selenization and sulphurization in CVD reactions. Formation of selenization is harder than sulphurization thus higher temperature are optimized.

The chalcogenide exchange mechanism (CEM) is exchanging of alloyed atom in host lattice site of the structure. By using CEM is selenium rich alloy is produced at higher temperatures. Full width at half maximum of photoluminescence spectra of $MoS_{2(1-x)}Se_{2x}$ alloy is measured between 19.0 nm and 37.0 nm. The intensities of Pl emissions are uniform, evidencing monolayer property [29].

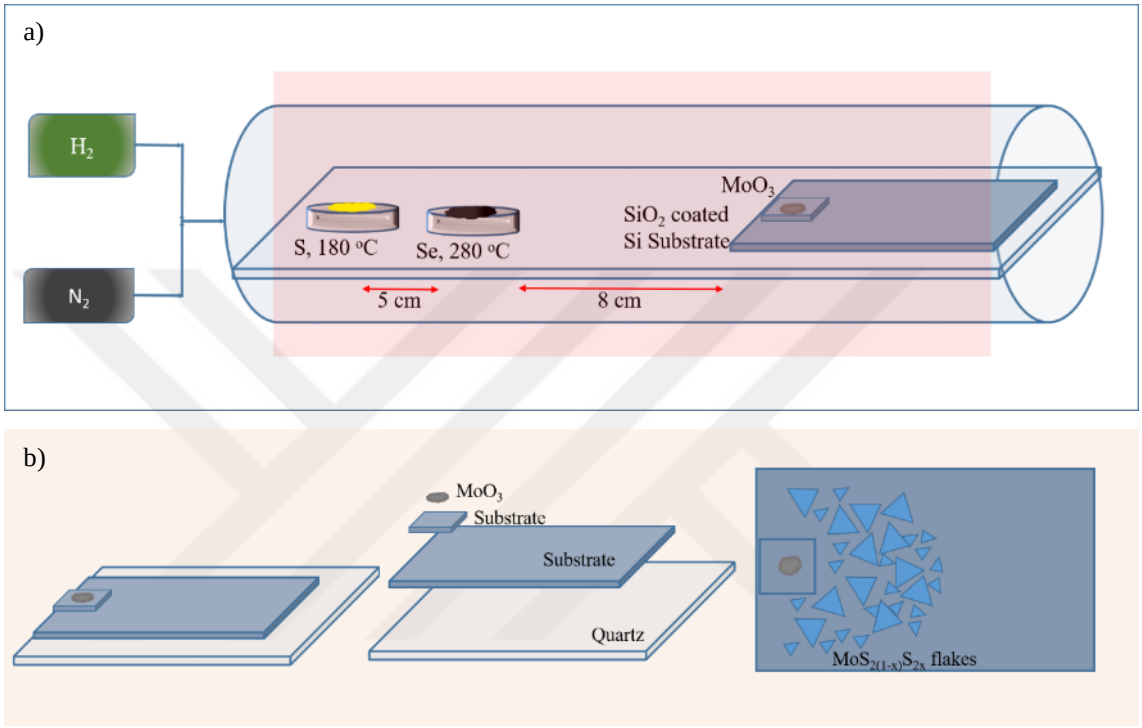

Figure 5-1 *a) CVD system scheme b) Illustration of substrate and monolayer* $MoS_{2(1-x)}Se_{2x}$

CVD system scheme is shown in Figure 5.1 a. Nitrogen (N_2) and hydrogen (H_2) gases are used as a precursor. Locations of sulphur, selenium, MoO_3 and SiO_2 substrates are placed from left to right side of the CVD system. The distance between selenium powder and MoO_3 powder is 8 cm and the distance sulphur and selenium powder is 5 cm. Illustration of substrate and monolayer $MoS_{2(1-x)}Se_{2x}$ is shown in Figure 5.1 b . Edge size of the flakes are counted from about over 90 flakes for indicated compositions. A statistical analysis is performed on the data. Images including size labels have been shown in Figure 5-2 indicating sampling area. Produced monolayer flake size distributions is calculated for the samples; x=0.20, x=0.42, x=0.78, x=1.0. Average flake size is found 33-44 μm and the standard deviation is found as 14-17 μm. Single layer flake size is changing between 9-87 μm. Experimental studies on the flake size demonstrate that flake size depends on the concentration gradient of the precursors on the substrate surface or

along the growth chamber which directly affect the number of formed nuclei on the surface [114]. Higher concentration ensures high nucleation density decreasing the distance between growth centers, lowering the flake size, and even triggering film formations with overlapping multilayer grain-boundaries. Increasing precursor to substrate distance lowers nucleation density and flakes found space to grow. Further increase of the substrate distance or a lower local concertation zone on the substrate suppress the nucleation density too much and flakes cannot find enough “fuel” to grow laterally. Kinetic Monte Carlo simulations benefiting from experimental observations based on concentration gradient explanation also predicts accurate shape and size of the grown crystals [130].

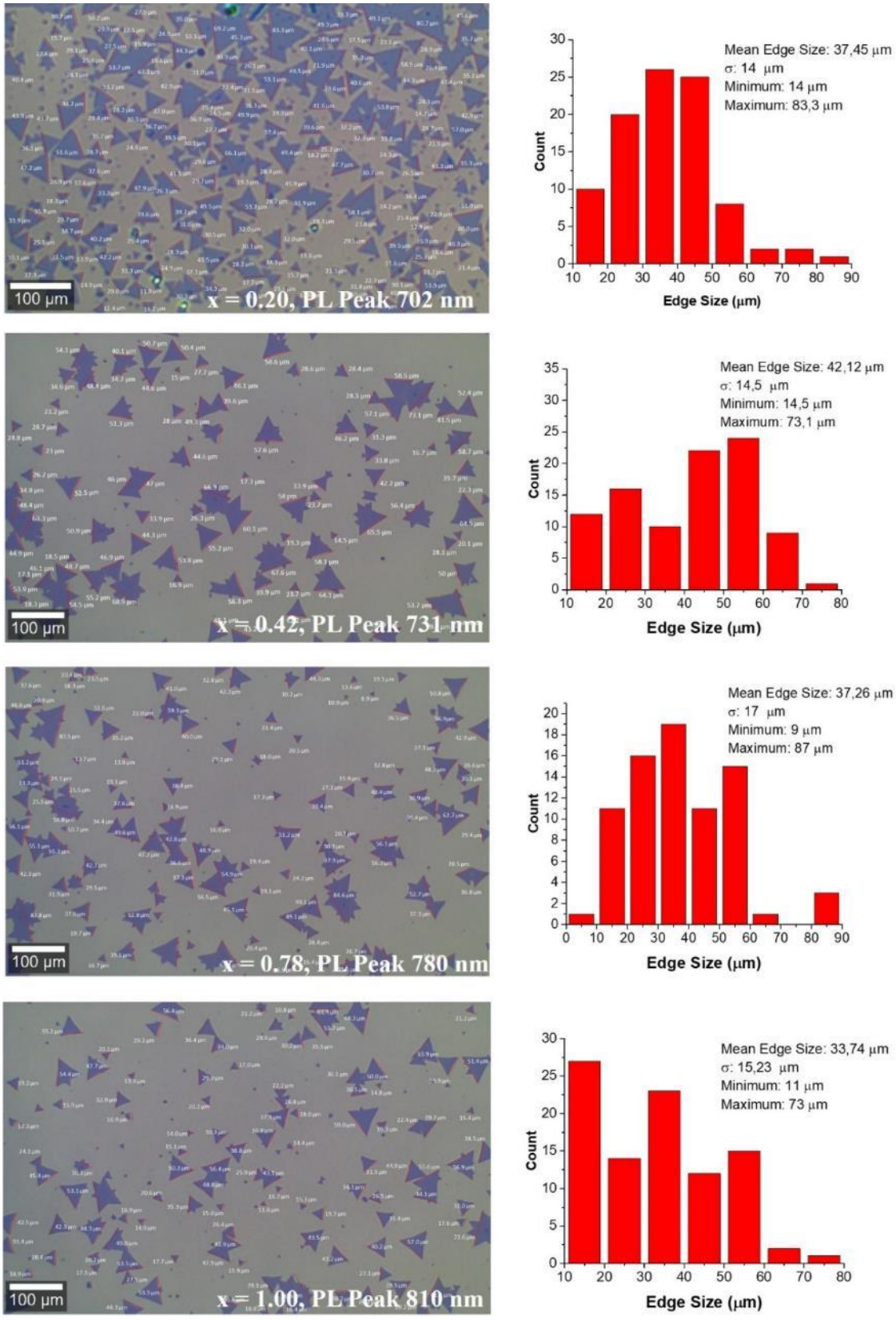

Figure 5-2 *Left column is region of interest for the statistical analysis and right column is the frequency count of the flakes' edge size together with mean, standard deviation (σ) minimum and maximum sizes.*

5.1.Experimental

A custom-built (CVD) system is used for growth of single layer $MoS_{2(1-x)}Se_{2x}$ (x=0-1) alloys by changing growth parameters such as, reaction temperature locations of powders, locations of substrates and sulphur/selenium ratio. In CVD system there three heat zone for three different precursor, selenium, sulphur, molybdenum trioxide. Nitrogen (N_2) and hydrogen (H_2) gases are used as a carrier gases. Locations of sulphur (in the first zone 180 °C), selenium (in the second zone 280 °C), MoO_3 and SiO_2 substrates (in the third zone 750 °C - 900 °C) are placed from left to right side of the CVD system. The distance between selenium powder and MoO_3 powder is 8 cm and the distance sulphur and selenium powder is 5 cm (Figure 5.1 a). Illustration of substrate and produced monolayer $MoS_{2(1-x)}Se_{2x}$ flakes is shown in Figure 5.1 b. Controlling of the distinct temperature of powders is important and after CVD reaction process, fast cooling of the system is used to finish chemical reaction as soon as possible. This cooling method, prevent monolayer structures growing as multilayer flakes. We clean the substrate by three solvents. While cleaning process we should not touch the surface of the substrate even using sterile gloves. MoO_3 precursor is placed on SiO_2 substrate (0.5 cm×0.5 cm). We use small substrate (0.5 cm×0.5 cm) as a carrier substrate, CVD reactions start on it. We observe, there are multilayer structures on the center of carrier substrate. Using small substrate enhances lateral growth of monolayer $MoS_{2(1-x)}Se_{2x}$ (x=0-1) alloys on bigger substrate (2.5 cm×5 cm) (Figure 5-1). The ratio of hydrogen and nitrogen carrier gases is studied; selenium powder is 300 mg for each experiment. Sulphur powder is decreased with a reaction temperature 750 ^oC for x value is between up to 0.52. Reaction temperature and selenium powder is increased for x value is between 0.52 and 1.0. For characterizations, we use optical microscopy, PL, Raman spectroscopy, Atomic force microscopy.

i. It's possible to grow $MoSe_2$ (x = 1) or MoS_2 (x = 0) at 750 °C with optimized gas flow rates and precursor amounts that forms the two-extreme ends of the Table 5-1.

ii. By keeping the temperature constant at 750 °C and by only changing the S/Se ratios, we observed that the Se content can be increased up to only x=0.5 but not further. We observed that when a small amount of Sulfur (up to 10 wt. %, 30 mg

Sulfur – 300 mg Selenium) is utilized, we always end up with Sulfur rich flakes even though amount of the Se is 10x higher than that of the S at 750 °C.

iii. Therefore, we increased the temperature to 900 °C with a heating rate of 10 °C/min to see its effect on the composition change. We observed that Se incorporation increases beyond x=0.52 up to x = 0.85.

Thus, this is the reason why growth temperatures of x=1 and x=0.85 is so different. Increase of the temperature also comes with an additional 25 minutes of extra heating period to reach from 750 °C to 900 °C. Since we know that S rich flakes are grown at 750 °C, we consider that this extra time is used as chalcogenide exchange mechanism that Se vapor replaces with S host atoms in as grown flakes initially deposited at 750 °C.

Table 5-1 *Critical growth parameters: S, Se amount,3rd zone temperature and resulting PL peak centers with compositions.*

Mo (mg)	Se (mg)	S (mg)	Temperature (°C)	PL Peak (nm)	X Composition
1	0	30	750	675	0
0.1	300	28	750	702	0.20
0.1	300	25	750	718	0.32
0.1	300	23	750	731	0.42
0.1	300	20	750	745	0.52
0.1	300	17	900	755	0.60
0.1	300	13	900	780	0.78
0.1	300	8	900	790	0.85
0.1	300	0	750	810	1

5.1.Results and Discussions

The total gas flow rate of precursors (N_2+H_2) is kept constant at 100 sccm and CVD growth experiments are done with the same conditions (300 mg Se, 28 mg S and 750 °C). The percentage values of H_2 precursor gas are adjusted as 5 %, 25 % and 50 %. As an ion source H_2 is used as 5 percentage surface coverage of the substrate is low due to incomplete CVD reactions (Figure 5-3 a). When the percentage of H_2 is 25 %, larger flakes are produced and the surface coverage is enhanced due to adequate ion source H_2 (Figure 5-3 b). However, the percentage of H_2 is 50 %, produced flakes are very small, and the surface coverage is decreased due to excessive ion source (Figure 5-3 c). AFM result is shown in Figure 5-3 d. The thickness of the monolayer flake is 0.70 nm [58, 85, 90, 91, 131-159]. Raman spectra and Photoluminescence spectra of $MoS_{2(1-x)}Se_{2x}$ (x=0, 0.20, 0.32, 0.42, 0.52, 0.60, 0.78, 0.85, 1) flakes are shown in Figure 5-5 a and Figure 5-

5 a, PL peak position (nm) with respect to x value of $MoS_{2(1-x)}Se_{2x}$ flakes. Inset: Optical image and PL intensity map of x=0.2 are shown in Figure 5-5 c. Pl spectra and Raman spectra verify that selenium and sulphur atoms alloyed by CVD reactions for monolayer growth (5 %, 25 % and 50 %. H_2 inclusion) (Figure 5-3 e) and (Figure 5-3 f).Raman spectra of monolayer flakes shows that $MoS_{2(1-x)}Se_{2x}$ alloy is produced by having distinctive Raman peaks of $MoSe_2$ and MoS_2 concurrently (Figure 5-5 a) [127]. Raman finger prints of MoS_2 are E^1_{2g} is at 400 cm^{-1} and A^1_g is at 380 cm^{-1}. Raman finger prints of $MoSe_2$ are E^1_{2g} is at 238 cm^{-1}, consistent with the literature [58, 90, 91, 138, 139, 145-164]. Sulphur powder is decreased with a reaction temperature 750 ^oC for x value is between up to 0.52. Reaction temperature and selenium powder is increased for x value is between 0.52 and 1.0. The temperature is increased to 900 ^oC to enhance selenization and CEM in CVD reactions

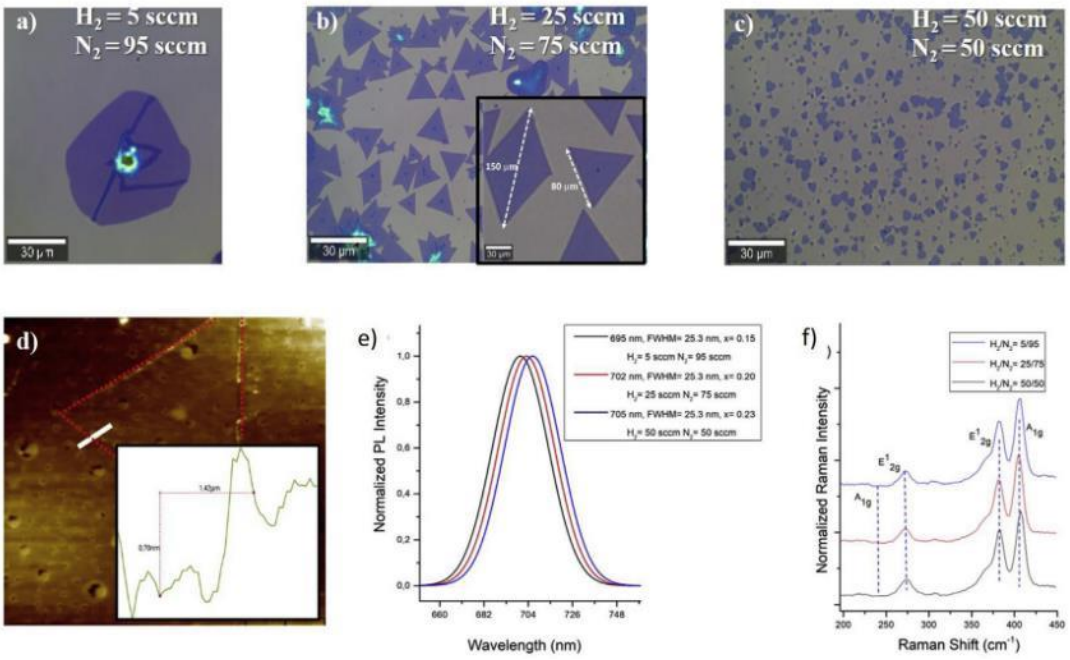

Figure 5-3 *Optical image of $MoS_{2(1-x)Se2x}$ for a) H_2=5 sccm, N_2=95 sccm N_2 b) H_2=25 sccm, N_2=75 sccm N_2 c) H_2=50 sccm, N_2=50 sccm d) and AFM measurement of the flakes. Inset shows thickness of monolayer flake (0.7 nm) e) PL measurement f) Raman measurement of $MoS_{2(1-x)}Se_{2x}$ for H_2/N_2=5/95, 25/75, 50/50.*

Selenium content of produced flake is increased via S-Se CEM, concentration of x is between 0.5 and 1 (Figure 5-4). PL imaging at a specific wavelength and line scans on monolayer flake (x=0.23) is shown in Figure 5-6 a. There is a small variation of x concentration between center and edges of the flake. Edge of the flake is brighter (x=30),

selenium atom is more in the alloy lattice due to CEM [165]. At center of flake is x value is 0.23. Monolayer flakes are homogeneously produced with no boundary.

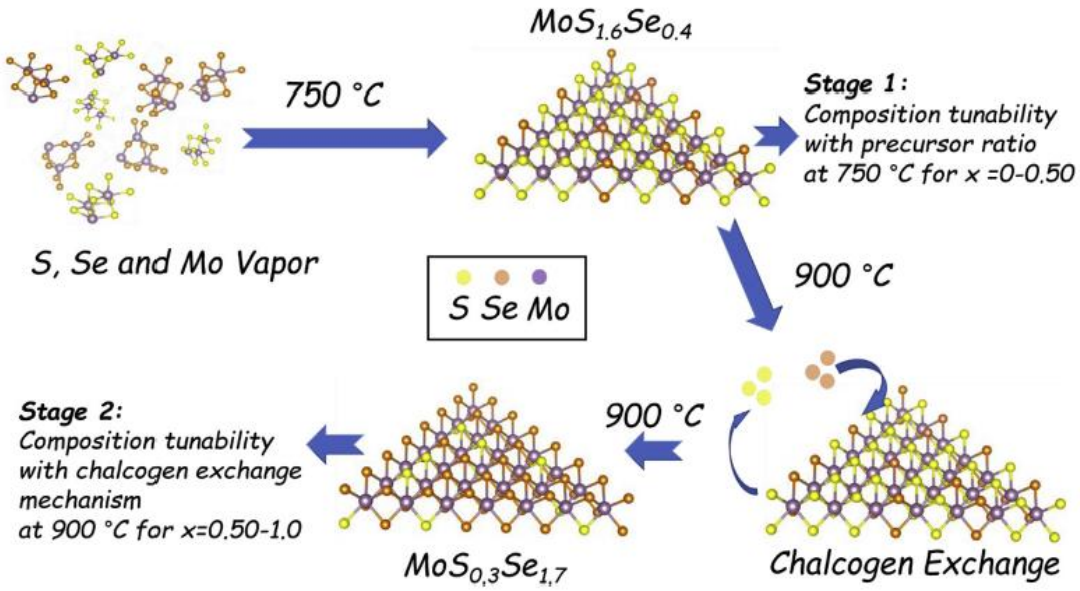

Figure 5-4 *Schematic illustration of the growth mechanism for triplet $MoS_{2(1-x)}Se_{2x}$ (x=0–1) system via chalcogenide exchange mechanism[29]*

Demonstration of monolayer alloy flakes having same S and Se content but having different atomic configurations isn't possible due to the complete miscibility of the S and Se in the alloy system and complexity of the required experimental effort. Such an experimental effort requires much advanced characterization tools like dedicated STEM or STM techniques and combination of band-gap measurements from the region of interest. Moreover, investigation will be limited with the probe area of such techniques which won`t be representative for the entire flake or flakes [166-168]. In the case of PL measurement that is largely utilized by other researchers cited in our manuscript, the laser spot size is roughly between 0.400 μm to 1 μm depending on the laser wavelength and numerical aperture of the objective. These researchers report single spectra and band-edge transition values correspond to specific compositions but not different values for the same composition. The large spot size with respect to the local changes of atomic configurations can be assumed smaller than spot size of the beam. Therefore, PL spectra reflects the average composition of the flake. However, the composition can still be varied inside the flake and can be tracked by PL peak center maps. For example, Honglai et al.

[43] synthesizes the graded atomic layer Mo-S-Se flakes where mole fraction of the Se changes within the single flake from 0 (center of the flake) to 0.7 (edge of the flake) gradually. In our PL peak center maps we get largely homogenous PL peak center (Figure 5-6 a) indicating homogeneous band-gap through the flakes [169-171]. Edges of the flakes have slightly rich in Se composition than that of the center, which is attributed to the chalcogenide exchange mechanism (CEM). However, it is still interesting to note that DFT calculations can give useful insights about the ordering in the alloy flakes. For example, extensive DFT studies on about 17000 symmetry inequivalent systems of Mo-Se-S have been studied by Kang et al [172]. They have reported stable ordered alloy structures with the concentrations of 1/3, 1/2 and 2/3 and they have reported that clustering of S or Se atoms is not favored. Yet, they report single band-gap values even though they investigate different atomic configurations [172]

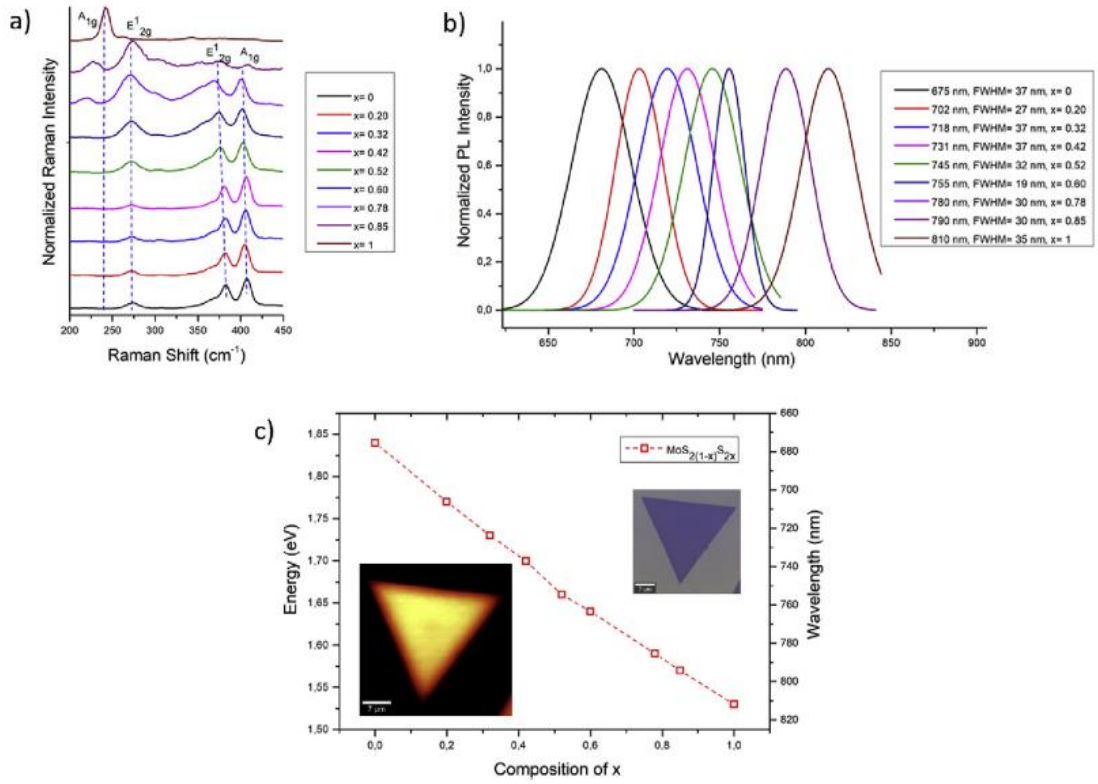

Figure 5-5 *a) Raman and b) PL spectra of $MoS_{2(1-x)}Se_{2x}$ (x=0, 0.20, 0.32, 0.42, 0.52, 0.60, 0.78, 0.85, 1) flakes. C) PL peak position (nm) versu x value of $MoS_{2(1-x)}Se_{2x}$ flakes. Inset: Optical image and PL imaging measurement of x=0.2 [29]*

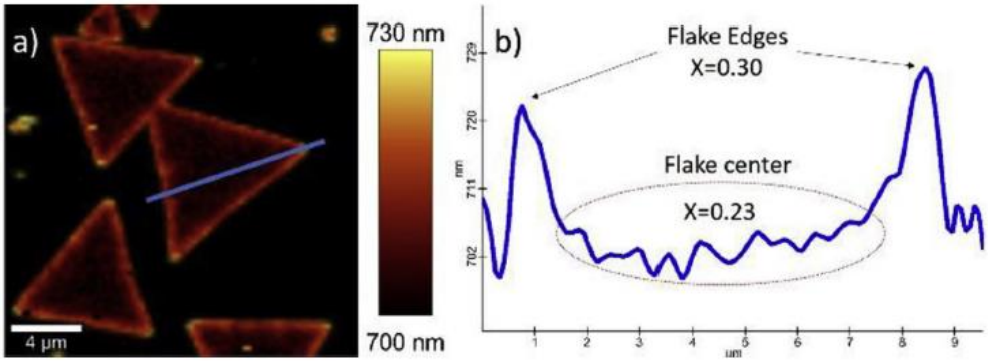

Figure 5-6 *a) PL peak center map of x=0.23 flake and b) PL peak center line scan [29]*

Color scale bar of Figure 5-6 indicates not intensity distribution but indicate photoluminescence peak center. As also the line analysis across the flake (Figure 5.b) demonstrates flake edges emit at 730 nm (brighter) and the flake center emits at 723 and seems dimmer (x = 0.23) according to the used color scale bar. Result indicate that edges are slightly rich in Se than that of the center. This is attributed to the usage of less amount of sulphur with respect to selenium, its higher activity and early consumption [173-175]. We believe that rest of selenium atoms would rather be deposited at the edges or exchange with the S inside the alloy lattice. In this example, the first suggestion is more likely to occur because of the growth temperature of the sample (750 °C). In addition, the edges of the flakes are more active than that of the basal plane of the flakes because there is the presence of dangling bonds. Therefore, S-Se exchange would be rather more pronounced than that of the center of the flake. On the other hand, inset of the Figure 5-5 c demonstrates intensity distribution of the flake where edges are dimmer with respect to center.

The emission energy interpreted that a bowing as the x (x=0-1) changes this is called band gap bowing which can be denoted by quadratic equation (5.1) (Table 5-1). The Pl spectra is used to explain x value by using a bowing parameter equation for MoS_2 (1.82 eV 675 nm) and for $MoSe_2$ (1.55 eV 810 nm). $MoS_{2(1-x)}S_{2(x)}$, (x=0-1) composition is calculated by this equation (5.1). The resulting formula calculated for 136 different wavelengths values between 765 nm (x=0) and 810 nm (x=1) by MATLAB programming. Pl peak position versus composition for $MoS_{2(1-x)}Se_{2x}$ shown in Figure A1-11 and emission energy versus composition for $MoS_{2(1-x)}Se_{2x}$ shown in Figure A1-12.

Using MATLAB programing, x value is calculated for 136 different Pl peak values between 675 nm (MoS_2, x=0) – 810 nm ($MoSe_2$, x=1) (Table A1-2).

$$Eg(MoS_{2(1-x)}S_{2(x)}) = (1-x) \times Eg(MoS_2) + x \times Eg(MoSe_2) - (b) \times (x) \times (1-x)) \quad \textbf{(5.1)}$$

$Eg(MoS_{2(1-x)}S_{2(x)})$, $Eg(MoSe_2)$ and $Eg(MoS_2)$ are the band gaps of the alloy and the and materials, and b is the bowing parameter. comparing the bowing parameter of the other alloys, $MoS_{2(1-x)}S_{2(x)}$ alloy has small bowing parameter which is 0.05 [39, 44, 47, 172].

$Egap = hc/\lambda$

$Egap = (6.626070040 \times 10^{-34} (joule\ second) \times 3 \times 10^{8} (meter\ per\ second)) / \lambda$

$Egap = 1240/\lambda$

$Eg(MoS_{2(1-x)}S_{2(x)}) = (1-X) \times Eg(MoS_2) + X \times Eg(MoSe_2) - (b) \times (X) \times (1-x))$

$Eg(MoS_2) = 1240/675$

$Eg(MoS_2) = 1240/810$

$b(MoS_{2(1-x)}S_{2(x)}) = 0.05$ (Table 6-1)

$Eg(MoS_{2(1-x)}S_{2(x)}) = 1240/\lambda$

$1240/\lambda = (1-X) \times (1240/810) + X \times (1240/675) - (b) \times (X) \times (1-x))$

$(0.05)X^2 - (0.3561728395)X + (1.837037037 - (1240/\lambda)) = 0$

$X_1 = 3.561728395 - ((24800/\lambda) - 24.0548318)^{0.5}$

$X_2 = 3.561728395 + ((24800/\lambda) - 24.0548318)^{0.5}$ since $0 \leq X \leq 1$ the root X_2 out of the range.

For $MoS_{2(1-x)}Se_{2(x)}$ *photoluminescence* peak is measured at 675 nm if we calculate it is simply, MoS_2

$x_1 = 3.561728395 - ((24800/675) - 24.0548318)^{0.5}$

$x_1 = 0$

For $MoS_{2(1-x)}$ $Se_{2(x)}$ photoluminescence peak is measured at 725 nm if we calculate it is simply, $MoS_{2(0.6245)}Se_{2(0.3755)}$

$x_1=3.561728395-((24800/800) - 24.0548318)^{0.5}$

$x_1=0.3755$

For $MoS_{2(1-x)}Se_{2(x)}$ photoluminescence peak is measured at 810 nm if we calculate it is simply, $MoSe_2$

$x_1=3.561728395-((24800/800) - 24.0548318)^{0.5}$

$x_1=1$

5.1.Conclusions

In summary, we demonstrate bandgap tuning control of single layer $MoS_{2(1-x)}Se_{2x}$ (x=0–1) alloys by changing and optimizing CVD reaction parameters. Bandgap of monolayer $MoS_{2(1-x)}Se_{2x}$ (x=0-1) is tuned between 1.82 eV ($MoSe_2$) and 1.55 eV (MoS_2). Selenium and sulphur ratio and reaction temperature are the most important parameters to produce monolayer $MoS_{2(1-x)}Se_{2x}$ (x=0-1). By using CEM is selenium rich alloy is produced at higher temperatures. Single layer $MoS_{2(1-x)}Se_{2x}$ (x=0–1) alloys by CVD has a good potentiality due to band gap tuning in optoelectronic device applications [1, 29, 38, 81].

6. MONOLAYER GROWTH OF MOLYBDENUM DISELENIDE ($MoSe_2$) BY CVD

In Chapter 6, monolayer growth of molybdenum diselenide ($MoSe_2$) on different substrates such as glass and SiO_2 is explained. The experimental details, the effects of impurities of glass substrate and different salts are investigated. The characterization of the produced monolayer $MoSe_2$ such as, optical measurements, photoluminescence and photoluminescence mapping measurement, Raman and Raman mapping measurement, bright field and dark field optical measurements, atomic force microcopy measurement are interpreted.

6.1. Introduction

2D Transition metal dichalcogenide (TMDC) can be used in various applications including microelectronics, photonics and catalysis [41, 42, 51, 98, 176, 177]. 2D MoS2 has already been studied by numerous groups and attracted significant attention up to now[161, 178-181]. In this regard, the reports on 2D $MoSe_2$ is comparatively few among the TMDCs, however, it also presents a high potential considering its high mobility [41, 51, 59-62]. Similar to MoS_2, as its thickness is reduced to monolayer, there is a transition from indirect band gap to direct band gap. To realize the 2D films, we used the CVD system by carefully changing the process parameters such as substrate temperature, gas flow rates, precursor amounts etc. CVD technique enables us to control the thickness and quality of films with optimization of reaction parameters. We used two different heating zones as it is needed to reach 2 distinct melting points for Molybdenum trioxide (MoO_3) precursor and selenium (Se) precursor. Nitrogen (N_2) and hydrogen (H_2) gases are the carrier gases, which transport the precursors to the substrates . The gas flow rates are adjusted to 80 sccm for N_2, 20 sccm for H_2 at ambient pressure.

6.2. Experimental

After several experiments a CVD recipe is developed to produce homogenous, monolayer MoS_2, $MoS_{2(1-x)}Se_{2(x)}$ (x=0-1), $MoSe_2$ flakes by CVD method, The recipe has many parameters such as, CVD reaction temperature, flow ratios of the carrier gases, amount of precursor powders etc. The produced unified flake size is up to 1375-micrometers size in one side and single flake size is up to 150-micrometers in one side. Experimental procedures are applied cautiously to grow monolayer $MoSe_2$ structures.

Glass substrates are beneficial, because glass substrates are melting in CVD reactions. While glass substrates are, melting NaCl molecules are activating as a catalyzer in CVD reactions. NaCl molecules support the monolayer $MoSe_2$ growth positively. The coverage of the flakes are adequate to produce FET device. However, there is a disadvantage of the glass substrates, after CVD reactions melted glass substrates solidified; this solidification makes the boundaries of substrate, irregular shapes. Transferring of the produced monolayer MoSe2 flakes grown on glass substrate to SiO_2 substrate is a solution for irregular surface problem. It is simply transferring of monolayer flakes from glass to SiO_2 coated silicon substrate. Using glass as a substrate is beneficial to produce monolayer TMDCs but, it is not fully understood whether the glass surface reactions or glass impurities such as Na, Mg, Ca and etc. To understand the effect of these elements, new salts can be used as catalyzers such as, NaCl, CaCl, KCl, and KIO_2. These salts are soluble in distilled water. 0.05 molar NaCl solution is prepared and it is used to prepare a thin layer on SiO_2 substrate by using spinner. The results of the CVD production is surprisingly good, fully coverage is achieved. The details of the survey are explained in subsection 6.2.

6.3. Results and Discussions

6.3.1. 2D $MoSe_2$ growth by face down face down configuration

CVD scheme for $MoSe_2$ by face down configuration and optical image of laterally largest grown $MoSe_2$ flake are shown in Figure 6-1. We tried to produce monolayer $MoSe_2$ flakes on SiO_2 substrate by using face down configuration, Maximum size of the produced $MoSe_2$ flake is 40 μm on edge side of triangular flake (Figure 6-1 b). However, the surface coverage is low; the flakes are produced on one edge side of SiO_2 substrate, which is not sufficient for device fabrication. Hygrogen (H_2), Argon (Ar), Nitrogen (N_2) gases are used as carrier gases. Locations of powders, location substrate, flow rates, reaction temperatures are optimized. SiO_2 substrate is placed on quartz pot with face down (Figure 6-1 a). This configuration adversely affects the laminar gas flow, which is important monolayer growth. Carrier gases enters CVD system through a needle tipped valve and laminar flow formed inside the quartz tube. There is very small gap between quartz pot and substrate (face down). Vaporized selenium atoms that are carried by carrier gases through the quartz tube, cannot sufficiently enters in this gap. Therefore, CVD reactions take place in adequately and surface coverage of the film is low.

To increase laminar flow we design a rectangular plate (3 mm*6 mm*300 mm) made from quartz material and face up configuration (more details of face up configuration of are explained in subsection 6.2 and 6.3). Substrates, quartz holders and powders are stood fixed on rectangular quartz plate, which is important for CVD parameters such as distances between powders and substrates.

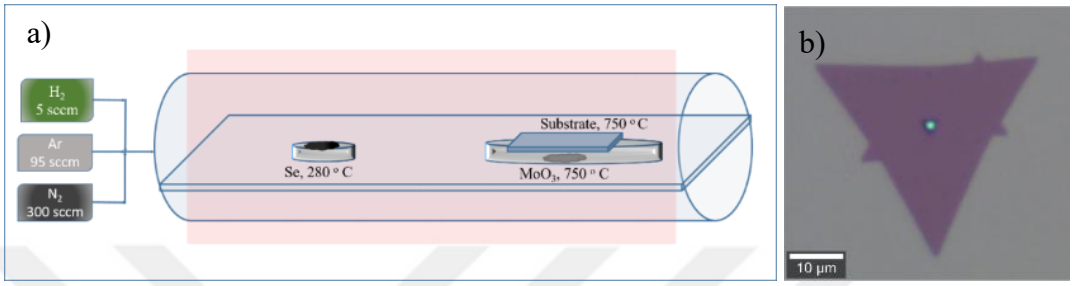

Figure 6-1 *a) CVD scheme for $MoSe_2$ b) Optical image of the largest produced $MoSe_2$ by flake face down configuration*

6.3.2. 2D $MoSe_2$ growth on glass substrate

Using glass as a substrate is reported to be favorable in chemical vapor deposition (CVD) reactions, extending the lateral growth of monolayer $MoSe_2$ [104]. However, there are several issues to be clarified regarding the role of a glass substrate in monolayer formation. For example, it is not fully understood whether the glass surface reactions or glass impurities such as Na, Mg, and Ca etc. function as a catalyzer or supporter to produce homogeneous, large-area and monolayer $MoSe_2$ flakes. CVD scheme is shown in Figure 6-2. Optical image of $MoSe_2$ flake, and photoluminescence measurement emissions at 810 nm (Figure 6-3). Horizontal CVD configuration and using glass as a catalyzer are advantageous to obtain high coverage and large monolayer $MoSe_2$ flakes. Thus, glass impurities such as Na, Mg, and Ca support the monolayer growth [81, 104, 182, 183].

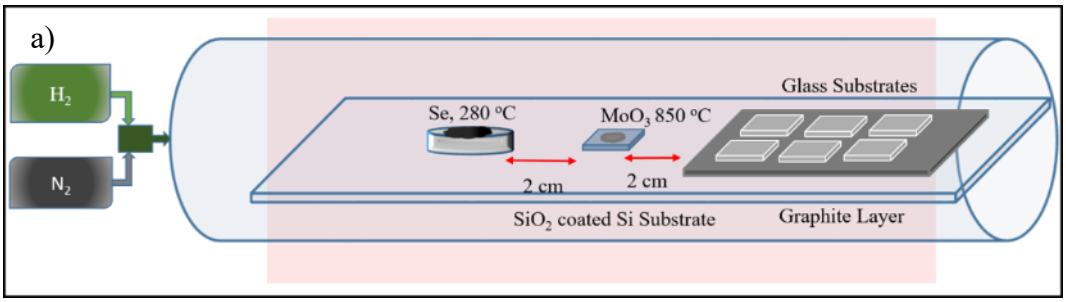

Figure 6-2 *CVD scheme for $MoSe_2$ .Optical image Raman and Pl measurements*

Raman spectra of monolayer $MoSe_2$ grown on glass substrate has distinctive peaks at 240 cm^{-1} which is out of plane A_{1g} mode, monolayer $MoSe_2$ flake show two distinctive peaks located at 240 cm^{-1}, 220 cm^{-1} and 270 cm^{-1}, A_{1g} mode and E^1_{2g} mode shown in Figure 6-3 c. In addition, Pl spectra of $MoSe_2$ flakes are fitted by nonlinear curve fitting (Figure 6.3 b). Bright field and dark field microscopy images of $MoSe_2$ grown on glass substrate are shown in Figure 6-3 d, f. Glass substrate is transparent material and the surface is not smoot as SiO_2 substrate due to CVD reactions (Figure 6-3 a). By using glass substrate high coverage is obtained, however, the surface is not smooth to fabricate a device. Transferring of the monolayer flakes is need; the details of transferring processes are explained in subsection 7.2.

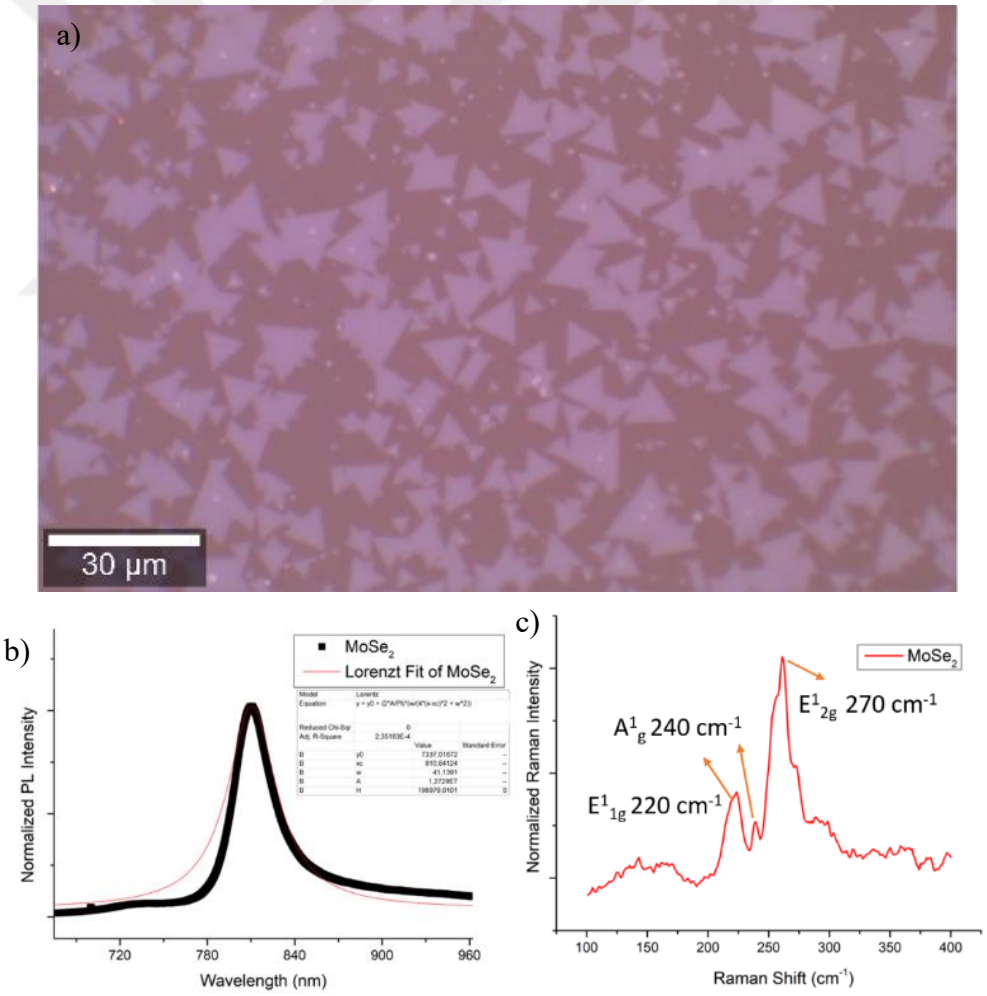

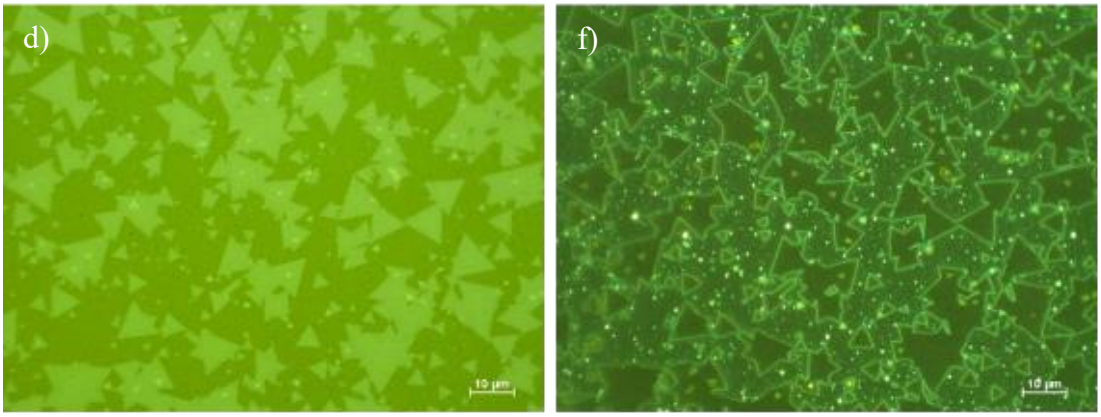

Figure 6-3 *a) Optic image of $MoSe_2$ flake. b) Lorenzt fit and Pl spectra of $MoSe_2$ flake. c) Raman spectra of $MoSe_2$ flake. d) Raman measurement of $MoSe_2$ flake. e)*

6.3.3. NaCl Salt assisted $MoSe_2$ growth

Monolayer $MoSe_2$, a member of 2D two dimensional TMDCs family has attracted considerable attention due to its direct bandgap and high mobility suitable for both optoelectronic and electronic devices [38, 51, 184, 185]. However, to produce uniform and large-area $MoSe_2$ monolayer structures over the whole substrate with a high coverage is still a challenging issue due to the difficulty in controlling the growth of single-layer structures[41, 46, 53]. Using glass as a substrate is reported to be favorable in CVD reactions, extending the lateral growth of monolayer $MoSe_2$ [98, 104, 186, 187]. However, there are several issues to be clarified regarding the role of a glass substrate in monolayer formation. For example, it is not fully understood whether the glass surface reactions or glass impurities such as Na, Mg, Ca etc. function as a catalyzer or supporter to produce homogeneous, large-area and monolayer $MoSe_2$ flakes. Carrier gases, configuration of substrates, locations ofMoO_3 and selenium powders illustrated in CVD system scheme (Figure 6-4).

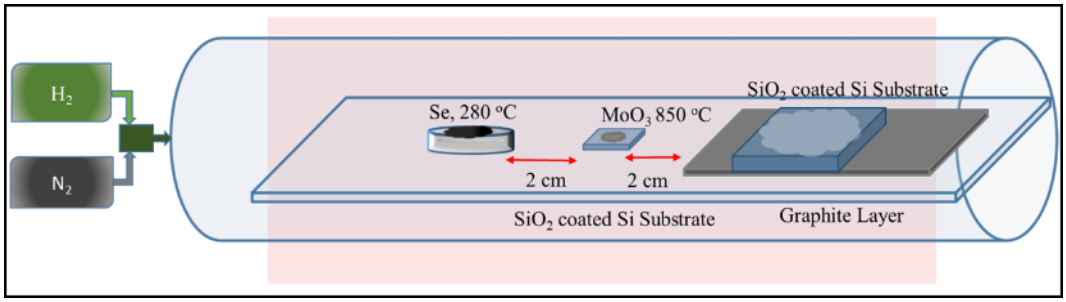

Figure 6-4 *CVD scheme for $MoSe_2$*

Hence, in this study, we report the synthesis and characterization of monolayer $MoSe_2$ structures formed on 300 nm SiO_2 coated Si substrate where NaCl salt is used as a catalyzer in CVD process. We have also fabricated and compared the electronic properties of a back-gate field effect transistors (FET) based on these salts induced flakes and conventionally CVD grown $MoSe_2$ flakes. 0.05 molar NaCl solution is dropped and spinned on a SiO_2/Si substrate (4 cm x 4 cm) by 500 rpm for 120 seconds. After the spinning process, the substrate is kept for 120 seconds on a hot plate (70 ^oC) as shown in Figure 6-5 a). Molybdenum trioxide (MoO_3), selenium (Se) powders, and NaCl coated substrate are placed on a quartz tube in the CVD chamber (Figure 6-4). CVD reactions take place under ambient pressure conditions with a temperature ramping rate of 20 °C min^{-1} where the growth temperature is 850^oC and reaction period is 5-minutes. Single layer $MoSe_2$ flakes with a thickness of ~0.70 nm and a lateral dimension up to 100 μm are uniformly produced. Raman spectroscopy, photoluminescence (PL) spectroscopy, atomic force microscopy (AFM) and optical microscopy are used for characterizing the formed structures. The photoluminescence peak of A exciton emission of NaCl salt assisted $MoSe_2$ is observed at 812 nm . Raman peak, out of plane mode (A^1_g) observed at 238 cm^{-1}. It is assigned to monolayer $MoSe_2$ flake formations shown in Figure 6-5 c and Figure 6-5 d. Lorentz fitting analysis is performed for Raman spectra of NaCl salt assisted monolayer $MoSe_2$ (Figure 6-5 e). Optical measurements are performed by bright field and dark field microscopy to show grain boundaries, uniform growth and the obtained sizes of the salt assisted grown $MoSe_2$ flakes (Figure 6-6).

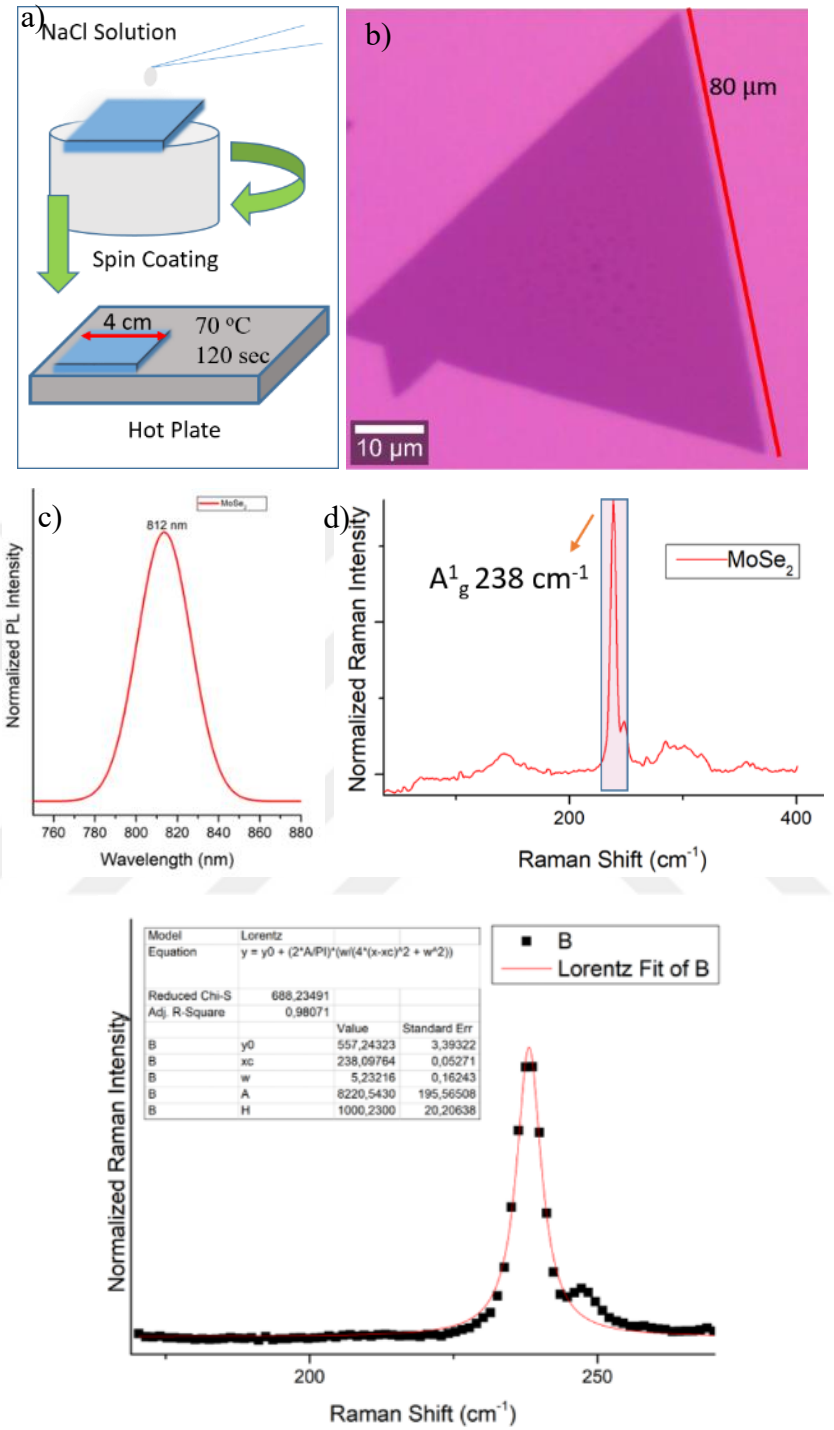

Figure 6-5 a) *Coating process of NaCl on SiO_2 substrate b) Optical microscope image of $MoSe_2$ c) Pl spectra of NaCl salt assisted monolayer $MoSe_2$ d) Raman spectra of NaCl salt assisted monolayer $MoSe_2$ e) Lorentz fitting analysis of Raman spectra of NaCl salt assisted monolayer $MoSe_2$*

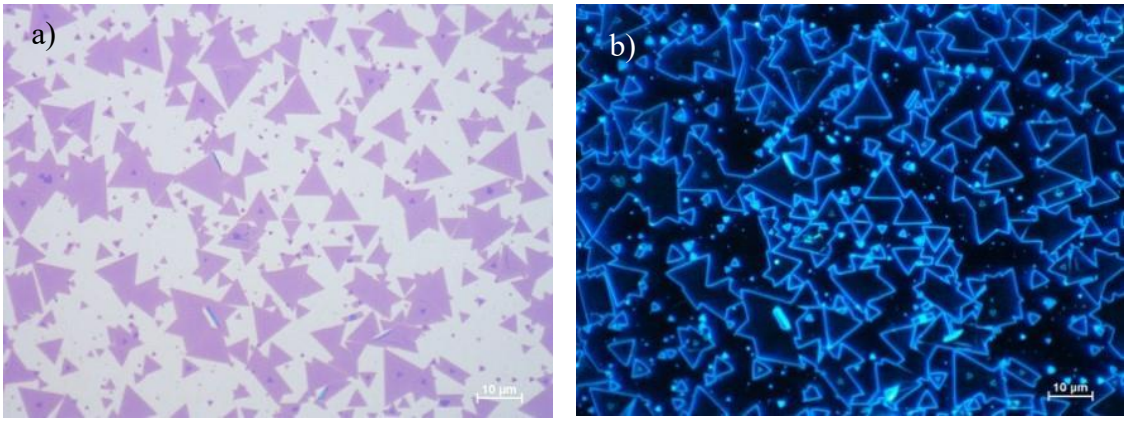

Figure 6-6 *a) BF microscope image of NaCl salt assisted monolayer $MoSe_2$ b) DF microscope image of NaCl salt assisted monolayer $MoSe_2$*

Optical images of NaCl salt assisted $MoSe_2$ and $MoSe_2$ flakes grown on glass are shown in Figure 6-7 b and Figure 6-7 e. Both monolayer flakes have similar triangular shapes with no boundary. However, their Raman spectrum are different, For NaCl salt assisted $MoSe_2$, Raman peak is located at 238 cm^{-1} that matches 2H $MoSe_2$ and Raman peaks. For $MoSe_2$ flakes grown on glass Raman peaks are located at 220 cm^{-1}, 238 cm^{-1}, 270 cm^{-1} these are Raman fingerprints of 1T $MoSe_2$ (Figure 6-7 a Figure 6-7 d) [91, 144, 159, 188]. In addition, it is possible to compare NaCl salt assisted $MoSe_2$ with $MoSe_2$ flakes grown on glass by Raman imaging measurements of the flakes at different Raman shift values. For Raman imaging of NaCl salt assisted $MoSe_2$, the spectral center of Raman shift is 238 cm^{-1}, homogenous and bright colors prove that, the flake is 2H $MoSe_2$ (Figure 6-7 c). For Raman imaging of $MoSe_2$ grown on glass, the spectral centers of Raman shift are 220 cm^{-1}, 238 cm^{-1}, 270 cm^{-1}, homogenous and bright colors prove that, the flake is 2T $MoSe_2$ (Figure 6-7 f, Figure 6-7 g, Figure 6-7 h) [91, 144, 159, 188]. In Figure 6-7 f, the spectral center of Raman shift is 220 cm^{-1} edges of the flake are brighter than the center of flake. In Figure 6-7 g and Figure 6-7 h, for the spectral centers of Raman shift 240 cm-1 and 270 cm^{-1} center of the flake are brighter than the edges of flake. These color differences are due to metallic phase (1T) of $MoSe_2$.1T is metallic phase that, in a unit cell 3 molybdenum atoms have chemical bonding with selenium or sulphur atoms, there is trimerization and the structure have metallic phase [41, 91, 144, 159].

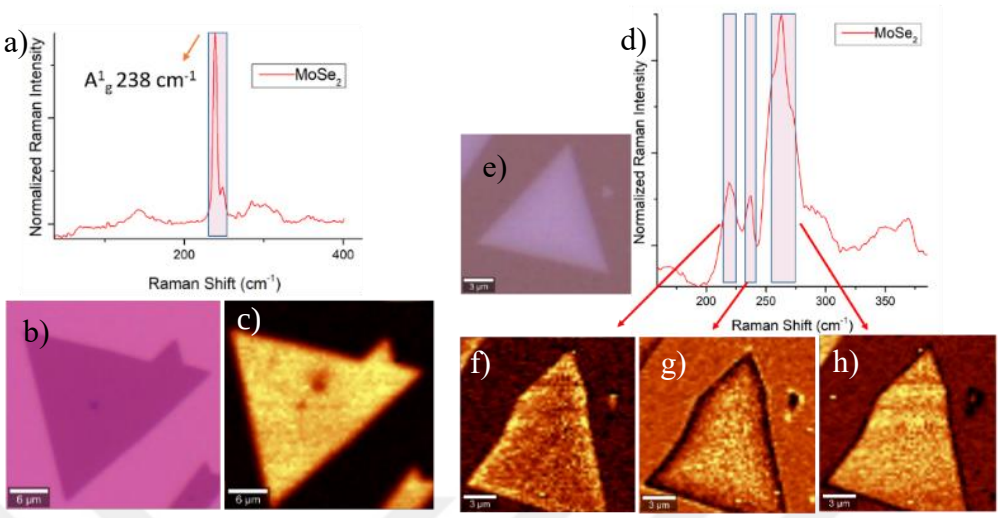

Figure 6-7 *a) Raman spectra NaCl salt assisted $MoSe_2$. b) Optical image of NaCl salt assisted $MoSe_2$. c) Raman imaging of NaCl salt assisted $MoSe_2$ (centered at 238 cm^{-1}). d) Raman spectra of $MoSe_2$ flakes grown on glass. e) Optical image of $MoSe_2$ flakes grown on glass. f) Raman imaging of $MoSe_2$ flakes grown on glass (centered at 220 cm^{-1}). g) Raman imaging of $MoSe_2$ flakes grown on glass (centered at 240 cm^{-1}). h) Raman imaging of $MoSe_2$ flakes grown on glass (centered at 270 cm^{-1}).*

We use spinning for NaCl coating on SiO_2 substrate. Before spinning process, 0.05 M NaCl solution is dropped on the surface of SiO_2 substrate. This solution is fully coated and it is waited for 60 second due to possible weak bonding. To understand the effect of NaCl solution, NaCl solution is partially dropped and is it waited for 60 seconds (Figure 6-8 a). After CVD process, on the area which is the partially dropped and waited fully monolayer growth. The other parts of the substrate surface coverage is very low.

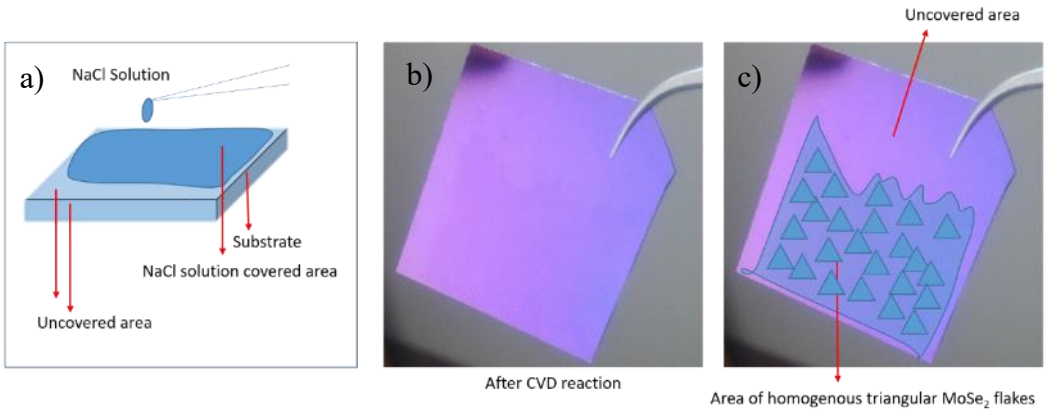

Figure 6-8 *a) Demonstration of NaCl solution on SiO_2 substrate b) SiO_2 substrate after CVD growth c) Demonstration of growth location*

Bright field and dark field microscope images of NaCl salt assisted monolayer $MoSe_2$ are shown in Figure 6-9 b. The surface coverage is high and flakes are monolayer with no grain boundary. BF and DF optical images of triangular and unified triangular shapes of $MoSe_2$ flake prove that there is no boundary inside of the unified triangular flakes (Figure 6-9 c and Figure 6-9 d) which is important for device quality [2, 38, 105, 189].

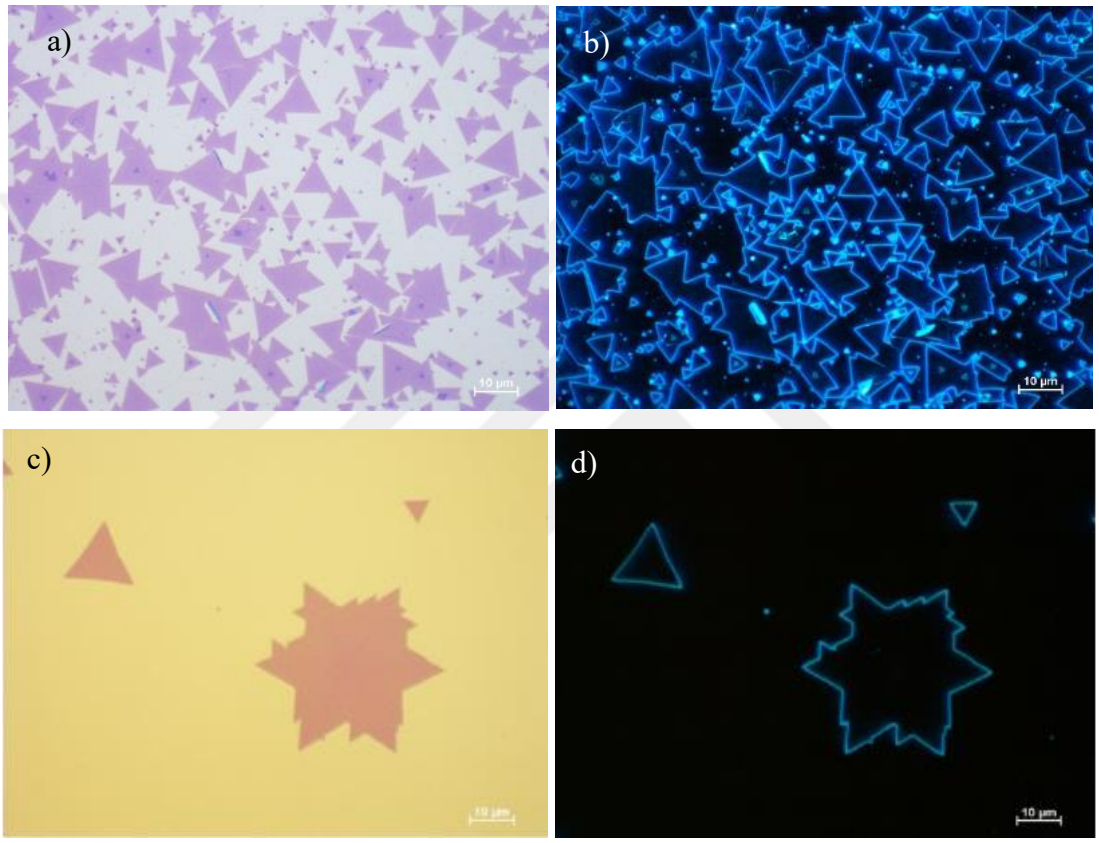

Figure 6-9 *a) BF microscope image of NaCl salt assisted monolayer $MoSe_2$ b) DF microscope image of NaCl salt assisted monolayer $MoSe_2$ (unified triangular shapes) c) BF optical images of $MoSe_2$ flake d) DF optical images of $MoSe_2$ (unified triangular shapes)*

Atomic force microscopy (AFM) measurement of NaCl assisted $MoSe_2$ flake is shown in Figure 6-12. The thickness of the samples are found as 0.76 nm (Figure 6-15 a), 0.70 nm (Figure 6-12 b), 0.72 nm (Figure 6-12 c AFM measurements signify that the $MoSe_2$ flakes are monolayer. The step heights is appropriate atomic height of $MoSe_2$ [164, 190-192].

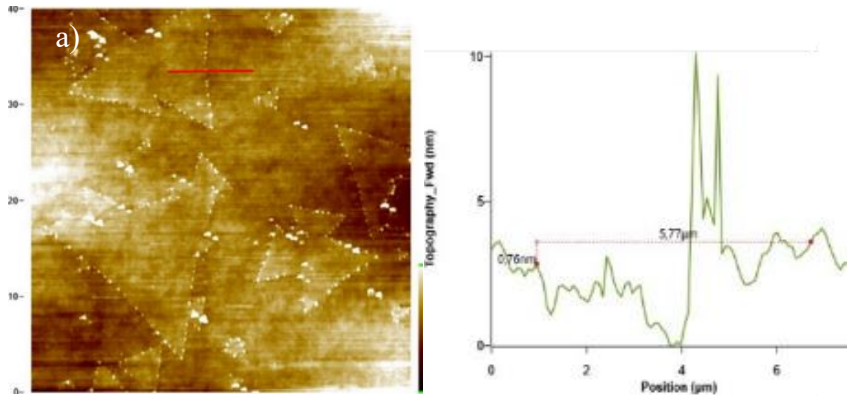

Figure 6-10 *AFM measurement of NaCl assisted $MoSe_2$ flake (thicness=0.76 nm)*

6.4. Conclusions

In conclusion, using glass as a substrate is beneficial to produce monolayer TMDCs. To understand the effect of these elements in glass such as Na, Mg, Ca and etc., new salts can be used as catalyzers such as, NaCl, CaCl, KCl, and KIO_2. NaCl Involvement in CVD process enables large area $MoSe_2$ flakes with full substrate coverage, which was not possible with process without any salt [5]. Hence, we confirm that NaCl develops CVD kinetics via reducing strength of interlayer bonds of $MoSe_2$ flakes and enlarges homogeneous, laterally grown monolayer device-quality $MoSe_2$ flakes, which is crucial for practical applications of 2D TMDCs.

7. TMDC BASED FIELD EFFECT TRANSISTOR (FET) DEVICE FABRICATION

In Chapter 7, two dimensional transition metal dichalgonides (2D-TMDCs) based field effect transistor (FET) device fabrication, transfer processes, lithography processes, metal coating processes, and electrical performance measurements of produced field effect transistors are explained.

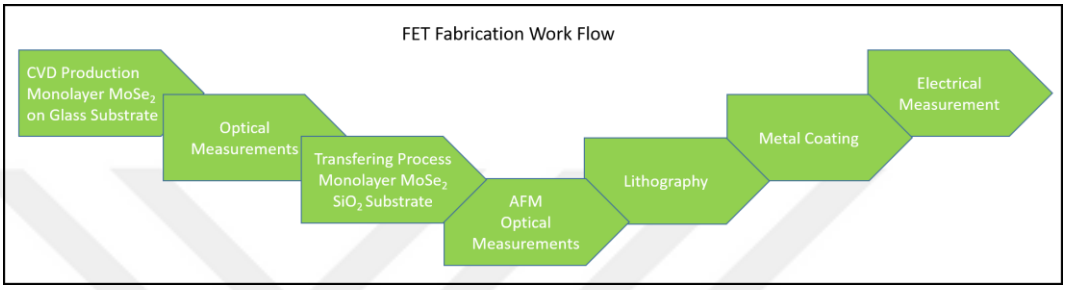

Figure 7-1 *a) Fabrication workflow of $MoSe_2$ FET*

7.1. Field Effect Transistors (FET's)

In many study, the FET devices using 2D $MoS_{2(1-x)}Se_{2(x)}$, MoS_2, $MoSe_2$ flakes are fabricated on highly doped 300 nm SiO_2 coated silicon substrates [2, 82, 83, 193-207]. The typical device fabrication is UV-lithography followed by thermal evaporation of Titanium/Gold (10nm/90nm) metal contacts [2, 46, 51]. The silicon substrate is used as the back gate contact. Electrical characterization of fabricated devices are performed with a home-built probe station (Figure 7-1) [37, 99] .

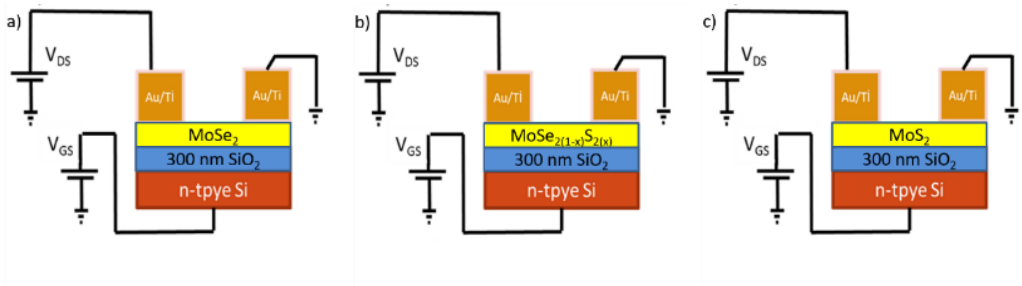

Figure 7-2 *a) Back gate configuration of $MoSe_2$ FET b) Back gate configuration of $MoS_{2(1-x)}Se_{2(x)}$, FET c) Back gate configuration of MoS_2 FET*

FETs devices are fabricated on monolayer $MoSe_2$ that behave n-type. The electron mobility of the monolayer $MoSe_2$ is relatively high compared with 2D MoS_2 with the same back-gate configuration [36, 51, 73, 106]. FETs based on $MoSe_2$ has advantageous mobility, which is about 50 $cm^2 V^{-1} s^{-1}$, mobility of MoS_2 is between 4-20 $cm^2 V^{-1} s^{-1}$ [46, 52, 105]. Back gate configuration of $MoSe_2$ FET and the optical image of a large $MoSe_2$ flake and gating voltage and drain current measurement are shown in Figure 7-2 [105, 208].

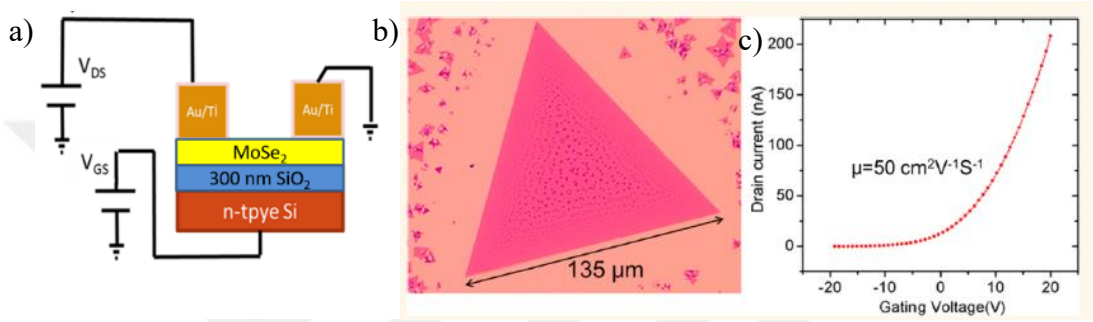

Figure 7-3 *a) Back gate configuration of $MoSe_2$ FET. b) Optic image of $MoSe_2$ flake [105]. c) Gating voltage vs source/drain current measurement [105].*

7.2. Transfer Processes of Monolayer Structures

Using glass as a substrate is reported to be beneficial in CVD reactions, extending the lateral growth of monolayer $MoSe_2$ [104, 209]. Glass impurities such as Na, Mg, Ca and etc. function as a catalyzer or supporter to produce homogeneous, large-area and monolayer $MoSe_2$ flakes. However, after CVD reactions the surface of the glass substrate is not appropriate for device fabrication thus solidification and melting of glass adversely effect on surface of glass substrate. Monolayer $MoSe_2$ flakes grown on glass substrate can be transferred on to a SiO_2 substrate by transfer process (Figure 7-5).

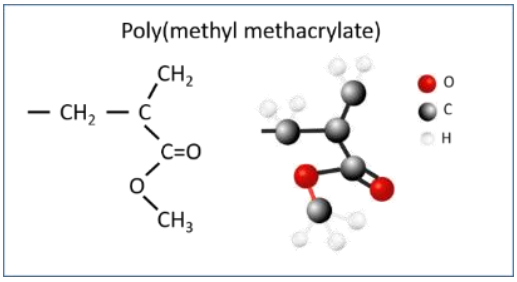

Figure 7-4 *Molecular structure of Poly(methyl methacrylate)*

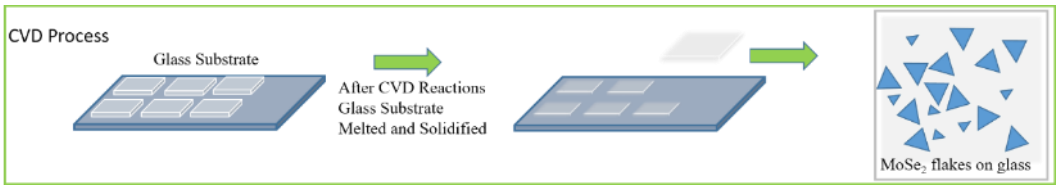

Figure 7-5 *Chemical vapor deposition process with glass substrates*

Transfer process of monolayer structures is carried out by using Poly(methyl methacrylate) (PMMA) (Figure 7-6). The molecular structure of PMMA is shown in Figure 7-4. $MoSe_2$ grown glass substrate is put on spinning device. Carefully a few drops of PMMA are put on glass substrate and wait for 30 seconds. Then spinning device is started with 500 rpm for 40 seconds. Homogeneously produced PMMA layer on glass substrate is need to be dried thus; substrate is waited on heater at 70 ^oC for 120 seconds. The borders of the glass substrates are carefully scraped with a knife. Glass and PMMA layer are slowly separated via dipping in to distilled water. PMMA layer is transferred on to SiO_2 substrate by reverse dipping movement. By using acetone at 70 ^oC, PMMA layer is vanished in 60 minutes. $MoSe_2$ flakes are now on SiO_2 substrate (Figure 7-6).

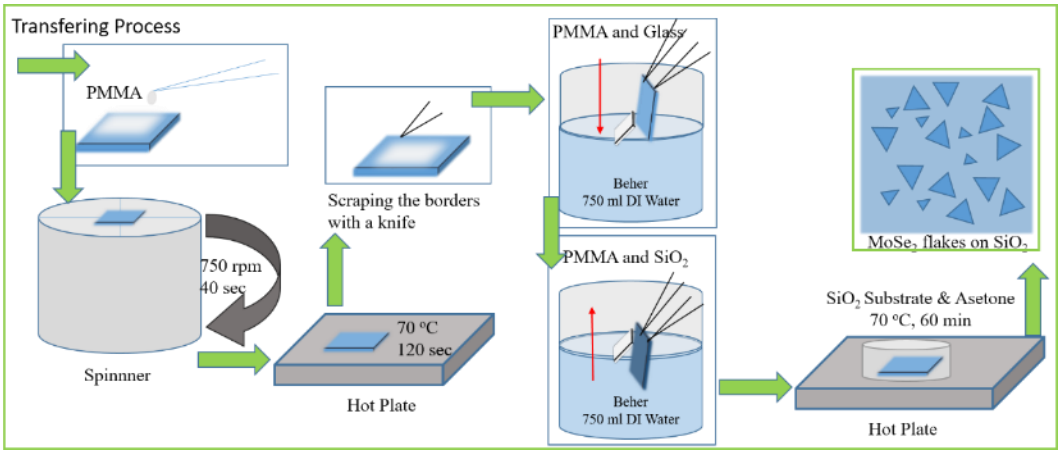

Figure 7-6 *Transferring process scheme*

In Figure 7-7 a, b Bright field and dark field microscopy images of $MoSe_2$ grown on glass substrate are shown before transferring processes. Glass substrate is transparent material and the surface is not smoot as SiO_2 substrate due to CVD reactions. In Figure 7-7 c, d Bright field, and dark field microscopy images of monolayer $MoSe_2$ transferred on SiO_2 substrate are shown, the boundaries of the produced flakes are now easily

distinguished. The surface of the substrate smooth which is beneficial for device fabrication.

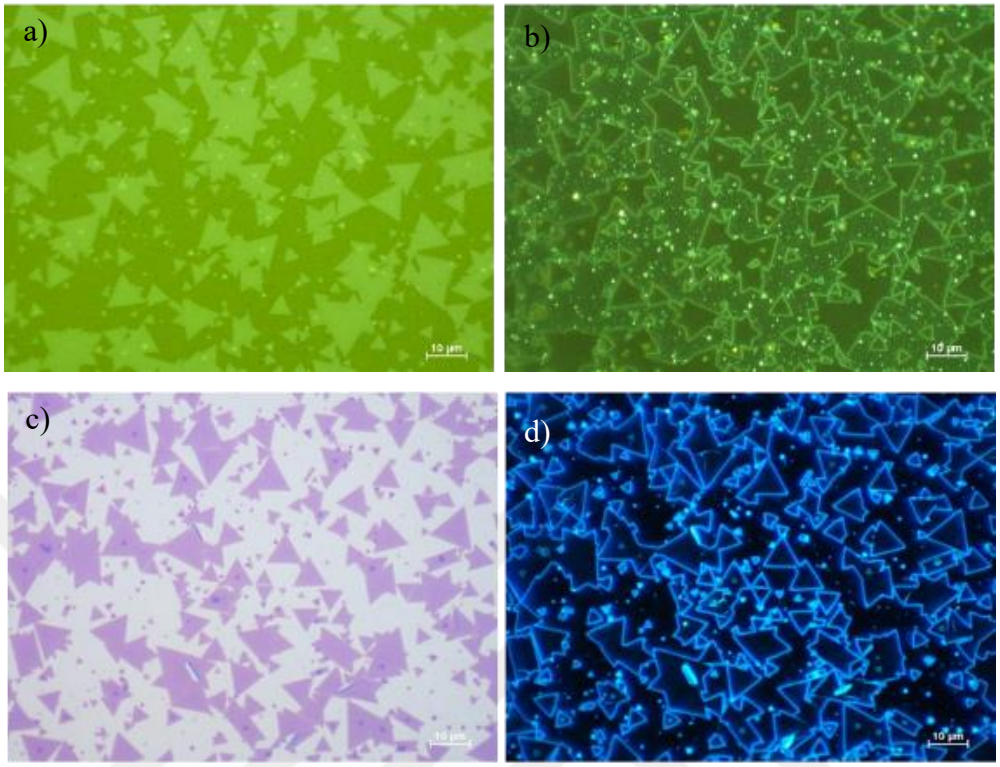

Figure 7-7 *a) BF microscopy image of monolayer $MoSe_2$ grown on glass substrate b) DF microscopy image of monolayer $MoSe_2$ grown on glass substrate c) BF microscopy image of monolayer $MoSe_2$ transferred on SiO_2 substrate d) DF microscopy image of monolayer $MoSe_2$ transferred on SiO_2 substrate*

7.3. Lithography

Photoresist and developer are used to be ready for mask aligner, the mask is on a flat glass (10 cm *10 cm) the photoresist is AZ350, which is very important, and one dropped to SiO_2 substrate than it is spinned with a spin velocity 750 rpm for 40 seconds. After photoresist is coated homogeneously, it is heated to 70 ^{o}C for 120 seconds. Now it is ready to for lithography.

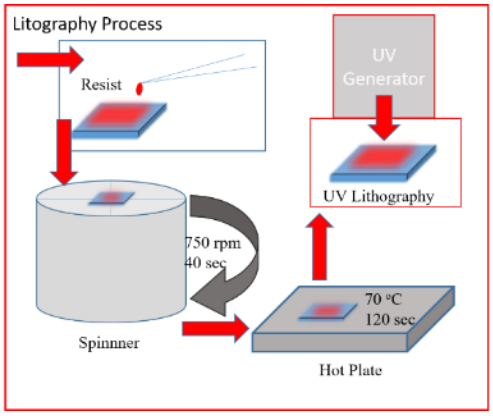

Figure 7-8 *Lithography process scheme*

Lithography process is very critical because, there are a lot of preparing steps, such as focusing the laser, matching the substrate and mask. There are two kinds of mask one is positive mask that we use, in this time of mask, the dark parts are stationary other parts are perish by UV, the second one is negative mask which remains only bright side and the dark parts are perish by UV light (Figure 7-9). Positive mask are far more useful and user friendly, because it can be easily seen which part will be remain and perish. While replacing the mask and SiO_2 substrate the movements have to be slowly and carefully, because it can easily damage to flakes and the mask can be broken. (Figure 7-8).

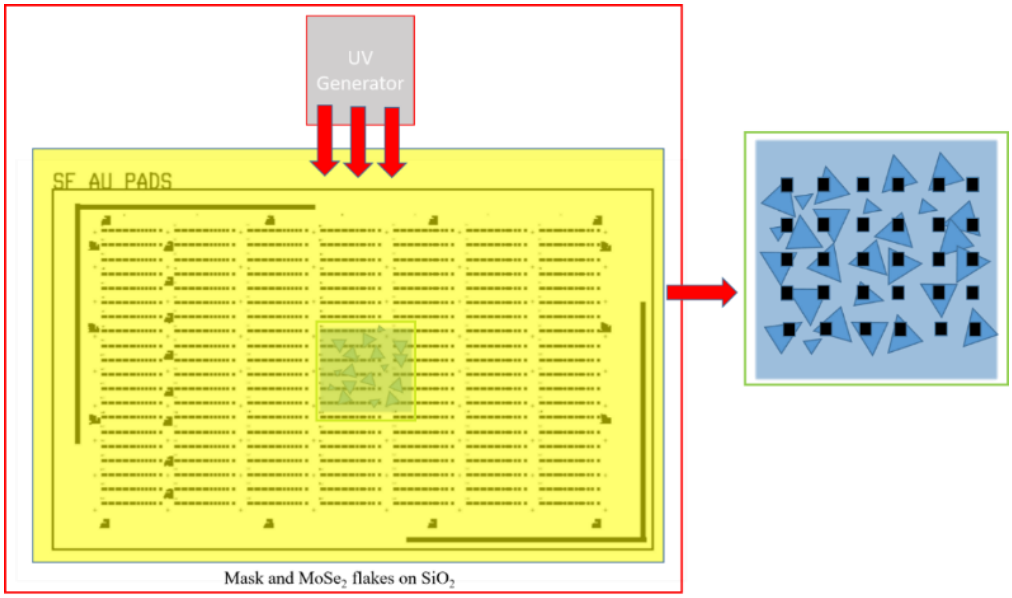

Figure 7-9 *Lithography process mechanism*

7.4. Metal Coating Process

After UV lithography, photoresist coated flakes are ready to be metal coated, this process is very important because the metal contact of the FET devices are fabricated in this process. In metal coating process, thermal evaporation of Titanium/Gold (10nm/90nm) metal contacts is carried out carefully (Figure 7-10). 1500 ampere goes through the copper line. This heat makes powder gas phase quickly, after coating process; the metal layer has to be lifted off by using acetone (Figure 7-11).

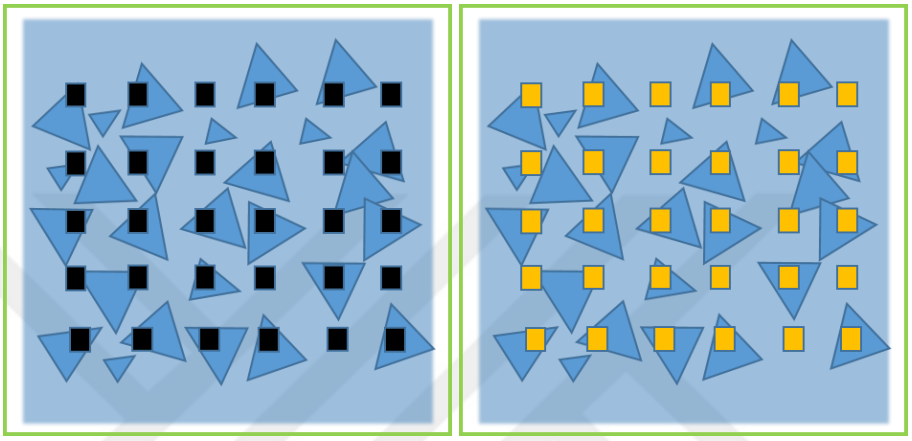

Figure 7-10 *Metal coating process scheme*

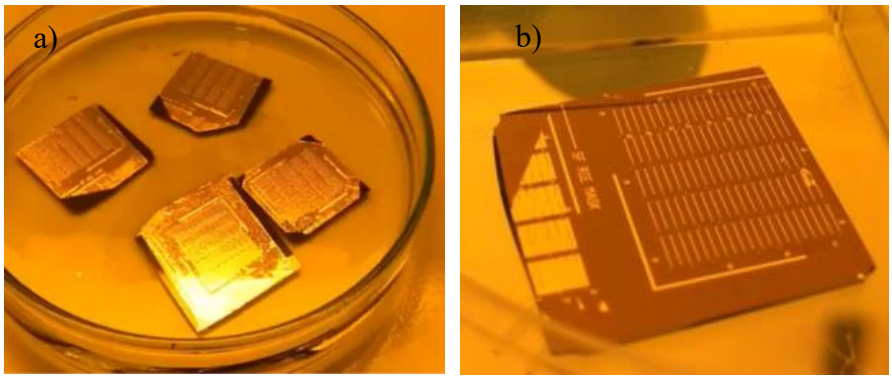

Figure 7-11 *a) Lift off process of metal coating a) After liftoff process, metal contacts are seen*

7.5. Electrical Measurements

Back gate configuration of $MoSe_2$ FET is shown in Figure 7-12 a. The silicon substrate is used as the back gate contact. Electrical characterizations of fabricated devices are performed with a home-built probe station (Figure 7-12 b) [37, 99] .

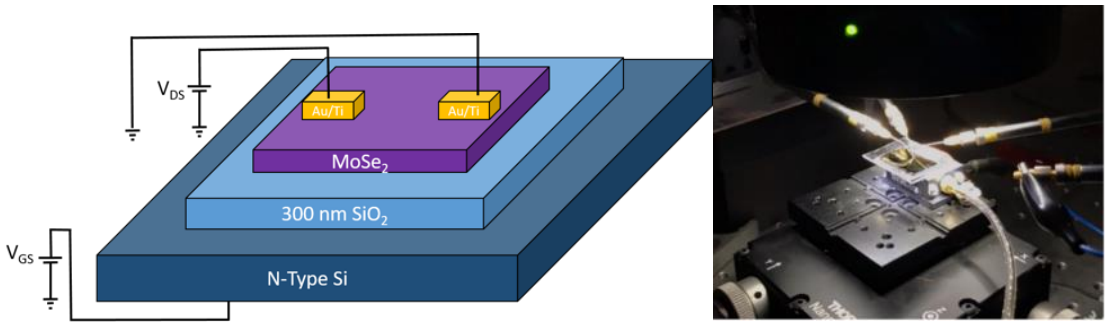

Figure 7-12 a) *Back gate configuration of $MoSe_2$ FET b) Electrical measurements of FET*

Threshold Voltage is calculated as 94.4 Volts (7.1). The voltage between drain and source is kept constant 6 Volts. In addition, the channel length is fabricated as 4 micrometers; the channel width is 2.66 micrometers. ON/OFF ratio is founded 10^4. The mobility of FET device fabricated on monolayer $MoSe_2$ is calculated as 37 $cm^2\ V^{-1}\ s^{-1}$ (Figure 7-13 & Figure 7-14).

$$\mu = \frac{L_{ch}}{W_{ch}} \cdot \frac{1}{V_d \cdot C_{ox}} \cdot \frac{dI_{ds}}{dV_{ds}}$$
$$C_{ox} = \epsilon_0 \cdot \epsilon_r / t \qquad (7.1)$$

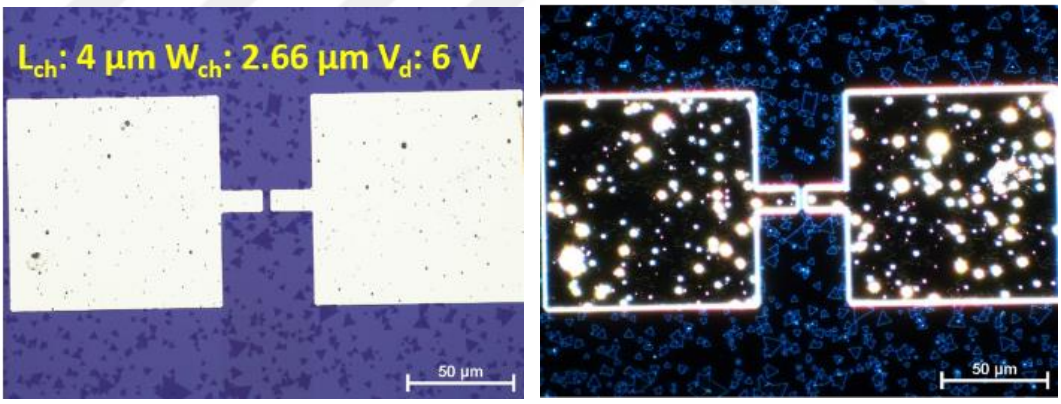

Figure 7-13 *a) BF microscopy image Back gate configuration of $MoSe_2$ FET b) DF microscopy image Back gate configuration of $MoSe_2$ FET*

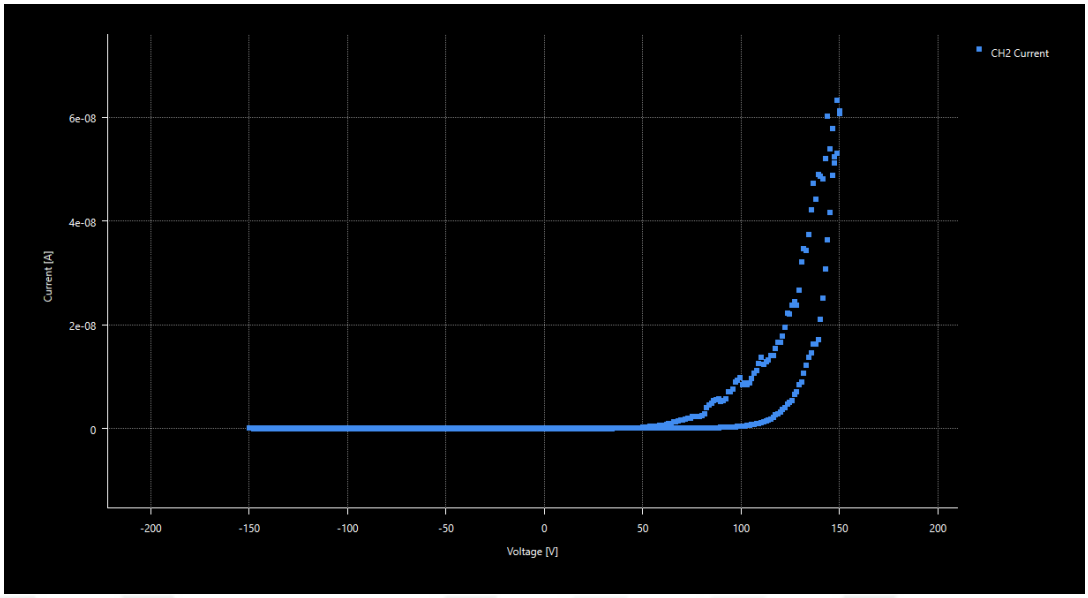

Figure 7-14 *I/V measurements of fabricated $MoSe_2$ FET*

8. CONCLUSION AND FUTURE WORKS

Two-dimensional transition metal dichalcogenide (2-D, TMDC) and their alloys such as, molybdenum sulphide (MoS_2), molybdenum sulphoselenide ($MoS_{2(1-x)}$-Se_{2x} (x=0-1)), molybdenum selenide ($MoSe_2$), and their alloys are successfully produced by CVD technique. These TDMCs have important potential as candidates for new devices in optoelectronics, semiconductor electronics, photodetectors, photovoltaics and energy harvesting. We present repeatable MoS_2, $MoS_{2(1-x)}$-Se_{2x}, $MoSe_2$ monolayer growth through systematic investigation of CVD growth parameters such as gas flow rates, substrate temperature and precursor concentration (S/Se ratio). We obtained a full control of the x value (x=0-1) allowing for bandgap modify between 1.82 eV (MoS_2) and 1.56 eV ($MoSe_2$). We obtain the reaction temperature and S/Se ratio are the most important parameters, to control the composition (x=0-1) of the monolayer alloy TMDCs. We performed measurements, which include photoluminescence (PL) measurement, Raman spectroscopy measurement, and dark field image measurement, atomic force microscopy (AFM) measurements, scanning electron microcopy (SEM) measurements. The field effect transistor (FET) devices using 2D $MoSe_2$ flakes are fabricated and the performance measurements are demonstrated. Horizontal CVD configuration and using glass as a catalyzer are advantageous to obtain high coverage and large monolayer $MoSe_2$ flakes. Thus, glass impurities such as Na, Mg, and Ca support the monolayer growth. We confirm that NaCl supports CVD kinetics for monolayer formation by reducing the strength of Van der Waals bonds between interlayers of $MoSe_2$ flakes and hindering multi-layer formation and enlarges homogeneous, laterally grown monolayer device-quality $MoSe_2$ flakes, which is crucial for practical applications of 2D TMDCs.

Using glass positively effects monolayer growth due to glass impurity, Na, Mg, and Cas. To understand the effects of these elements, new salts can be used as catalyzers such as, NaCl, CaCl, KCl, and KIO_2. Reaction temperature, precursor ratio, fast cooling are the most important CVD parameters, more parameters can be optimized with different salts as catalyzers for a better growth recipe for producing high quality monolayer films. Using optimized recipe, new heterostructures of TMDCs can be produced in one-step CVD process. New design of FETs devices structures can be fabricated from these heterostructures and other members of TMDCs family.

REFERENCES

[1] F. Crowne, Classical gradual-channel modeling of graphene field-effect transistors (FETS), 2012, pp. 1-54.
[2] F. Crowne, Classical Gradual-Channel Modeling of Graphene Field-Effect Transistors (FETs), DOI (2010) 78.
[3] B. B Wymore, Electrochemically Prepared Graphene Field Effect Transistors and Magnetoresistive Devices, DOI (2014).
[4] M. Velický, P.S. Toth, From two-dimensional materials to their heterostructures: An electrochemist's perspective, Applied Materials Today, 8 (2017) 68-103.
[5] S. Mao, Graphene Field-Effect Transistor Sensors, 2018, pp. 113-132.
[6] A. K. N. Geim, K.S. Novoselov, The Rise of Graphene, Nature materials, 6 (2007) 183-191.
[7] K.S. Novoselov, D. Jiang, F. Schedin, T.J. Booth, V.V. Khotkevich, S.V. Morozov, A.K. Geim, Two-dimensional atomic crystals, Proceedings of the National Academy of Sciences of the United States of America, 102 (2005) 10451.
[8] K.S. Novoselov, A.K. Geim, S.V. Morozov, D. Jiang, M.I. Katsnelson, I.V. Grigorieva, S.V. Dubonos, A.A. Firsov, Two-dimensional gas of massless Dirac fermions in graphene, Nature, 438 (2005) 197-200.
[9] A.K. Geim, I.V. Grigorieva, Van der Waals heterostructures, Nature, 499 (2013) 419.
[10] P. Miró, M. Audiffred, T. Heine, An atlas of two-dimensional materials, Chemical Society reviews, 43 (2014).
[11] P.R. Wallace, The Band Theory of Graphite, Physical Review, 71 (1947) 622-634.
[12] L. Madkour, Carbon Nanomaterials and Two-Dimensional Transition Metal Dichalcogenides (2D TMDCs), 2019, pp. 165-245.
[13] M.S. Dresselhaus, P.T. Araujo, Perspectives on the 2010 Nobel Prize in Physics for Graphene, ACS Nano, 4 (2010) 6297-6302.
[14] J. Liu, C. Poh, D. Zhan, L. Lai, S. Lim, L. Wang, X. Liu, N. Sahoo, C. Li, Z. Shen, J. Lin, Improved synthesis of graphene flakes from the multiple electrochemical exfoliation of graphite rod, Nano Energy, 2 (2013) 377-386.
[15] Y. Xu, H. Cao, Y. Xue, B. Li, W. Cai, Liquid-Phase Exfoliation of Graphene: An Overview on Exfoliation Media, Techniques, and Challenges, Nanomaterials, 8 (2018) 942.
[16] C. Xu, T. Peng, M. Guan, Q. Zhang, X. Ma, The preparation and the photoelectric characteristics of graphene/MoSe 2 heterojunction, IOP Conference Series: Materials Science and Engineering, 397 (2018) 012055.
[17] H. Jisong, W. Duan, H. He, H. Lv, C. Huang, X. Ma, A Promising Strategy to Tune the Schottky Barrier of MoS2(1-x)Se2x/ graphene Heterostructure by Asymmetric Se Doping, Journal of Materials Chemistry C, DOI 10.1039/C9TC01873E(2019).
[18] T. Taira, T. Shinohara, S. Obata, K. Saiki, Real-time observation on hot-filament-assisted CVD growth of graphene, Japanese Journal of Applied Physics, 58 (2019) SIIB24.
[19] A. Ramasubramaniam, D. Naveh, E. Towe, Tunable Band Gaps in Bilayer Graphene−BN Heterostructures, Nano Letters, 11 (2011) 1070-1075.
[20] S. Ebadzadeh, H. Goudarzi, M. Khezerlou, Tuneable superconducting effective gap in graphene-TMDC heterostructures, 2019.
[21] A. Kolobov, J. Tominaga, Magnetism in 2D TMDC, 2016, pp. 365-388.

[22] D. Alameri, J. R Nasr, D. Karbach, Y. Liu, R. Divan, S. Das, I. Kuljanishvili, Mask-free patterning and selective CVD-growth of 2D-TMDCs semiconductors, Semiconductor Science and Technology, 34 (2019) 085010.
[23] R. Mishra, Ultrafast Characterization 2D Semiconducting TMDC for Nanoelectronics Application, 2018.
[24] A. David, G. Burkard, A. Kormányos, Effective theory of monolayer TMDC double quantum dots, 2D Materials, 5 (2018).
[25] A. Kolobov, J. Tominaga, Emerging applications of 2D TMDCs, 2016, pp. 473-512.
[26] H.O. Pierson, 2 - Fundamentals of Chemical Vapor Deposition, Handbook of Chemical Vapor Deposition (CVD) (Second Edition), William Andrew Publishing, Norwich, NY, 1999, pp. 36-67.
[27] H.O. Pierson, 3 - The Chemistry of CVD, Handbook of Chemical Vapor Deposition (CVD) (Second Edition), William Andrew Publishing, Norwich, NY, 1999, pp. 68-83.
[28] H.O. Pierson, 5 - CVD Processes and Equipment, Handbook of Chemical Vapor Deposition (CVD) (Second Edition), William Andrew Publishing, Norwich, NY, 1999, pp. 108-146.
[29] M. Bay, A. Özden, F. Ay, N.K. Perkgöz, Bandgap tuning of Monolayer MoS 2(1-x) Se 2x alloys by optimizing parameters, Materials Science in Semiconductor Processing, 99 (2019) 134 - 139.
[30] M.D. Allendorf, T.M. Besmann, R.J. Kee, M.T. Swihart, Chapter 3 Modeling CVD Processes, Chemical Vapour Deposition: Precursors, Processes and Applications, The Royal Society of Chemistry2009, pp. 93-157.
[31] M. Azad Malik, P. O'Brien, Chapter 5 Basic Chemistry of CVD and ALD Precursors, Chemical Vapour Deposition: Precursors, Processes and Applications, The Royal Society of Chemistry2009, pp. 207-271.
[32] V. Kranthi Kumar, S. Dhar, T.H. Choudhury, S.A. Shivashankar, S. Raghavan, A predictive approach to CVD of crystalline layers of TMDs: the case of MoS2, Nanoscale, 7 (2015) 7802-7810.
[33] N. Changbin, Y. Leyong, W. Xingzhan, S. Jun, L. Wenqiang, C. Weimin, F. Shuanglong, S. Haofei, Ultrafast growth of large-area monolayer MoS 2 film via gold foil assistant CVD for a highly sensitive photodetector, Nanotechnology, 28 (2017) 275203.
[34] A.B. Leese, A.R. Mills, Chapter 13 Commercial Aspects of CVD, Chemical Vapour Deposition: Precursors, Processes and Applications, The Royal Society of Chemistry2009, pp. 535-570.
[35] D.K. Ferry, Semiconductors, Bonds and bands, IOP Publishing, 2013.
[36] RadisavljevicB, RadenovicA, BrivioJ, GiacomettiV, KisA, Single-layer MoS2 transistors, Nat Nano, 6 (2011) 147-150.
[37] B.G. Streetman, Solid state electronic devices, Prentice-hall, New Jersey :, 1980.
[38] L. Yu, D. El-Damak, U. Radhakrishna, X. Ling, A. Zubair, Y. Lin, Y. Zhang, M.-H. Chuang, Y.-H. Lee, D. Antoniadis, J. Kong, A. Chandrakasan, T. Palacios, Design, Modeling, and Fabrication of Chemical Vapor Deposition Grown MoS2 Circuits with E-Mode FETs for Large-Area Electronics, Nano Letters, 16 (2016) 6349-6356.
[39] L.M. Xie, Two-dimensional transition metal dichalcogenide alloys: preparation, characterization and applications, Nanoscale, 7 (2015) 18392-18401.
[40] J. Zheng, X. Yan, Z. Lu, H. Qiu, G. Xu, X. Zhou, P. Wang, X. Pan, K. Liu, L. Jiao, High-Mobility Multilayered MoS2 Flakes with Low Contact Resistance Grown by Chemical Vapor Deposition, Advanced Materials, 29 (2017) 1604540.
[41] U. Gupta, S.N. Boddu, U. Maitra, A. Singh, S. Shirodkar, U. Waghmare, C.N.R. Rao, Characterization of few-layer 1T-MoSe2 and its superior performance in the visible-light induced hydrogen evolution reaction, 2014.

[42] D. Nam, J.-U. Lee, H. Cheong, Excitation energy dependent Raman spectrum of MoSe2, Scientific Reports, 5 (2015) 17113.
[43] H. Li, X. Duan, X. Wu, X. Zhuang, H. Zhou, Q. Zhang, X. Zhu, W. Hu, P. Ren, P. Guo, L. Ma, X. Fan, X. Wang, J. Xu, A. Pan, X. Duan, Growth of Alloy MoS2xSe2(1–x) Nanosheets with Fully Tunable Chemical Compositions and Optical Properties, Journal of the American Chemical Society, 136 (2014) 3756-3759.
[44] Q. Feng, N. Mao, J. Wu, H. Xu, C. Wang, J. Zhang, L. Xie, Growth of MoS2(1–x)Se2x (x = 0.41–1.00) Monolayer Alloys with Controlled Morphology by Physical Vapor Deposition, ACS Nano, 9 (2015) 7450-7455.
[45] C. Jung, S. Min Kim, H. Moon, G. Han, J. Kwon, Y.K. Hong, I. Omkaram, Y. Yoon, S. Kim, J. Park, Highly Crystalline CVD-grown Multilayer MoSe2 Thin Film Transistor for Fast Photodetector, 2015.
[46] C. Jung, S.M. Kim, H. Moon, G. Han, J. Kwon, Y.K. Hong, I. Omkaram, Y. Yoon, S. Kim, J. Park, Highly Crystalline CVD-grown Multilayer MoSe2 Thin Film Transistor for Fast Photodetector, Scientific Reports, 5 (2015) 15313.
[47] J. Kang, S. Tongay, J.J. Li, J. Wu, Monolayer semiconducting transition metal dichalcogenide alloys: Stability and band bowing, 2013.
[48] J.C. Shaw, H. Zhou, Y. Chen, N.O. Weiss, Y. Liu, Y. Huang, X. Duan, Chemical vapor deposition growth of monolayer MoSe2 nanosheets, Nano Research, 7 (2014) 511-517.
[49] C. Jung, S.M. Kim, H. Moon, G. Han, J. Kwon, Y.K. Hong, I. Omkaram, Y. Yoon, S. Kim, J. Park, Highly Crystalline CVD-grown Multilayer MoSe(2) Thin Film Transistor for Fast Photodetector, Scientific Reports, 5 (2015) 15313.
[50] A.S. Pawbake, M.S. Pawar, S.R. Jadkar, D.J. Late, Large area chemical vapor deposition of monolayer transition metal dichalcogenides and their temperature dependent Raman spectroscopy studies, Nanoscale, 8 (2016) 3008-3018.
[51] Y.-H. Chang, W. Zhang, Y. Zhu, Y. Han, J. Pu, J.-K. Chang, W.-T. Hsu, J.-K. Huang, C.-L. Hsu, M.-H. Chiu, T. Takenobu, H. Li, C.-I. Wu, W.-H. Chang, A.T.S. Wee, L.-J. Li, Monolayer MoSe2 Grown by Chemical Vapor Deposition for Fast Photodetection, ACS Nano, 8 (2014) 8582-8590.
[52] X. Lu, M.I.B. Utama, J. Lin, X. Gong, J. Zhang, Y. Zhao, S.T. Pantelides, J. Wang, Z. Dong, Z. Liu, W. Zhou, Q. Xiong, Large-Area Synthesis of Monolayer and Few-Layer MoSe2 Films on SiO2 Substrates, Nano Letters, 14 (2014) 2419-2425.
[53] Y. Zhao, H. Lee, W. Choi, W. Fei, C.J. Lee, Large-area synthesis of monolayer MoSe2 films on SiO2/Si substrates by atmospheric pressure chemical vapor deposition, RSC Advances, 7 (2017) 27969-27973.
[54] Y. Lei, S. Pakhira, K. Fujisawa, X. Wang, O.O. Iyiola, N. Perea López, A. Laura Elías, L. Pulickal Rajukumar, C. Zhou, B. Kabius, N. Alem, M. Endo, R. Lv, J.L. Mendoza-Cortes, M. Terrones, Low-temperature Synthesis of Heterostructures of Transition Metal Dichalcogenide Alloys (WxMo1–xS2) and Graphene with Superior Catalytic Performance for Hydrogen Evolution, ACS Nano, 11 (2017) 5103-5112.
[55] P. Nihan Kosku, B. Mehmet, Investigation of Single-Wall MoS2 Monolayer Flakes Grown by Chemical Vapor Deposition, Nano-Micro Letters, 8 (2015).
[56] Q. Gong, L. Cheng, C. Liu, M. Zhang, Q. Feng, H. Ye, M. Zeng, L. Xie, Z. Liu, Y. Li, Ultrathin MoS 2(1– x) Se 2 x Alloy Nanoflakes For Electrocatalytic Hydrogen Evolution Reaction, ACS Catalysis, 5 (2015) 2213-2219.
[57] J. Sun, X. Li, W. Guo, M. Zhao, X. Fan, Y. Dong, C. Xu, J. Deng, Y. Fu, Synthesis Methods of Two-Dimensional MoS2: A Brief Review, Crystals, 7 (2017) 198.

[58] T.-J. Dai, X.-D. Fan, Y.-X. Ren, S. Hou, Y.-Y. Zhang, L.-X. Qian, Y.-R. Li, L. Xing-Zhao, Layer-controlled synthesis of wafer-scale MoSe2 nanosheets for photodetector arrays, Journal of Materials Science, 53 (2018).
[59] K.F. Mak, C. Lee, J. Hone, J. Shan, T.F. Heinz, Atomically Thin ${\mathrm{MoS}}_{2}$: A New Direct-Gap Semiconductor, Physical Review Letters, 105 (2010) 136805.
[60] H. Wang, D. Zhu, F. Jiang, P. Zhao, H. Wang, Z. Zhang, x. chen, C. Jin, Revealing the microscopic CVD growth mechanism of MoSe2 and the role of hydrogen gas during the growth procedure, Nanotechnology, 29 (2018).
[61] Y. Li, K. Zhang, F. Wang, Y. Feng, Y. Li, Y. Han, D. Tang, B. Zhang, H.S.P. Wong, Scalable Synthesis of Highly Crystalline MoSe2 and Its Ambipolar Behavior, ACS Applied Materials & Interfaces, 9 (2017).
[62] S. Zhao, M. Lu, S. Xue, L. Yan, M. Peng, Y. Hang, X. Wang, Z. Liu, y. Wang, L. Tao, Y. Sui, Y. Wang, A Se vacancy induced localized Raman mode in two-dimensional MoSe2 grown by CVD, 2019.
[63] W. Zhang, X. Li, T. Jiang, J. Song, Y. Lin, L. Zhu, X. Xu, CVD synthesis of Mo (1−x) W x S 2 and MoS 2(1−x) Se 2x alloy monolayers aimed at tuning the bandgap of molybdenum disulfide, Nanoscale, 7 (2015).
[64] H. Taghinejad, D. Rehn, C. Muccianti, A. Eftekhar, M. Tian, T. Fan, X. Zhang, Y. Meng, Y. Chen, t.-v. Nguyen, S. Shi, P. M. Ajayan, J. Schaibley, E. Reed, A. Adibi, Defect-Mediated Alloying of Monolayer Transition-Metal Dichalcogenides, ACS Nano, 12 (2018).
[65] J. Gusakova, V. Gusakov, B.K. Tay, DFT study of structural and electronic properties of MoS 2(1−x) Se 2x alloy (x = 0.25), Journal of Applied Physics, 123 (2018) 161594.
[66] S. Hussain, K. Akbar, D. Vikraman, H.-S. Kim, S.-H. Chun, J. Jung, Few-layer thickness of MoSSe alloy by RF sputtering–CVD route for enhanced hydrogen evolution reaction, 2018.
[67] H. Mogi, Y. Kobayashi, A. Taninaka, R. Sakurada, T. Takeuchi, S. Yoshida, O. Takeuchi, Y. Miyata, H. Shigekawa, Scanning tunneling microscopy/spectroscopy on MoS 2 embedded nanowire formed in CVD-grown Mo 1− x W x S 2 alloy, Japanese Journal of Applied Physics, 56 (2017) 08LB06.
[68] F.-Q. Huang, W. Zhao, J. Pan, F. Yuqiang, X. Che, D. Wang, b. Kejun, Metastable MoS2 : Crystal Structure, Electronic Band Structure, Synthetic Approach and Intriguing Physical Properties, Chemistry, 24 (2018).
[69] M. Yi, Z. Shen, A review on mechanical exfoliation for scalable production of graphene, J. Mater. Chem. A, 3 (2015).
[70] P. R, R. S, M. Savith, M. Balachandar, REVIEW OF PHYSICAL VAPOUR DEPOSITION (PVD) TECHNIQUES, 2013.
[71] R. W. Johnson, A. Hultqvist, S. Bent, A brief review of atomic layer deposition: From fundamentals to applications, Materials Today, 17 (2014).
[72] K. Piglmayer, M. Boman, M. Lindstam, R. Chabicovsky, Photon assisted CVD, Journal De Physique Iv - J PHYS IV, 11 (2001).
[73] X. Tong, E. Ashalley, F. Lin, H. Li, Z. M. Wang, Advances in MoS2-based field-effect transistors (FETs), Nano-Micro Letters, 7 (2015).
[74] D. Andrzejewski, H. Myja, M. Heuken, A. Grundmann, H. Kalisch, A. Vescan, T. Kuemmell, G. Bacher, Scalable large-area p-i-n light emitting diodes based on WS 2 monolayers grown via MOCVD, ACS Photonics, DOI 10.1021/acsphotonics.9b00311(2019).

[75] M. Sial, M. Usman, B. Zheng, Y.-N. Yu, A. Mavrič, Q. Fangzhu, M. Valant, Z. M. Wang, CVD Growth of Molybdenum Diselenide Surface Structures with Tailored Morphology, CrystEngComm, 20 (2018).
[76] P. Yang, A.-G. Yang, L. Chen, J. Chen, Y. Zhang, H. Wang, L. Hu, R.-J. Zhang, R. Liu, X.-P. Qu, Z.-J. Qiu, C. Cong, Influence of seeding promoters on the properties of CVD grown monolayer molybdenum disulfide, Nano Research, DOI 10.1007/s12274-019-2294-y(2019).
[77] R. Sharma, K. Sahoo, P. Rastogi, R. Biroju, W. Theis, T. Narayanan, On the Synthesis of Morphology Controlled Transition Metal Dichalcogenides via CVD for Electrochemical Hydrogen Generation, physica status solidi (RRL) - Rapid Research Letters, DOI 10.1002/pssr.201900257(2019).
[78] S. Irvine, D. Lamb, photo-assisted cvd, 2008, pp. 477-493.
[79] G.A. Saenz, C. de Anda Orea, A. Bandyopadhyay, A. B. Kaul, Photocurrent enhancement of CVD MoS2 photodetector via nanoplasmonics, 2019.
[80] J. Creighton, P. Ho, Introduction to Chemical Vapor Deposition (CVD), ASM International, DOI (2001).
[81] S. Li, S. Wang, D.-M. Tang, W. Zhao, H. Xu, L. Chu, Y. Bando, D. Golberg, G. Eda, Halide-assisted atmospheric pressure growth of large WSe2 and WS2 monolayer crystals, Applied Materials Today, 1 (2015) 60-66.
[82] M. T. Thompson, Introduction to Field-Effect Transistors (FETs) and Amplifiers, 2014, pp. 297-339.
[83] T. Yamada, Analysis of Carbon Nanotube Field-Effect-Transistors(FETs), 1999.
[84] S. Ahmed, J. Yi, Two-Dimensional Transition Metal Dichalcogenides and Their Charge Carrier Mobilities in Field-Effect Transistors, Nano-Micro Letters, 9 (2017) 50.
[85] T. Dai, Y. Liu, X. Liu, D. Xie, Y. Li, High performance photodetectors constructed on atomically thin few-layer MoSe2 synthesized using atomic layer deposition and a chemical vapor deposition chamber, Journal of Alloys and Compounds, 785 (2019).
[86] I. Omkaram, Y.K. Hong, S. Kim, Transition Metal Dichalcogenide Photodetectors, 2018.
[87] P. Kumar, H. Abuhimd, W. Wahyudi, M. Li, J. Ming, L. Li, Review—Two-Dimensional Layered Materials for Energy Storage Applications, ECS Journal of Solid State Science and Technology, 5 (2016) Q3021-Q3025.
[88] D.R. Kumar, S. Sahoo, E. Joanni, D.R. Singh, r.m. Yadav, R. Verma, D. Singh, W. Tan, A. Pérez Del Pino, S. Moshkalev, A. Matsuda, A review on synthesis of graphene, h-BN and MoS2 for energy storage applications: Recent progress and perspectives, Nano Research, 12 (2019).
[89] R. Krishna, T. Unsworth, R. Edge, Raman Spectroscopy and Microscopy, 2016.
[90] S. Sugai, T. Ueda, K. Murase, Raman Scattering in MoS2, MoSe2 and α-MoTe2, J. Phys. Colloques, 42 (1981) 320-322.
[91] T. Sekine, M. Izumi, T. Nakashizu, K. Uchinokura, E. Matsuura, Raman Scattering and Infrared Reflectance in 2H-MoSe2, Journal of The Physical Society of Japan - J PHYS SOC JPN, 49 (1980) 1069-1077.
[92] D. Tuschel, Photoluminescence spectroscopy using a Raman spectrometer, 31 (2016) 14-21.
[93] K.V.R. Murthy, H. Virk, Luminescence Phenomena: An Introduction, Defect and Diffusion Forum, 347 (2013) 1-34.
[94] W. Zhou, R. Apkarian, Z. Wang, D. Joy, Fundamentals of Scanning Electron Microscopy (SEM), 2006, pp. 1-40.

[95] J. Seyforth, Scanning Electron Microscopy (SEM): An Introduction to the use of SEM for character- ising the Surface Topology and Composition of Matter with Further Applications, DOI (2015).
[96] X. Wang, K. Kang, S. Chen, R. Du, E.-H. Yang, Location-Specific Growth and Transfer of Arrayed MoS2 Monolayers with Controllable Size, 2D Materials, 4 (2017).
[97] P. Goodhew, General Introduction to Transmission Electron Microscopy (TEM), 2011, pp. 1-19.
[98] J. C. Shaw, H. Zhou, Y. Chen, N. O. Weiss, Y. Liu, Y. Huang, X. Duan, Chemical vapor deposition growth of monolayer MoSe2 nanosheets, 2015.
[99] D. Neamen, AN INTRODUCTION TO SEMICONDUCTOR DEVICES, MCGRAW HILL HIGHER EDUCATION, BOSTON BURR RIDGE, 2006.
[100] D.L. Plata, A.J. Hart, C.M. Reddy, P.M. Gschwend, Early Evaluation of Potential Environmental Impacts of Carbon Nanotube Synthesis by Chemical Vapor Deposition, Environmental Science & Technology, 43 (2009) 8367-8373.
[101] R.S. Balmer, J.R. Brandon, S.L. Clewes, H.K. Dhillon, J.M. Dodson, I. Friel, P.N. Inglis, T.D. Madgwick, M.L. Markham, T.P. Mollart, N. Perkins, G.A. Scarsbrook, D.J. Twitchen, A.J. Whitehead, J.J. Wilman, S.M. Woollard, Chemical vapour deposition synthetic diamond: materials, technology and applications, Journal of Physics: Condensed Matter, 21 (2009) 364221.
[102] Y. Yue, Y. Feng, J. Chen, D. Zhang, W. Feng, Two-dimensional large-scale bandgap-tunable monolayer MoS2(1-x)Se2x/graphene heterostructures for phototransistors, Journal of Materials Chemistry C, 5 (2017) 5887-5896.
[103] T. Chen, Y. Zhou, Y. Sheng, X. Wang, S. Zhou, J. Warner, Hydrogen-Assisted Growth of Large-Area Continuous Films of MoS 2 on Monolayer Graphene, 2018.
[104] J. Chen, X. Zhao, S.J.R. Tan, H. Xu, B. Wu, B. Liu, D. Fu, W. Fu, D. Geng, Y. Liu, W. Liu, W. Tang, L. Li, W. Zhou, T.C. Sum, K.P. Loh, Chemical Vapor Deposition of Large-Size Monolayer MoSe2 Crystals on Molten Glass, Journal of the American Chemical Society, 139 (2017) 1073-1076.
[105] X. Wang, Y. Gong, G. Shi, W.L. Chow, K. Keyshar, G. Ye, R. Vajtai, J. Lou, Z. Liu, E. Ringe, B.K. Tay, P.M. Ajayan, Chemical Vapor Deposition Growth of Crystalline Monolayer MoSe2, ACS Nano, 8 (2014) 5125-5131.
[106] D. Dumcenco, D. Ovchinnikov, K. Marinov, P. Lazić, M. Gibertini, N. Marzari, O.L. Sanchez, Y.-C. Kung, D. Krasnozhon, M.-W. Chen, S. Bertolazzi, P. Gillet, A. Fontcuberta i Morral, A. Radenovic, A. Kis, Large-Area Epitaxial Monolayer MoS2, ACS Nano, 9 (2015) 4611-4620.
[107] N. Perkgoz, CVD GROWTH and CHARACTERIZATION OF 2D TRANSITION METAL DICHALCOGENIDES, MoS2 and WS2, ANADOLU UNIVERSITY JOURNAL OF SCIENCE AND TECHNOLOGY A - Applied Sciences and Engineering, 18 (2017) 1-1.
[108] K. Tae-Young, S. Younggul, C. Kyungjune, A. Matin, A. Geun Ho, K. Jae-Keun, P. Jinsu, C. Seungjun, J. Ali, L. Takhee, Analysis of the interface characteristics of CVD-grown monolayer MoS 2 by noise measurements, Nanotechnology, 28 (2017) 145702.
[109] D. Wu, J. Shi, X. Zheng, J. Liu, W. Dou, Y. Gao, X. Yuan, F. Ouyang, H. Huang, CVD Grown MoS2 Nanoribbons on MoS2 Covered Sapphire(0001) Without Catalysts, physica status solidi (RRL) - Rapid Research Letters, DOI 10.1002/pssr.201900063(2019).
[110] X. Chen, Y. Ju Park, M. Kang, S.-K. Kang, J. Koo, S. Shinde, J. Shin, S. Jeon, G. Park, Y. Yan, M. Macewan, W. Ray, K.-M. Lee, J. A Rogers, J.-H. Ahn, CVD-grown monolayer MoS2 in bioabsorbable electronics and biosensors, Nature Communications, 9 (2018).

[111] A. Kis, Electrical transport in MOS2: A prototypical semiconducting tmdc, 2017, pp. 295-309.
[112] A. Pezo, M. Paes Lima, M. Costa, A. Fazzio, Electronic transport properties of MoS2 nanoribbons embedded on butadiene solvent, Physical Chemistry Chemical Physics, 21 (2019).
[113] M.-Y. Li, J. Pu, J.-K. Huang, Y. Miyauchi, K. Matsuda, T. Takenobu, L.-J. Li, Self-Aligned and Scalable Growth of Monolayer WSe2–MoS2 Lateral Heterojunctions, Advanced Functional Materials, 28 (2018) 1706860.
[114] S. Wang, Y. Rong, Y. Fan, M. Pacios, H. Bhaskaran, K. He, J.H. Warner, Shape Evolution of Monolayer MoS2 Crystals Grown by Chemical Vapor Deposition, Chemistry of Materials, 26 (2014) 6371-6379.
[115] S. Withanage, M. Lopez, W. Sameen, V. Charles, S. Khondaker, Elucidation of the growth mechanism of MoS2 during the CVD process, MRS Advances, DOI 10.1557/adv.2018.660(2018) 1-6.
[116] S. Hong, A. Krishnamoorthy, C. Sheng, R. K. Kalia, A. Nakano, P. Vashishta, A Reactive Molecular Dynamics Study of Atomistic Mechanisms During Synthesis of MoS2 Layers by Chemical Vapor Deposition, MRS Advances, 3 (2018) 1-5.
[117] Q. Fu, X. Wang, J. Zhou, J. Xia, Q. Zeng, D. Lv, C. Zhu, X. Wang, Y. Shen, X. Li, Y. Hua, F. Liu, Z. Shen, C. Jin, Z. Liu, One-Step Synthesis of Metal/Semiconductor Heterostructure NbS2/MoS2, Chemistry of Materials, 30 (2018).
[118] G.A. Saenz, C. de Anda Orea, A. Kaul, Single and Few-Layer MoS2: CVD Synthesis, Transference, and Photodetection Application, MRS Advances, 2 (2017) 1-6.
[119] X. Lee, X.M. Li, X. Zang, M. Zhu, Y. He, K. Wang, D. Xie, H. Zhu, Role of hydrogen in chemical vapor deposition growth of MoS2 atomic layers, Nanoscale, 7 (2015).
[120] K.F. Mak, K. He, C. Lee, G.H. Lee, J. Hone, T.F. Heinz, J. Shan, Tightly bound trions in monolayer MoS2, Nat Mater, 12 (2013) 207-211.
[121] C. Beatriz López-Posadas, Y. Wei, W. Shen, D. Kahr, M. Hohage, L. Sun, Direct observation of the CVD growth of monolayer MoS 2 using in situ optical spectroscopy, Beilstein Journal of Nanotechnology, 10 (2019) 557-564.
[122] Z. Li, X. Meng, Z. Zhang, Recent Development on MoS 2 -based Photocatalysis: a Review, Journal of Photochemistry and Photobiology C: Photochemistry Reviews, 35 (2017).
[123] R. Laishram, S. Praveen, M. Guisan, P. Garg, J. S. Rawat, C. Prakash, Structural properties of MoS 2 layers grown by CVD technique, Integrated Ferroelectrics, 194 (2018) 16-20.
[124] I. Abid, W. Chen, J. Yuan, S. Najmaei, E. C. Peñafiel, R. Péchou, N. Large, J. Lou, A. Mlayah, Surface enhanced resonant Raman scattering in hybrid MoSe 2 @Au nanostructures, Optics Express, 26 (2018) 29411.
[125] Y. Hwang, N. Shin, Hydrogen-assisted Step-edge Nucleation of MoSe 2 monolayers on Sapphire Substrates, Nanoscale, 11 (2019).
[126] F. Ersan, G. Gökoğlu, A. Ethem, Adsorption and Diffusion of Lithium on Monolayer Transition Metal Dichalcogenides (MoS 2(1-x) Se 2x) Alloys, The Journal of Physical Chemistry C, 119 (2015).
[127] S. Sampath, K. Vankayala, D. Mukherjee, R. Jenjeti, Active Guests in MoS2 / MoSe2 Host Lattice: Efficient Hydrogen Evolution Using Few-Layer Alloys of MoS2(1-x)Se2x, Nanoscale, 6 (2014).
[128] S. Umrao, J. Jeon, S. Min Jeon, Y. Choi, S. Lee, A Homogeneous Atomic Layer MoS2(1-x)Se2x Alloy Prepared by Low-Pressure Chemical Vapor Deposition, and its Properties, Nanoscale, 9 (2016).

[129] L. Yang, Q. Fu, W. Wang, J. Huang, J. Huang, Z. Fan, J. Zhang, B. Xiang, Large-area synthesis of monolayer MoS2(1-x)Se2x with a tunable band gap and its enhanced electrochemical catalytic activity, Nanoscale, 7 (2015).
[130] A. Govind Rajan, J.H. Warner, D. Blankschtein, M.S. Strano, Generalized Mechanistic Model for the Chemical Vapor Deposition of 2D Transition Metal Dichalcogenide Monolayers, ACS Nano, 10 (2016) 4330-4344.
[131] K. Kim, J.-U. Lee, D. Nam, H. Cheong, Davydov Splitting and Excitonic Resonance Effects in Raman Spectra of Few-Layer MoSe2, ACS nano, 10 (2016).
[132] V. Kuraganti, O. Meiron, A. Enyashin, R. Bar-Ziv, M. Bar-Sadan, The Effect of Ru Doping on the Properties of MoSe2 Nanoflowers, The Journal of Physical Chemistry C, 123 (2019) 1987-1994.
[133] H. In Jeong, S. Park, H.I. Yang, W. Choi, Electrical properties of MoSe2 metal-oxide-semiconductor capacitors, Materials Letters, 253 (2019).
[134] H. Shu, Y. Wang, M. Sun, Enhancing electronic and optical properties of monolayer MoSe2 via MoSe2/Blue phosphorene heterobilayer, Physical Chemistry Chemical Physics, 21 (2019).
[135] M. Iqbal, X. Lu, D. Zhan, T. Ha, Y. Yuan, Z. Shen, Q. Xiong, Etching-free patterning on 2D materials for electrical characterizations of CVD-grown MoSe2, Nanoscale, DOI (2014).
[136] D. Nam, J.-U. Lee, H. Cheong, Excitation energy dependent Raman spectrum of MoSe2, Scientific Reports, 5 (2015).
[137] S. Shree, M. A. Semina, C. Robert, B. Han, T. Amand, A. Balocchi, M. Manca, E. Courtade, X. Marie, T. Taniguchi, K. Watanabe, M. Glazov, B. Urbaszek, Exciton-phonon coupling in MoSe2 monolayers, 2018.
[138] B. Wen, Y. Zhu, D. Yudistira, A. Boes, L. Zhang, T. Yildirim, B. Liu, H. Yan, X. Sun, Y. Zhou, Y. Xue, Y. Zhang, L. Fu, A. Mitchell, H. Zhang, Y. Lu, Ferroelectric driven exciton and trion modulation in monolayer MoSe2 and WSe2, 2019.
[139] J. Ma, J. Zheng, X. Zhu, P. Liu, W. Li, B. Wang, First-principles calculations of thermal transport properties in MoS2/MoSe2 bilayer heterostructure, Physical Chemistry Chemical Physics, DOI 10.1039/C9CP01702J(2019).
[140] B. Wang, K. Ostrikov, T. Van der Laan, K. Zheng, R. Shao, M. Zhu, S. S. Zou, Growth and photoluminescence of oriented MoSe2 nanosheets produced by hot filament CVD, RSC Adv., 6 (2016).
[141] X. Mao, Z. Li, J. Zou, G. Zhao, D. Li, Z. Song, Growth controlling behavior of vertically aligned MoSe2 film, Applied Surface Science, 487 (2019).
[142] F. Göhler, E. C. Hadland, C. Schmidt, D. Zahn, F. Speck, D. Johnson, T. Seyller, Growth of Nanocrystalline MoSe2 Monolayers on Epitaxial Graphene from Amorphous Precursors, physica status solidi (b), 256 (2018).
[143] S.-Y. Chen, C. Zheng, M. S Fuhrer, J. Yan, Helicity resolved Raman scattering of MoS2, MoSe2, WS2 and WSe2 atomic layers, Nano letters, 15 (2015).
[144] Y. Yu, G.-H. Nam, Q. He, X.-J. Wu, K. Zhang, Z. Yang, J. Chen, Q. Ma, M. Zhao, Z. Liu, F.-R. Ran, X. Wang, H. Li, X. Huang, B. Li, Q. Xiong, Q. Zhang, Z. Liu, L. Gu, Y. Du, W. Huang, H. Zhang, High phase-purity 1T′-MoS2- and 1T′-MoSe2-layered crystals, Nature Chemistry, 10 (2018) 638-643.
[145] J.-Y. Baek, D. Yin, N. Liu, I. Omkaram, C. Jung, H. Im, S. Hong, S. Min Kim, Y.K. Hong, J. Hur, Y. Yoon, S. Kim, A highly sensitive chemical gas detecting transistor based on highly crystalline CVD-grown MoSe2 films, Nano Research, 10 (2016).
[146] N. Shelke, D. Late, Hydrothermal growth of MoSe2 nanoflowers for photo- and humidity sensor applications, Sensors and Actuators A Physical, 295 (2019) 160-168.

[147] F. Cheng, Z. Hu, H. Xu, Y. Shao, J. Su, Z. Chen, W. Ji, K. Loh, Interface Engineering of Au (111) for the Frowth of 1T'-MoSe2, ACS Nano, 13 (2019).
[148] Q. Duc Truong, N. Hung, Y. Nakayasu, K. Nayuki, Y. Sasaki, M.K. Devaraju, L.-C. Yin, T. Tomai, R. Saito, I. Honma, Inversion domain boundaries in MoSe2 layers, RSC Advances, 8 (2018) 33391-33397.
[149] C. Rogers, D. Gray, N. Bogdanowicz, H. Mabuchi, Laser Annealing for Radiatively Broadened MoSe2 grown by Chemical Vapor Deposition, Physical Review Materials, 2 (2018).
[150] Z. Lu, D. Rhodes, Z. Li, T. Dinh Van, Y. Jiang, J. Ludwig, Z. Jiang, Z. Lian, S.-F. Shi, J. Hone, H. Dery, D. Smirnov, Magnetic field mixing and splitting of bright and dark excitons in monolayer MoSe2, 2019.
[151] V. Kuraganti, A. Jain, R. Bar-Ziv, A. Ramasubramaniam, M. Bar-Sadan, Manganese Doping of MoSe2 Promotes Active Defect Sites for Hydrogen Evolution, ACS Applied Materials & Interfaces, 11 (2019).
[152] X. Zhao, Q. Yang, H. Zhang, Y. Gao, H. Wang, T. Wang, S. Wei, Modulating electronic and magnetic properties of zigzag MoSe2 nanoribbons with different edge structures, Physica E: Low-dimensional Systems and Nanostructures, 109 (2019).
[153] H. Xue, Y. Wang, Y. Dai, W. Kim, H. Jussila, M. Qi, J. Susoma, Z. Ren, Q. Dai, L. Peng, K. Halonen, H. Lipsanen, X. Wang, X. Gan, Z. Sun, A MoSe2/WSe2 Heterojunction-Based Photodetector at Telecommunication Wavelengths, Advanced Functional Materials, 28 (2018).
[154] H. S. Patel, S. P. Shukla, H. Parmar, Optical Response of MoSe2 Crystals, International Journal of Trend in Scientific Research and Development, Volume-1 (2017).
[155] B. Zaidi, C. Shekhar, B. Hadjoudja, S. Gagui, B. Chouial, Optimization of highly efficient monolayer MoSe2 based solar cells, Acta Physica Polonica Series a, 135 (2019).
[156] N. Morell, S. Tepsic, A. Reserbat-plantey, A. Cepellotti, M. Manca, I. Epstein, A. Isacsson, X. Marie, F. Mauri, A. Bachtold, Optomechanical measurement of thermal transport in two-dimensional MoSe2 lattices, 2019.
[157] Z. Ya-Ping, D. Wen-Ming, Z.H.U. Hai-Feng, H. Cheng-Xing, Y.U. Lian-Qing, W. Yong-Qiang, L.I. Zhe, X.U. Fei, Photoelectrochemical Properties of MoSe2 Modified TiO2 Nanotube Arrays, Journal of Inorganic Materials, DOI 10.15541/jim20180463(2019) 1.
[158] N. Berahim, I. Sadegh Amiri, T. Anwar, S.R. Azzuhri, M.N.S. Mohd Nasir, R. Zakaria, W.Y. Chong, C. Lai, S.H. Lee, H. Ahmad, M.A. Ismail, P. Yupapin, Polarizing effect of MoSe2-coated optical waveguides, Results in Physics, 12 (2018).
[159] E. C. Hadland, F. Göhler, G. Mitchson, S. S. Fender, C. Schmidt, D. Zahn, T. Seyller, D. Johnson, Synthesis and Properties of (BiSe)0.97MoSe2: A Heterostructure Containing Both 2H-MoSe2 and 1T-MoSe2, Chemistry of Materials, DOI 10.1021/acs.chemmater.9b01899(2019).
[160] X. Zhang, Z. Yangyang, Y. Zhang, W.-J. Jiang, Q.-H. Zhang, Y.-G. Yang, L. Gu, J.-S. Hu, L.-J. X Wan, Y.Y. Zhang, Y. Zhang, W.J. Zhang, J.S. Jiang, L.J. Hu, Wan, X. Zhang, W.J. Jiang, J.S. Hu, L.J. Wan, L. Gu, Control of 1T-MoSe2 NiSe Heterostructure Nanowire Arrays, 2019.
[161] A. Surrente, D. Dumcenco, Z. Yang, A. Kuc, Y. Jing, T. Heine, Y.-C. Kung, D. Maude, A. Kis, P. Plochocka, Defect Healing and Charge Transfer-Mediated Valley Polarization in MoS2/MoSe2/MoS2 Trilayer van der Waals Heterostructures, Nano Letters, 17 (2017) 4130–4136.
[162] W. Xue, J. Liu, H. Zong, X. Lai, P. Sahoo, H. Rodriguez Gutierrez, D. Voronine, Nano-optical imaging of monolayer MoSe2-WSe2 lateral heterostructure, DOI (2017).

[163] X. Tian, R. Wei, S. Liu, Y. Zhang, J. Qiu, Photoluminescence nonuniformity from self-seeding nuclei in CVD grown monolayer MoSe2, Nanoscale, 10 (2017).
[164] L. Wu, S. Shi, Q. Li, X. Zhang, X. Cui, TiO2 nanoparticles modified with 2D MoSe2 for enhanced photocatalytic activity on hydrogen evolution, International Journal of Hydrogen Energy, 44 (2018).
[165] A. Agarwal, Y. Qin, B. Chen, M. Blei, K. Wu, L. Liu, Y. Shen, D. Wright, M. D Green, H. L. Zhuang, S. Tongay, Anomalous Isoelectronic Chalcogen Rejection in 2D Anisotropic vdW TiS3(1-x)Se3x Trichalcogenides, Nanoscale, 10 (2018).
[166] T. Chen, G. Hao, L. Kou, C. Wang, J. Zhong, Controllable epitaxial growth of MoSe2-MoS2 lateral heterostructures with tunable electrostatic properties, Nanotechnology, 29 (2018).
[167] A.O. Wei-Dong, L.I.U. Yan, M.A. Qing-Shan, L.I.U. Huan, Z. Bin, Z. Xiao-Jia, Y.U. Dong-Qi, Z. Wen-Hua, Controllable Synthesis of Vertically Aligned ReS 2(1-x) Se 2x Nanosheets with Tunable Chemical Compositions and Bandgaps, Journal of Inorganic Materials, 33 (2018) 1083.
[168] Y. Li, F. Wang, D. Tang, J. Wei, Y. Xing, K. Zhang, Controlled synthesis of highly crystalline CVD-derived monolayer MoSe2 and shape evolution mechanism, Materials Letters, 216 (2018) 261-264.
[169] S. Hussain, K. Akbar, D. Vikraman, K. Karuppasamy, H.-S. Kim, S.-H. Chun, J. Jung, Synthesis of MoS2(1-x)Se2x and WS2(1-x)Se2x alloy for enhanced hydrogen evolution reaction performance, Inorg. Chem. Front., 4 (2017).
[170] X. Gu, C.Y. Zhao, Thermal conductivity of single-layer MoS2(1−x)Se2x alloys from molecular dynamics simulations with a machine-learning-based interatomic potential, Computational Materials Science, 165 (2019) 74-81.
[171] Q.-F. Gong, L. Cheng, C. Liu, M. Zhang, Q. Feng, H.-L. Ye, M. Zeng, L.-M. Xie, Z. Liu, Y. Li, Tuning the Chemical Composition of Ultrathin MoS2(1-x)Se2x Nanoflakes Toward Optimal Electrocatalytic Activity for Hydrogen Evolution Reaction, ACS Catalysis, DOI (2015).
[172] J. Kang, S. Tongay, J. Li, J. Wu, Monolayer semiconducting transition metal dichalcogenide alloys: Stability and band bowing, Journal of Applied Physics, 113 (2013) 143703.
[173] B. Rajbanshi, S. Sarkar, P. Sarkar, The electronic and optical properties of MoS2(1-x)Se2x and MoS2(1-x)Te2x monolayers, Physical chemistry chemical physics : PCCP, 17 (2015).
[174] D. Tang, F. Wang, B. Zhang, Y. Li, Y. Li, Y. Feng, Y. Han, J. Ma, T. Ren, K. Zhang, Field effect properties of single-layer MoS2(1−x)Se2x nanosheets produced by a one-step CVD process, Journal of Materials Science, 53 (2018).
[175] D.H. Lü, D.C. Zhu, C. Jin, Preferential substitution of selenium along the grain boundaries in monolayer MoS2(1−x)Se2x alloy, Wuli Huaxue Xuebao/ Acta Physico - Chimica Sinica, 33 (2017) 1514-1519.
[176] Y. Liu, X. Ma, H. Wang, Y. Li, Z. Jin, CdS Photocorrosion Protection by MoSe2 Modification for Photocatalytic Hydrogen Production, Catalysis Surveys from Asia, DOI 10.1007/s10563-019-09275-3(2019).
[177] J.A. Wilson, F.J. Di Salvo, S. Mahajan, Charge-density waves and superlattices in the metallic layered transition metal dichalcogenides, Advances in Physics, 24 (1975) 117-201.
[178] S. Jun Yang, Y. Lee, J. Hong Kim, H.J. Kim, B.K. Choi, H.Y. Jeong, K. Pyo Kim, J. Sik Choi, Y.J. Chang, Single-step synthesis of wrinkled MoSe2 thin films, Current Applied Physics, 19 (2018).

[179] J.W. Huang, L.Q. Luo, B. Jin, S. Chu, R.F. Peng, Synthesis and photoluminescence property of hexangular star MoSe2 bilayer, Wuli Xuebao/Acta Physica Sinica, 66 (2017).
[180] N. Masurkar, N. Kumar, L. Arava, CVD-Grown MoSe2 Nanoflowers with Dual Active Sites for Efficient Electrochemical Hydrogen Evolution Reaction, ACS Applied Materials & Interfaces, 10 (2018).
[181] W.-J. Liu, M. Liu, Y. OuYang, H. Hou, M. Lei, Z. Wei, CVD-grown MoSe2 with high modulation depth for ultrafast mode-locked erbium-doped fiber laser, Nanotechnology, 29 (2018).
[182] W. Zhan, X. Yong, W. Haolin, W. Ruixue, N. Tang, Z. Yongjie, S. Jing, J. Teng, Z. Ying, L. Yimin, Y. Mei, W. Weidong, Z. Qing, M. Xiaohua, H. Yue, NaCl-assisted one-step growth of MoS 2 –WS 2 in-plane heterostructures, Nanotechnology, 28 (2017) 325602.
[183] Z. Wang, Y. Xie, H. Wang, R. Wu, T. Nan, Y. Zhan, J. Sun, T. Jiang, Y. Zhao, Y. Lei, M. Yang, W. Wang, Q. Zhu, X. Ma, Y. Hao, NaCl-assisted one-step growth of MoS 2 –WS 2 in-plane heterostructures, 2017.
[184] P. Campbell, A. Friedman, A. T. Hanbicki, S. V. Sivaram, A. J. Kusterbeck, V. K. Nguyen, R. McGill, Chemical vapor sensing with CVD-grown monolayer MoSe 2 using photoluminescence modulation, Applied Physics Letters, 113 (2018) 163106.
[185] M. Chhowalla, H.S. Shin, G. Eda, L.-J. Li, K.P. Loh, H. Zhang, The chemistry of two-dimensional layered transition metal dichalcogenide nanosheets, Nature Chemistry, 5 (2013) 263.
[186] Q. Feng, M. Zhu, Y. Zhao, H. Liu, L. Meng, J. Zheng, H. Xu, Y. Jiang, Chemical vapor deposition growth of sub-centimeter singlecCrystal WSe2 monolayer by NaCl assistant, Nanotechnology, 30 (2018).
[187] P. Sherrell, P. Palczynski, M. Sokolikova, F. Reale, F. Pesci, M. Och, C. Mattevi, Large-Area CVD MoS2/WS2 Heterojunctions as a Photoelectrocatalyst for Salt Water Oxidation, ACS Applied Energy Materials, DOI 10.1021/acsaem.9b01008(2019).
[188] S. Deng, C. Ai, M. Luo, B. Liu, Y. Zhang, Y. Li, S. Lin, G. Pan, Q. Xiong, Q. Liu, X. Wang, X. Xia, J. Tu, Coupled Biphase (1T-2H)-MoSe2 on Mold Spore Carbon for Advanced Hydrogen Evolution Reaction, Small (Weinheim an der Bergstrasse, Germany), DOI 10.1002/smll.201901796(2019) e1901796.
[189] F. Ersan, G. Gökoğlu, E. Aktürk, Adsorption and Diffusion of Lithium on Monolayer Transition Metal Dichalcogenides (MoS2(1–x)Se2x) Alloys, The Journal of Physical Chemistry C, 119 (2015) 28648-28653.
[190] R. Jagtap, A. Ambre, Atomic force microscopy (AFM): Basics and its important applications for polymer characterization: An overview, Indian Journal of Engineering & Materials Sciences, 13 (2006) 368-384.
[191] Y. Wang, R. Huang, F. Kong, B. Gao, G. Li, F. Liang, G. Hu, Tunable electronic and optical properties of the MoS2/MoSe2 heterostructure nanotubes, Superlattices and Microstructures, 132 (2019) 106156.
[192] X. Chen, G. Liu, Y. Hu, W. Cao, P.a. Hu, W. Hu, Vertical MoSe2-MoOx p-n heterojunction and its application in optoelectronics, Nanotechnology, 29 (2017).
[193] J. Park, H.H. Nguyen, W. Abdela, M. Kim, Applications of Field-Effect Transistor (FET)-Type Biosensors, Applied Science and Convergence Technology, 23 (2014) 61-71.
[194] M. Fallah, R. Faez, A. Sadr, The Effect of Strain on Carbon Nanotube Field Effect Transistors (FETs), 2012.
[195] W. Wróblewski, B. Mirzyńska, Z. Brzózka, Field Effect Transistors (FETs) as Transducers in Electrochemical Sensors, Chemia Analityczna, 41 (1996) 697-706.

[196] P. Chavarkar, U.K. Mishra, Field effect transistors: FETs and HEMTs, Thin Films, 28 (2001) 71-145.
[197] H.F. Storm, Field-effect transistor (FET) bibliography, Electron Devices, IEEE Transactions on, 14 (1967) 710-717.
[198] L. Ming, A Field-Effect Transistor (FET) model for ASAP, NASA STI/Recon Technical Report N, 76 (1965) 10377.
[199] K. K. Chan, W. E. Haensch, E. Leobandung, M. Yang, Field-effect transistor (FET) with source-drain contact over gate spacer, 2015.
[200] L.L. Chang, H.N. Yu, The Germanium Insulated-Gate Field-Effect Transistor (FET), Proceedings of the IEEE, 53 (1965) 316-317.
[201] H. Fang, S. Chuang, T.C. Chang, K. Takei, T. Takahashi, A. Javey, High-Performance Single Layered WSe2 p-FETs with Chemically Doped Contacts, Nano Letters, 12 (2012) 3788-3792.
[202] J.-B. Yau, J.O. Chu, K.T. Shiu, S.L. Cheng, I. Lauer, Nanowire field effect transistor (FET) and method for fabricating the same, 2016.
[203] M. Elena Sánchez-Vergara, L. Hamui, S. González Habib, New Approaches in Flexible Organic Field-Effect Transistors (FETs) Using InClPc, Materials, 12 (2019) 1712.
[204] W. Hoong. Kan, Parylene as a dielectric layer in a field effect transistor (FET), DOI (2019).
[205] W. Hwan Park, K. Soup Song, pH Sensitive Graphene Field-Effect Transistor(FET), Journal of the Institute of Electronics and Information Engineers, 53 (2016) 117-122.
[206] A.M. Ball, Silicon Field Effect Transistors (FETs), 1981, pp. 86-97.
[207] K. Datta, A. Shadman, E. Rahman, Q.D.M. Khosru, Trilayer TMDC Heterostructures for MOSFETs and Nanobiosensors, Journal of Electronic Materials, DOI 10.1007/s11664-016-5078-0(2016).
[208] H. Yoo, S. Hong, H. Moon, S. On, H. Ahn, H.-K. Lee, S. Kim, Y.K. Hong, J.-J. Kim, Chemical Doping Effects on CVD-Grown Multilayer MoSe 2 Transistor, Advanced Electronic Materials, 4 (2018) 1700639.
[209] K. Nowakowski, R. van Bremen, H. J. W. Zandvliet, P. Bampoulis, Control of the Metal/TMDC Contact Properties Using 2-Dimensional Buffer Layers, Nanoscale, 11 (2019).

APPENDIX-1

$MoS_{2(1-x)}S_{2(x)}$, (x=0-1) x value Calculation

The emission energy interpreted that a bowing as the x (x=0-1) changes this is called band gap bowing which can be denoted by quadratic equation. $MoS_{2(1-x)}S_{2(x)}$, (x=0-1) composition calculated by this equation. The resulting formula calculated for 136 different wavelengths values between 765 nm (X=0) and 810 nm (X=1) by MATLAB programming. Pl peak position versus composition for $MoS_{2(1-x)}Se_{2x}$ shown in Figure A1-11 and emission energy versus composition for $MoS_{2(1-x)}Se_{2x}$ shown in Figure A1-12

$$Eg(MoS_{2(1-x)}S_{2(x)}) = (1-x)\times Eg(MoS_2) + x\times Eg(MoSe_2) - (b)\times(X)\times(1-x)) \quad (1)$$

$Eg(MoS_{2(1-x)}S_{2(x)})$, $Eg(MoSe_2)$ and $Eg(MoS_2)$ are the band gaps of the alloy and the and materials, and b is the bowing parameter. From Table A1-1 comparing the bowing parameter of the other alloy, $MoS_{2(1-x)}S_{2(x)}$ alloy has small bowing parameter which is 0.05 [39, 44, 47].

$Egap = hc/\lambda$

$Egap = (6.626070040\times10^{-34}(joule\ second) \times 3\times10^{8}(meter\ per\ second)) / \lambda$

$Egap = 1240/\lambda$

$Eg(MoS_{2(1-x)}S_{2(x)}) = (1-X)\times Eg(MoS_2) + X\times Eg(MoSe_2) - (b)\times(X)\times(1-x))$

$Eg(MoS_2) = 1240/675$

$Eg(MoS_2) = 1240/810$

$b(MoS_{2(1-x)}S_{2(x)}) = 0.05$ (Table 6-1)

$Eg(MoS_{2(1-x)}S_{2(x)}) = 1240/\lambda$

$1240/\lambda = (1-X)\times(1240/810) + X\times(1240/675) - (b)\times(X)\times(1-x))$

$(0.05)X^2-(0.3561728395)X+(1.837037037-(1240/\lambda))=0$

$X_1=3.561728395-((24800/\lambda)-24.0548318)^{0.5}$

$X_2=3.561728395+((24800/\lambda)-24.0548318)^{0.5}$ since $0 \le X \le 1$ the root X_2 out of the range.

For $MoS_{2(1-x)}Se_{2(x)}$ *photoluminescence* peak is measured at 675 nm if we calculate it is simply, MoS_2

$X_1=3.561728395-((24800/675)-24.0548318)^{0.5}$

$X_1=0$

For $MoS_{2(1-x)}$ $Se_{2(x)}$ photoluminescence peak is measured at 725 nm if we calculate it is simply, $MoS_{2(0.6245)}Se_{2(0.3755)}$

$X_1=3.561728395-((24800/800)-24.0548318)^{0.5}$

$X_1=0.3755$

For $MoS_{2(1-x)}Se_{2(x)}$ photoluminescence peak is measured at 810 nm if we calculate it is simply, $MoSe_2$

$X_1=3.561728395-((24800/800)-24.0548318)^{0.5}$

$X_1=1$

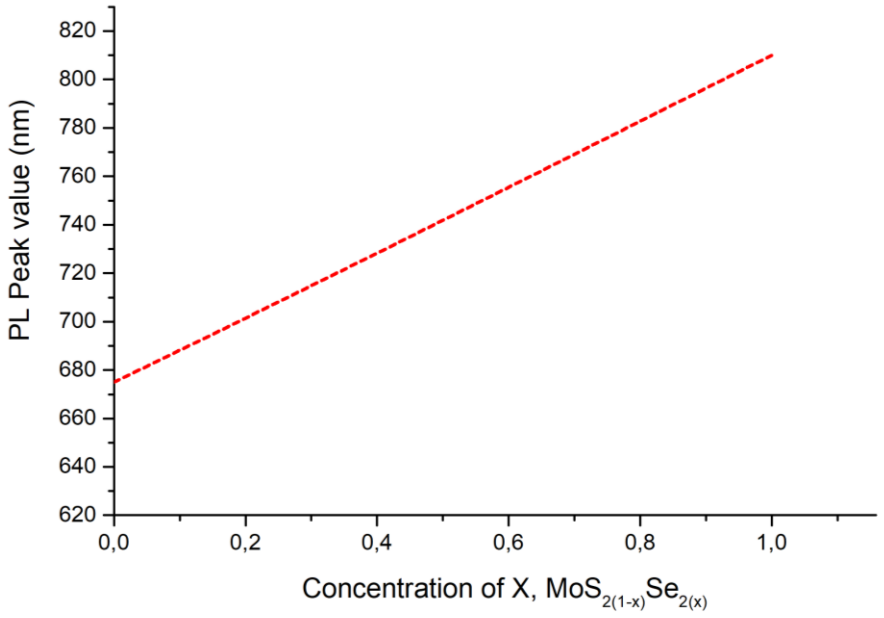

Figure A1- 1 *Pl peak position (nm) versus (x=0-1) for* $MoS_{2(1-x)}Se_{2(x)}$

```
function [X] = ConcentrationFunction(~)
v=[675 676 677 678 679 680 681 682 683 684 685 686 687 688 689 690 691 692 693 694 695 696 697 698 699 700
701 702 703 704 705 706 707 708 709 710 711 712 713 714 715 716 717 718 719 720 721 722 723 724 725 726 727
728 729 730 731 732 733 734 735 736 737 738 739 740 741 742 743 744 745 746 747 748 749 750 751 752 753 754
```

```
755 756 757 758 759 760 761 762 763 764 765 766 767 768 769 770 771 772 773 774 775 776 777 778 779 780 781
782 783 784 785 786 787 788 789 790 791 792 793 794 795 796 797 798 799 800 801 802 803 804 805 806 807 808
809 810];
X = 3.561728395 - sqrt((24800 ./v)-24.05483158);
```

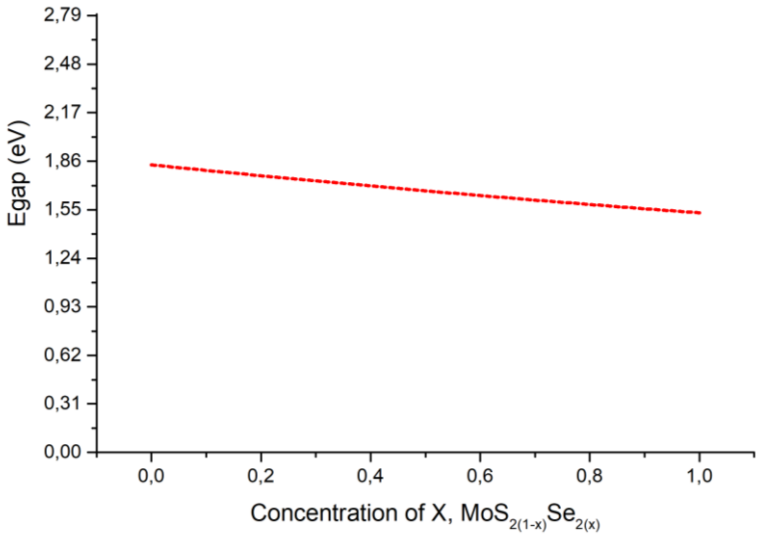

Figure A1- 2 *Emission energy (eV) versus x value (0-1) for $MoS_{2(1-x)}Se_{2(x)}$*

```
function [X] = eVfunction(~)
v=[675 676 677 678 679 680 681 682 683 684 685 686 687 688 689 690 691 692 693 694 695 696 697 698 699 700
701 702 703 704 705 706 707 708 709 710 711 712 713 714 715 716 717 718 719 720 721 722 723 724 725 726 727
728 729 730 731 732 733 734 735 736 737 738 739 740 741 742 743 744 745 746 747 748 749 750 751 752 753 754
755 756 757 758 759 760 761 762 763 764 765 766 767 768 769 770 771 772 773 774 775 776 777 778 779 780 781
782 783 784 785 786 787 788 789 790 791 792 793 794 795 796 797 798 799 800 801 802 803 804 805 806 807 808
809 810];
X = 1240./v;
```

Table A1- 1 *Pl peak value and x value of monolayer $MoS_{2(1-x)}Se_{2(x)}$*

The Table of PL peak value and X concentration value of monolayer $MoS_{2(1-x)}Se_{2(x)}$							
PL Peak Value (nm)	X value	PL Peak Value (nm)	X value	PL Peak Value (nm)	X value	PL Peak Value (nm)	X value
675	-1,39E-10	709	0,25658	743	0,50831	777	0,75766
676	0,00764	710	0,26404	744	0,51567	778	0,76498
677	0,01527	711	0,2715	745	0,52302	779	0,77231
678	0,0229	712	0,27895	746	0,53037	780	0,77964
679	0,03051	713	0,2864	747	0,53772	781	0,78696
680	0,03813	714	0,29384	748	0,54507	782	0,79429
681	0,04574	715	0,30129	749	0,55241	783	0,80162
682	0,05334	716	0,30872	750	0,55976	784	0,80894
683	0,06093	717	0,31616	751	0,5671	785	0,81627
684	0,06852	718	0,32359	752	0,57444	786	0,8236
685	0,07611	719	0,33101	753	0,58178	787	0,83093
686	0,08369	720	0,33844	754	0,58912	788	0,83827
687	0,09126	721	0,34586	755	0,59645	789	0,8456
688	0,09883	722	0,35327	756	0,60379	790	0,85293
689	0,10639	723	0,36068	757	0,61112	791	0,86027
690	0,11395	724	0,36809	758	0,61846	792	0,86761
691	0,1215	725	0,3755	759	0,62579	793	0,87494
692	0,12904	726	0,3829	760	0,63312	794	0,88228
693	0,13659	727	0,3903	761	0,64045	795	0,88962
694	0,14412	728	0,3977	762	0,64778	796	0,89697
695	0,15165	729	0,40509	763	0,65511	797	0,90431
696	0,15918	730	0,41248	764	0,66244	798	0,91166
697	0,1667	731	0,41987	765	0,66976	799	0,91901
698	0,17421	732	0,42725	766	0,67709	800	0,92636
699	0,18172	733	0,43463	767	0,68441	801	0,93371
700	0,18923	734	0,44201	768	0,69174	802	0,94107
701	0,19673	735	0,44939	769	0,69906	803	0,94843
702	0,20423	736	0,45676	770	0,70639	804	0,95579
703	0,21172	737	0,46413	771	0,71371	805	0,96315
704	0,21921	738	0,4715	772	0,72104	806	0,97051
705	0,22669	739	0,47887	773	0,72836	807	0,97788
706	0,23417	740	0,48623	774	0,73569	808	0,98525
707	0,24164	741	0,49359	775	0,74301	809	0,99262
708	0,24911	742	0,50095	776	0,75034	810	1

Table A1- 2 *Emission energy value and x value of monolayer* $MoS_{2(1-x)}Se_{2(x)}$

E_{gap} (eV)	X value	Egap (eV)	X value	Egap (eV)	X value	Egap (eV)	X value
1,83704	-1,39E-10	1,74894	0,25658	1,66891	0,50831	1,59588	0,75766
1,83432	0,00764	1,74648	0,26404	1,66667	0,51567	1,59383	0,76498
1,83161	0,01527	1,74402	0,2715	1,66443	0,52302	1,59178	0,77231
1,82891	0,0229	1,74157	0,27895	1,6622	0,53037	1,58974	0,77964
1,82622	0,03051	1,73913	0,2864	1,65997	0,53772	1,58771	0,78696
1,82353	0,03813	1,73669	0,29384	1,65775	0,54507	1,58568	0,79429
1,82085	0,04574	1,73427	0,30129	1,65554	0,55241	1,58365	0,80162
1,81818	0,05334	1,73184	0,30872	1,65333	0,55976	1,58163	0,80894
1,81552	0,06093	1,72943	0,31616	1,65113	0,5671	1,57962	0,81627
1,81287	0,06852	1,72702	0,32359	1,64894	0,57444	1,57761	0,8236
1,81022	0,07611	1,72462	0,33101	1,64675	0,58178	1,5756	0,83093
1,80758	0,08369	1,72222	0,33844	1,64456	0,58912	1,5736	0,83827
1,80495	0,09126	1,71983	0,34586	1,64238	0,59645	1,57161	0,8456
1,80233	0,09883	1,71745	0,35327	1,64021	0,60379	1,56962	0,85293
1,79971	0,10639	1,71508	0,36068	1,63804	0,61112	1,56764	0,86027
1,7971	0,11395	1,71271	0,36809	1,63588	0,61846	1,56566	0,86761
1,7945	0,1215	1,71034	0,3755	1,63373	0,62579	1,56368	0,87494
1,79191	0,12904	1,70799	0,3829	1,63158	0,63312	1,56171	0,88228
1,78932	0,13659	1,70564	0,3903	1,62943	0,64045	1,55975	0,88962
1,78674	0,14412	1,7033	0,3977	1,6273	0,64778	1,55779	0,89697
1,78417	0,15165	1,70096	0,40509	1,62516	0,65511	1,55583	0,90431
1,78161	0,15918	1,69863	0,41248	1,62304	0,66244	1,55388	0,91166
1,77905	0,1667	1,69631	0,41987	1,62092	0,66976	1,55194	0,91901
1,7765	0,17421	1,69399	0,42725	1,6188	0,67709	1,55	0,92636
1,77396	0,18172	1,69168	0,43463	1,61669	0,68441	1,54806	0,93371
1,77143	0,18923	1,68937	0,44201	1,61458	0,69174	1,54613	0,94107
1,7689	0,19673	1,68707	0,44939	1,61248	0,69906	1,54421	0,94843
1,76638	0,20423	1,68478	0,45676	1,61039	0,70639	1,54229	0,95579
1,76387	0,21172	1,6825	0,46413	1,6083	0,71371	1,54037	0,96315
1,76136	0,21921	1,68022	0,4715	1,60622	0,72104	1,53846	0,97051
1,75887	0,22669	1,67794	0,47887	1,60414	0,72836	1,53656	0,97788
1,75637	0,23417	1,67568	0,48623	1,60207	0,73569	1,53465	0,98525
1,75389	0,24164	1,67341	0,49359	1,6	0,74301	1,53276	0,99262
1,75141	0,24911	1,67116	0,50095	1,59794	0,75034	1,53086	1

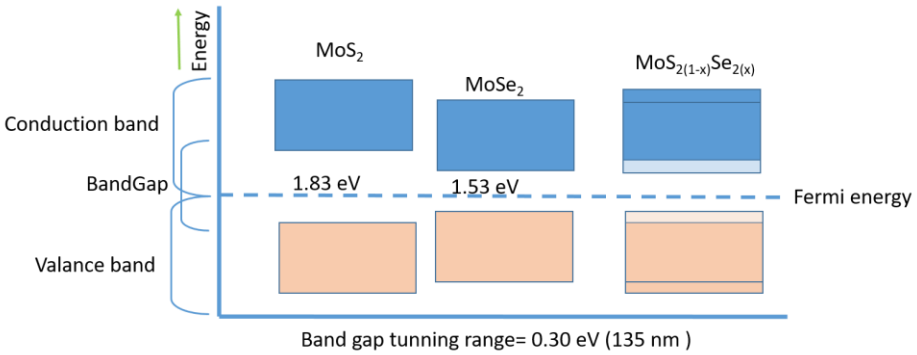

Figure A1- 3 *Bandgap models for 2D- TMDCs MoS_2, $MoSe_2$, $MoS_{2(1-x)}Se_{2(x)}$*

RESUME

Name Surname: Mehmet BAY

Foreign Language: English

Birth Place and Date: Gölcük / 05.09.1988

E-Mail: mehmetbay@eskisehir.edu.tr

EDUCATION

2012-2019, Eskişehir Technical University, Ph.D., Electrical and Electronics Engineering Department

2010-2012, Bahçeşehir University, M.Sc., Electrical and Electronics Engineering Department

2006-2010, Fatih University, B.Sc., Physics Department

EMPLOYMENT

2012-Current Research Assistant, Eskişehir Technical University Electrical and Electronics Engineering Department

2010-2012 Research Assistant, Bahçeşehir University, Electrical and Electronics Engineering Department

SCI PUBLICATIONS

1. M. Bay, A. Özden, F. Ay, N. K. Perkgöz, " Bandgap Tuning of Monolayer $MoS_{2(1-x)}Se_{2x}$ alloys by optimizing parameters" Materials Science in Semiconductor Processing, 2019

2. N. K. Perkgöz, M. Bay, "Investigation of Single-Wall MoS2 Monolayer Flakes Grown by Chemical Vapor Deposition" Nano-Micro Letters, 2016

CONFERENCES AND WORKSHOPS

1. M. Bay, A. Özden, F. Ay, N. K. Perkgöz, "Investigation of Large-Area $MoSe_2$ Monolayer Formation using NaCl Salt Catalyzer by Raman Scattering and Photoluminescence Spectroscopy" 4th International Turkish Congress on Molecular Spectroscopy, Aydın, Turkey. Oral Presentation, 2019

2. M. Bay, H. Şar, F. Ay, C. Sevik, N. K. Perkgöz, "Structural and Optical properties of CVD Grown $MoS_{2(1-x)}$-Se_{2x} Monolayer Alloys at Different x Compositions" 14th

International Nanoscience and Nanotechnology Conference, İzmir, Turkey. Poster Presentation, 2018

3. M. Bay, H. Şar, F. Ay, C. Sevik, N. K. Perkgöz, “Phototransistor Fabrication Based on CVD Grown 2D $MoSe_2$ films” 13th International Nanoscience and Nanotechnology Conference, Antalya, Turkey. Poster Presentation, 2017

4. N. K. Perkgöz, M. Bay, C. Sevik, F. Ay, “A Systematical Study of High Quality Monolayer $MoS_{2(1-x)}$-Se_{2x} AlloysGrown by CVD” 12th International Nanoscience and Nanotechnology Conference, Kocaeli, Turkey. Poster Presentation, 2016

5. M. Bay, A. Özden, A. Yeltik, C. Sevik, F. Ay, N. K. Perkgöz, “Controllable CVD Growth of Monolayer $MoS_{2(1-x)}$-Se_{2x} Alloys: Size and Bandgap Tuning” European MRS, Fall Meeting, Lille, France. Poster Presentation, 2016

6. N. K. Perkgöz, M. Bay, C. Sevik, F. Ay, “CVD Growth of Single-Wall MoS_2 Monolayer Flakes” European MRS, Fall Meeting, Lille, France. Poster Presentation, 2016